TOP AND HIGGS PHYSICS AT THE HADRON COLLIDERS

FERMILAB-PUB-13-570-E

SHABNAM JABEEN

Fermilab P.O. BOX 352, Batavia, USA
jabeen@fnal.gov

Received 30 August 2013
Accepted 9 September 2013
Published 21 October 2013

This review summarizes the recent results for top quark and Higgs boson measurements from experiments at Tevatron, a proton–antiproton collider at a center-of-mass energy of $\sqrt{s} = 1.96$ TeV, and the Large Hadron Collider, a proton–proton collider at a center-of-mass energy of $\sqrt{s} = 7$ TeV. These results include the discovery of a Higgs-like boson and measurement of its various properties, and measurements in the top quark sector, e.g. top quark mass, spin, charge asymmetry and production of single top quark.

Keywords: Top quark; Higgs boson; Tevatron; CDF; DØ, LHC; CMS; ATLAS.

PACS numbers: 12.38.Qk, 13.85.−t, 14.65.Ha, 14.80.Bn

Contents

1. Introduction

With the advent of the 21st century, we have entered an extraordinary era in the history of high energy physics. LHC recently discovered a new, Higgs-like particle after only a couple of years of data taking and Tevatron is still producing exciting results. Most of these results are, yet again, a testament to the validity of one of the most precisely tested theories, the standard model (SM) of particle physics.[1–4]

The SM is a gauge field theory based on the symmetry group $SU(3) \otimes SU(2) \otimes U(1)$, where $SU(2) \otimes U(1)$ describes the electroweak (EW) interactions[5–7] and $SU(3)$ describes the strong interactions Quantum Chromo-Dynamics (QCD).[8–12] The particle content of the SM includes a matter sector consisting of spin 1/2 fermion. This sector includes three generations of quark and lepton doublets. The interaction or the gauge sector includes the spin 1 gauge bosons: the photon (γ) for electromagnetic interaction; the weak gauge bosons Z and $W^{\pm}$ for weak interactions; and the eight gluons mediating the strong interaction. For the theory in its simplest form, with gauge symmetry unbroken, all these particles (bosons and fermions) are massless. The spontaneous breaking of this gauge symmetry in the EW sector of the SM is what gives mass to the weak gauge bosons. The mechanism used in the SM for this gauge symmetry breaking[13–15] is called Higgs mechanism or Englert–Brout–Higgs–Guralnik–Hagen–Kibble (EBHGHK) mechanism.[16–20] Particles in the matter sector become massive through their interaction with the quanta

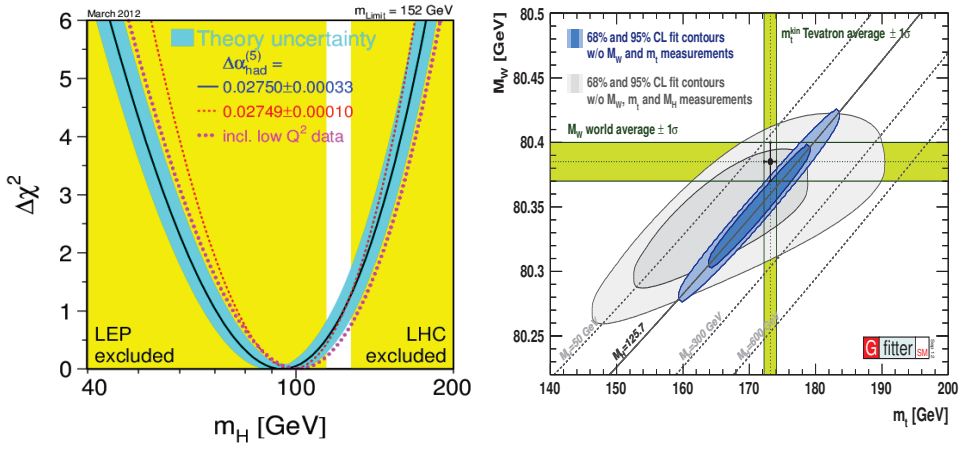

Fig. 1. (Color online) Left: the global χ^2 fit of the SM to precision data, projected onto the M_H axis. The blue band includes both the experimental and the theoretical uncertainties;[21] Right: constraints on the top quark and W boson masses resulting from direct measurements and a global SM fit including various values for the Higgs boson mass.[23]

of this new field, the Higgs boson. The fermion-Higgs couplings are in proportion to the fermion masses. The tantalizing fact that top quark's coupling to Higgs boson is almost 1, suggests that top quark might have some special role to play in EWSB. The mass of Higgs boson itself is a free parameter, not explained by the theory.

The study of top quark and Higgs boson are very much intertwined and both top quark and Higgs boson have been at the forefront of high energy physics for a long time. Since the SM theory is renormalizable, higher-order perturbative corrections can be reliably computed. These radiative corrections are very important for precision EW tests, which may be sensitive to new physics even if the new particles are too heavy for their direct production. It turns out that these radiative corrections are quite sensitive to the top mass (enhanced by a factor m_t^2/m_W^2) but only logarithmically dependent on the Higgs mass at one-loop level $\log(m_H^2/m_W^2)$. Higgs mass itself is driven by top quark radiative corrections. For the analysis of EW data in the SM, one can use the best measured input parameters and predict the value for any other parameters. For example, precise measurements of the top quark mass m_t together with the mass of the W boson m_W and other parameters of the EW theory can be used to indirectly constrain the mass of the Higgs boson, as shown in Fig. 1. The most recent global EW fits indicate that the Higgs boson should be light.[21–23] The value of top quark pole mass is one of the most important contributions to the limits on Higgs mass from vacuum stability conditions.

Apart from a very few possible deviations from its predictions in experiments, SM has proved to be an exceptionally successful theory. So far, there is no clear indication of new physics in the data collected and analyzed by different experiments. There are some measurements indicating some tension between the theory

and experimental observations[24] but nothing tangible enough to invalidate SM beyond any doubt. Yet, it does not answer all the open questions. Within SM, for example, instability of the SM with respect to quantum corrections is a problem, so is the observed mass of neutrinos. Also, baryogenesis, dark matter and dark energy are big issues not addressed by this theory. We also know that the EW symmetry breaking occurs at the TeV scale and new physics should lie around this scale. A large number of models beyond the SM try to describe nature and would be the main focus of experiments in coming years.

After the discovery of the top quark at the Tevatron in 1995 and of the τ neutrino at the DONUT experiment in 2000, the existence of a neutral boson, mark of the symmetry breaking mechanism, was still to be verified. Given that once a value for the Higgs boson mass is assumed, the properties of the SM Higgs boson are completely specified, precise predictions for production and decay rates and kinematics are possible. Based on these predictions, collider experiments have searched for the SM Higgs boson for the past many years. It took 25 years after the formulation of the Higgs mechanism until a significant mass range could be probed with the start of the operation of the Large Electron Positron (LEP) Collider at CERN in 1989. The search was continued at the Tevatron proton–antiproton collider from 2002 to 2011 at Fermilab. In 2010 the Large Hadron Collider (LHC) started taking data in proton–proton collisions. In the summer of 2012 a new particle, a neutral boson, very similar to one expected in SM, is discovered.[461,484,488]

Given the recent experimental results (discovery of a new Higgs-like particle and hints of possible deviations from SM expectations in top quark production, these two particles will remain the focus of collider experiments for a long time to come. This paper presents the current status of measurements concerning top quark and Higgs boson at the collider experiments.

This paper is organized as follows. After introduction (Sec. 1) a brief description of LHC and Tevatron colliders and Collider Detector at Fermilab (CDF), DØ, ATLAS and Compact Muon Solenoid (CMS) experiments are given (Sec. 2). General considerations for data analysis at colliders follow (Sec. 3). Next two sections contain the experimental results. The first section gives an account of current status of experimental studies of top quark (Sec. 4) and its properties and the second section describes SM Higgs boson searches and evidence and discovery of the Higgs-like particle at the LHC and Tevatron, respectively (Sec. 5).

A note to the reader: this paper only focuses on the experimental results either already published or submitted for publication. Exceptions to this rule are combinations of results between different channels in one experiment or within experiments. As is always the case, there is a lag between when the new results are publically available and when they are published. For a complete list of publically available recent results in top quark and Higgs boson physics please visit corresponding public webpages.[25–28]

2. Experimental Apparatus: Accelerators and Detectors

2.1. *Accelerators*: *Tevatron and LHC*

Tevatron collider at Fermi National Accelerator Laboratory in Chicago was the highest energy hadron collider in the world until the LHC at CERN in Geneva started taking data in 2009. The LHC is mainly a proton–proton collider whereas Tevatron is a proton–antiproton collider. This difference in initial states provides an opportunity to make complementary measurements along with the measurements at different center-of-mass (CM) energies. During Run II (defined by the period 2001–2011) Tevatron delivered 10 fb^{-1} integrated luminosity at 1.96 TeV CM energy to the CDF and DØ experiments each. The highest recorded instantaneous luminosity reached was $4.3 \times 10^{32}\ \text{cm}^2\,\text{s}^{-1}$ with about two multiple interactions on average.

At the LHC, the initial data taking started at 0.9 and 2.36 TeV CM energy, subsequently increasing to 7 TeV in 2010 and 8 TeV in 2012. The maximum instantaneous luminosity reached was $4 \times 10^{32}\ \text{cm}^2\,\text{s}^{-1}$ at 7 TeV and $8 \times 10^{33}\ \text{cm}^2\,\text{s}^{-1}$ at 8 TeV. One of the challenges specific to LHC is the number of multiple interactions per bunch crossing, which was about 20 on average with a maximum around 40 interactions per bunch crossing at 8 TeV. LHC stopped data taking at the end of 2012 for an upgrade to about 14 TeV, after delivering total integrated luminosity per experiment of about 5.5 fb^{-1} at 7 TeV and 23.5 fb^{-1} at 8 TeV.

2.2. *Detectors*: *CDF, DØ, ATLAS and CMS*

The final state of proton–proton or proton–antiproton collisions is expected to be comprised of some combination of leptons, jets and missing transverse energy $\not\!\!E_T$. All four experiments, CDF and DØ at the Tevatron and ATLAS and CMS at the LHC, are multipurpose detectors, built to reconstruct and analyze complete final states in hadron collisions.[29–36] The main components of these detectors are the tracking detectors, calorimeters and muon detectors. Typically, tracking detectors are located in the magnetic field of superconducting magnets to allow measurements of the momentum of charged particles.

At the Tevatron, the CDF weighs 5000 tons and is about 12 m in all three dimensions. The DØ detector has similar dimensions. Both CDF and DØ trigger system consists of three levels used to reduce the incoming collision rate of the order of 1 MHz to about 100 Hz.

All these detectors have very high object identification efficiencies. For example, the DØ primary vertex reconstruction and identification efficiency in data is above 97% and efficiencies to identify muons is about 80% for $p_T = 10$ GeV. CDF efficiency to identify electrons and photons is above 80%, and muon identification efficiency is about 95%.

In CDF, jets are reconstructed using a jet clustering algorithm.[37] In order to estimate the original parton energy from the observed jet energy in the calorimeter, observed jet energies are corrected for the losses in calorimeter and contributions

from multiple interactions in the event. In CDF these corrections are parametrized as function of η and for jets with transverse momentum above 50 GeV, the jet energy correction is determined with a 3% systematic uncertainty in the central region.[38] The jet reconstruction in DØ is performed using the Run II cone jet algorithm.[39] The jet energy scale (JES) corrections are η and p_T dependent and for a jet with $p_T = 100$ GeV and $\eta = 0.0$, the JES correction factor is 1.4 with 1.5% uncertainty.[40,41]

Many processes of interest, including top quark and Higgs boson production, are characterized by the presence of one or more b-quark jets in the final state. Thus identifying b-jets is an important part of signal selection and background rejection. Jets originating from the decay of b-quarks are identified using various methods including multivariate analysis (MVA) techniques. For CDF, typical b-tagging efficiency is about 50%–70% in the central region, with misidentification rates for light (u, d, s and gluon) jets of 0.5%–6%.[42–44] DØ also uses different algorithms to identify b-jets and typical efficiency for jets with p_T above 30 GeV for b-tagging is about 50%–80% with a light jet misidentification rate of 0.5%–10%, respectively.[45]

The luminosity measurement at the CDF is done using Cherenkov counter system.[46] At DØ, luminosity is measured using plastic scintillator arrays located in front of the end calorimeter cryostats.[32] The current CDF and DØ luminosity measurement uncertainty is about 6%.

At the LHC, the ATLAS detector[47] is 25 m high, 25 m wide and 46 m long, and has a total weight of 7000 tons. The CMS detector[48] is 21 m long, 15 m wide and 15 m high, and weighs 12,500 tons. A three-level trigger system is used to reduce the initial collision rate of the order of 10 MHz to about 200 Hz for ATLAS, and two-level CMS trigger system decreases the event rate to around 300 Hz, before data storage. CMS uses a global event reconstruction called Particle Flow (PF) to reconstruct and identify each particle produced in the event using information from all subdetectors.[49]

Electron reconstruction[50,51] efficiencies range from 70%–90% and for the most of relevant energy range, the electron energy scale is known to better than 0.5% (0.3%) in ATLAS (CMS), while the energy resolution is 2% (3%) or better. The probability to misidentify the electron charge is below 1%. The energy resolution for photons of $p_T = 100$ GeV is better than 1.5%.

For muons, the reconstruction efficiency is above 95% for both experiments and the muon p_T resolution is 3%–4% and 1%–2% in the relevant range for ATLAS[52] and CMS[53] detectors, respectively. Fake identification of a muon and the charge mis-identification are very small for both experiments.

For jet reconstruction anti-kt algorithm is used.[54–56] The typical jet energy resolution is about 8% (11%) at 100 GeV in the case of CMS[57] (ATLAS).[58] CMS benefits significantly from the use of PF algorithm to reconstruct jets. The JES uncertainty is less than 2% for $p_T > 45$ GeV.[57] For ATLAS, the JES uncertainty is less than 2.5% for central jets with $|\eta| < 0.8$ and $p_T = 60$–800 GeV.[57,59]

Like CDF and DØ experiments, ATLAS and CMS also use several algorithms based on the fact that B-hadrons travel inside the detector before decaying, resulting in secondary vertex in the event.[60–66] The b-jet identification efficiencies depend on the p_T and η of the jet, as well as the event sample used to measure these efficiencies. Typical values for the efficiencies and the rate of identifying a light flavor jet as a b-quark jet (mis-tag rate) are in the range 50%–70% and 0.5%–5%, respectively.[67–71]

Presence of a neutrino in the event is characterized by $\not\!\!E_T$, calculated as the negative of the vector sum of the p_T of all the particles in the final state. In ATLAS, $\not\!\!E_T$ is reconstructed from the deposited energy[72] where as CMS uses PF objects as input to $\not\!\!E_T$ calculation.[73] Even though ATLAS hadronic calorimeter has better resolution, the CMS $\not\!\!E_T$ resolution is comparable to ATLAS owing to the use of PF objects. The $\not\!\!E_T$ resolution is roughly $50\% \times \sqrt{\sum E_T}$ for both experiments.

The instantaneous luminosity is measured in both experiments by counting the rate of collisions for a given number of bunch crossings using various techniques and detectors.[74–80] In the case of ATLAS, the systematic uncertainty on the measured luminosity currently corresponds to 1.8% and 3.6% for 7 TeV and 8 TeV data, respectively.[81] For CMS, the corresponding uncertainties are 2.2 (4.4)% for 7 TeV and 8 TeV data, respectively.[77]

3. General Considerations for Searches at Hadron Colliders

In hadron collider experiments, the potential to search for new physics or to precisely measure a known process, depends on high trigger efficiency, efficient object identification, clever ideas to discriminate signal from the background and understanding sources of systematic uncertainties.

As is always the case, current experiments refine and enhance techniques and methods learned at the past experiments. Tevatron experiments started with a wealth of knowledge from UA1, UA2 and LEP experiments, for example, and added their own innovative methods, especially the use of multivariate techniques got a big boost at the Tevatron. The same is now being repeated at the LHC where old methods are being perfected and new methods are being continuously developed.

One of the biggest challenges at the hadron colliders lies in the fact that most of the rate of interesting collisions is very small compared to noninteresting collisions. Algorithms involved in selection of interesting collisions need constant tending with changing luminosity and analysis needs of the experiments. Once interesting collisions have been recorded, in order to increase the signal-to-background ratio, all experiments have developed methods to efficiently use detector information. Sophisticated techniques, e.g. matrix element information, artificial neural networks[82–86] and boosted decision trees,[87–91] are being used and improved regularly. The selection and classification of events is generally based on number and flavor of leptons, number of jets, quality and multiplicity of identified b-tagged jets, presence of missing transverse momentum $\not\!\!E_T$. These different channels have

different signal and background composition and help increase the sensitivity by exploiting these differences. For estimation of signal and the background processes to a process of interest, either Monte Carlo (MC) simulation or controlled samples in data, or a combination of both are used. There are several programs available to simulate various processes of interest at different CM energies and initial states. For all generated samples the hadronization is handled by PYTHIA[92] or HERWIG++[93] generators. In order to compare simulated events with experimental data, the simulated samples are processed through detector simulations based on the GEANT[94] framework. Finally, these simulated events are reconstructed and analyzed in exactly the same way as the real data events.

In order to separate signal from background, sophisticated analysis techniques have been developed. These techniques have been put to maximal use both in object identification as well as final signal discrimination. All experiments use MVA methods to combine information from many discriminating variables. Also, since analyses using different MVA techniques are not 100% correlated, it is becoming a normal practice to perform the search in a single channel with different MVA techniques and then combine their results to increase sensitivity. Using these techniques in series is common as well, where one discriminating technique is first applied for a certain background and then a cut is applied to the resulting discriminant to retain the signal enhanced subsample and then another MVA is applied to this subsample to reduce other backgrounds. At the Tevatron, these techniques have played a crucial role in many analyses including the observation of single top quark production and evidence for the Higgs-like boson.

The final most discriminating distributions either from a single reconstructed quantity or final output of a discriminating technique is used as the input for the statistical analysis. Experiments use both Bayesian and "CL_S" methods to set exclusion limits on new physics hypotheses. For details of these methods see Refs. 95–101.

4. *Top* Quark Physics at Hadron Colliders

4.1. *Introduction*

The top quark is the heaviest known fundamental particle. The mass of the top quark, m_t, is a fundamental parameter of the SM. It is partner of the b quark in the third generation weak isospin quark doublet and has charge $Q = +2/3e$ and weak isospin $T_3 = +1/2$. The existence of a sixth quark was postulated long before it was finally discovered in 1995 by the CDF and DØ collaborations at the Tevatron proton–antiproton ($p\bar{p}$) collider at Fermilab.[102,103] Its partner, the b quark, was discovered in 1977. The reason it took almost two decades to discover top quark, is its unexpectedly large mass which turns out to be $m_t = 173.2 \pm 0.9$ GeV, about 40 times heavier than the b-quark and comparable to the size of an atom of Gold. The top quark decays almost exclusively as $t \to Wb$. The decays of the top quark into a W boson and a quark of another isospin doublet $t \to Ws$ (BR $\sim 0.2\%$), $t \to Wd$

(BR $\sim 0.005\%$) are strongly suppressed in the SM. The top quark decay width predicted by the SM at next-to-leading-order (NLO) is $\Gamma_t = 1.33$ GeV for top mass $m_t = 172.5$ GeV,[104] which corresponds to a very short lifetime (about 10^{-25} s), an order of magnitude smaller than the typical formation time of hadrons. Thus top quark decays before it has a chance to hadronize, transferring information, e.g. about spin,[105] to its decay products, providing a unique opportunity to study the properties of a bare quark. The large value of m_t also implies a large coupling to the Higgs boson. The top quark Yukawa coupling is close to unity. This observation has often prompted the speculation that the top quark may play a special role in the EW symmetry breaking. The measured value of m_t together with the mass of the W boson (M_W) constrains the mass (m_H) of the Higgs boson through quantum corrections. Comparing this indirect prediction with a direct measurement of m_H provides a stringent test of the consistency of the SM.

Unitarity of the CKM matrix implies that the denominator of the ratio R of branching fractions (BR), defined as

$$R = \frac{\mathrm{BR}(t \to Wb)}{\mathrm{BR}(t \to Wq)} = \frac{|V_{tb}|^2}{|V_{tb}|^2 + |V_{ts}|^2 + |V_{td}|^2}\,, \tag{1}$$

is unity. Here $|V_{tx}|$ are CKM matrix elements. A deviation of R from unity may indicate presence of new physics beyond SM. Similarly, within SM the decays involving flavor changing neutral current (FCNC) $t \to Z/\gamma q/q$ have negligible branching ratios, and a deviation would indicate new physics. Thus precision measurements of the couplings of top quark are very important in order to validate SM. In general, precise measurements of the properties of the top quark and its interactions may reveal effects from new physics. In particular, there are many proposed models where new physics prefers to interact with third generation quarks. Also, experimental signatures involving top quark production often constitute an important background to various new physics scenarios. For these reasons, top quark physics is a major part of the research plan at both Tevatron and LHC.

After the discovery of the top quark at Tevatron, both CDF and DØ experiments have performed a large number of measurements to precisely determine its production and decay properties, as well as any hints of new physics involving top quarks. Now, this effort is being continued at the LHC. These measurements have been summarized in recent years (see, e.g. Refs. 106–108). The LHC is truly a top quark factory (millions of top quarks have been produced at the LHC so far. About 80,000 top quark pairs in 5 fb^{-1} at 7 TeV), and many properties will be measured more precisely at the LHC. However, because of the difference in initial states at both colliders, many measurements provide complementary information at the Tevatron and thus will remain relevant.

This section is arranged as follows. Subsection 4.2 describes top quark production and decay at Tevatron and LHC. In Subsec. 4.3, current status of top pair production cross-section measurements, measurement of branching fraction and some other related measurements are presented. Next section gives brief account

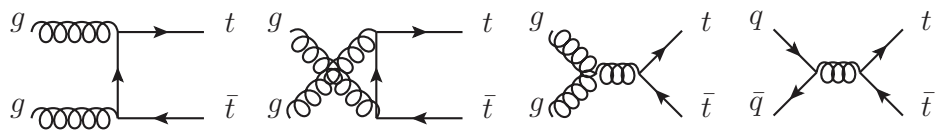

Fig. 2. Feynman diagrams for $t\bar{t}$ production at leading-order QCD.

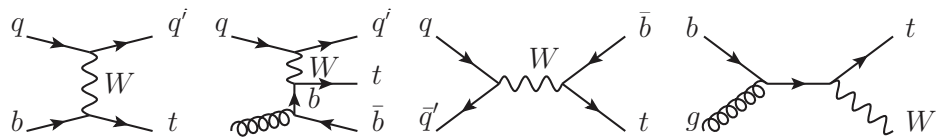

Fig. 3. Representative Feynman diagrams for single top quark production. From left to right: t-channel production as flavor excitation and as W-gluon fusion; s-channel production; tW production.

of measurement of differential cross-section (Subsec. 4.4). Direct and indirect top quark mass measurements are summarized in Subsec. 4.5, followed by mass difference (Subsec. 4.6), top quark charge (Subsec. 4.7), charge asymmetry (Subsec. 4.9), decay width (Subsec. 4.10), spin correlation (Subsec. 4.8), Wtb coupling and W polarization (Subsec. 4.11), and a study of color flow in top pair production is briefly discussed (Subsec. 4.12). Finally, measurements for EW production of single top quarks are presented (Subsec. 4.13).

4.2. *Top quark production and decay*

At hadron colliders, top quarks are produced either in pairs, through the strong interaction, or singly through the weak interaction. In SM, the dominant production mechanism for top quark pair production is mediated by the strong interaction. At the Tevatron, $q\bar{q}$ is responsible for $\approx 85\%$ of the total $t\bar{t}$ production cross-section and gluon fusion accounts for the rest. At the LHC these ratios are reversed and gluon fusion accounts for $\approx 90\%$ of the total $t\bar{t}$ production cross-section. Figure 2 depicts leading Feynman diagrams for $t\bar{t}$ production through gluon fusion and quark–antiquark annihilation. Figure 3 shows leading Feynman diagrams for three single top quark production channels: the t-channel production through a space-like W boson scattering off a b-quark; the s-channel production where time-like W boson is produced from incoming quarks; and the tW-channel where top quark is produced in association with a W boson.

The t-channel production mode is dominant at both Tevatron and LHC, followed by the tW associated production at LHC and s-channel production at Tevatron. The s-channel has very small cross-section at the Tevatron to be observed with 5 standard deviation (SD) significance at DØ or CDF alone, and the tW production has negligible cross-section. The increase in the cross-section for this channel from Tevatron to the LHC is significantly less than the increase in the main backgrounds, making it even harder to observe this channel at the LHC.

Table 1. Latest NNLO+NNLL theoretical predictions for top quark pair production for various colliders CM energies.[138]

Collider	$\sigma_{\rm tot}$ [pb]	Scales [pb]	PDF [pb]
Tevatron	7.164	$^{+0.110(1.5\%)}_{-0.200(2.8\%)}$	$^{+0.169(2.4\%)}_{-0.122(1.7\%)}$
LHC 7 TeV	172.0	$^{+4.4(2.6\%)}_{-5.8(3.4\%)}$	$^{+4.7(2.7\%)}_{-4.8(2.8\%)}$
LHC 8 TeV	245.8	$^{+6.2(2.5\%)}_{-8.4(3.4\%)}$	$^{+6.2(2.5\%)}_{-6.4(2.6\%)}$
LHC 14 TeV	953.6	$^{+22.7(2.4\%)}_{-33.9(3.6\%)}$	$^{+16.2(1.7\%)}_{-17.8(1.9\%)}$

Note that, being a proton–proton collider, for LHC, except for the tW production, the cross-sections for top quark production are larger than that for antitop quark production.

4.2.1. *Theoretical calculations for top quark production*

The NLO QCD corrections to the total $t\bar{t}$ production cross-section have been known for more than two decades.[109–115] Mixed QCD and weak[116–121] and QED and weak[122] corrections have been available at NLO as well. Various soft-gluon resummation logarithmic and approximate next-to-next-leading-order (NNLO) calculations have been done as well.[123–132] There are also calculations of $t\bar{t}$ production cross-section at NLO QCD which include the top quark decays and the correlations between production and decay, such as the information on the top quark spin.[133–137] Recently, exact NNLO calculations have been done[138] and latest NNLO + NNLL theoretical predictions for top quark pair production for various colliders and CM energies are given in Table 1. Figure 4 shows various NNLO approximate calculations at CM energies of 7 TeV and 8 TeV at LHC, and 1.96 TeV at Tevatron, along with exact NLO and NNLO calculations.

The NLO QCD differential cross-sections for the production of $t\bar{t}$+jets have been calculated at NLO.[115,139–143] For a detailed overview of the theoretical calculations see Refs. 144–147.

Theoretical calculations for single top quark production cross-section are available up to approximate NNLO for Tevatron as well as LHC.[148–161] Here, Refs. 148–160, 162 and 163 are up to NLO. References 161 and 164–167 are approximate NNLO. Reference 161 uses NLL resummation, while Refs. 164–167 use NNLL resummation.

For Tevatron $p\bar{p}$ collisions at 1.96 TeV, approximate NNLO single top t-channel and s-channel cross-sections are,

$$\sigma_{t\text{-channel}}(m_t = 173\ \text{GeV}) = 1.04^{+0.00}_{-0.02} \pm 0.06\ \text{pb} \quad \text{(Ref. 164)}\,,$$
$$\sigma_{s\text{-channel}}(m_t = 173\ \text{GeV}) = 0.523^{+0.001+0.030}_{-0.005-0.028}\ \text{pb} \quad \text{(Ref. 165)}\,.$$

Here, uncertainties are from scale and PDF variations, respectively. Single antitop production cross-section at the Tevatron is the same as for the single top cross-section. The tW production cross-section at Tevatron is negligible.

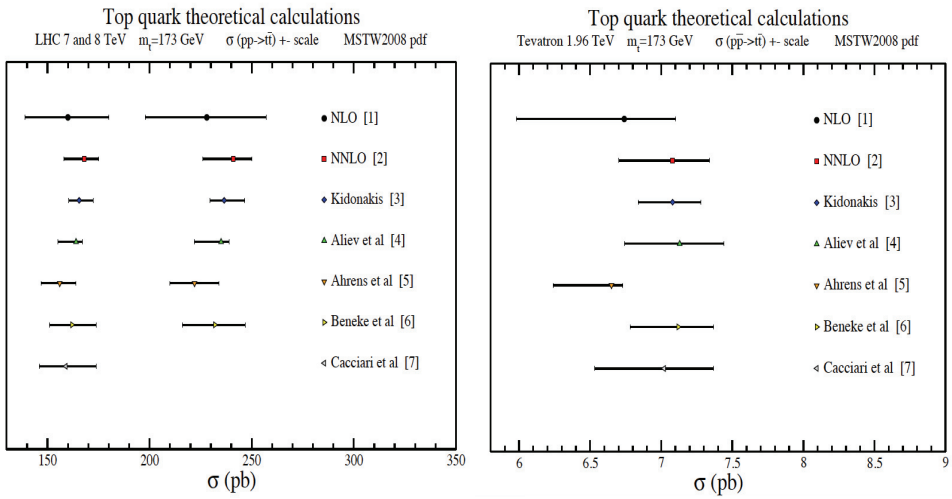

Fig. 4. NNLO exact[138] and approximate[123–127] results for the $t\bar{t}$ cross-section. Left: for LHC $\sqrt{s} = 7$ TeV (bars on the left) and $\sqrt{s} = 8$ TeV (right). Right: for Tevatron $\sqrt{s} = 1.96$ TeV. Plots taken from Ref. 132. Here, [1] corresponds to Refs. 109, 111, 112, [2] corresponds to Ref. 138 and [3], [4], [5], [6], [7] correspond to Refs. 123–127, respectively.

Table 2. Approximate NNLO QCD calculations of the total cross-sections for single top quark and antiquark production in pp collisions at $\sqrt{s} = 7$ TeV. The first (second) uncertainty corresponds to the scale (PDF) uncertainty.

Single top production mode	σ_t [pb]	$\sigma_{\bar{t}}$ [pb]
t-channel (Kidonakis[164])	$41.7^{+1.6}_{-0.2} \pm 0.8$	$22.5 \pm 0.5^{+0.7}_{-0.9}$
s-channel (Kidonakis[165])	$3.17 \pm 0.06^{+0.13}_{-0.10}$	$1.42 \pm 0.01^{+0.06}_{-0.07}$
s-channel (Zhu *et al.*[166])	$2.81^{+0.16}_{-0.10}$	$1.60^{+0.08}_{-0.05}$
tW-channel (Kidonakis[167])	$7.8 \pm 0.2^{+0.5}_{-0.6}$	$7.8 \pm 0.2^{+0.5}_{-0.6}$

For pp collisions at CM energy 7 TeV, these calculations are summarized in Table 2.

4.2.2. *Experimental signatures of top production*

The $t\bar{t}$ measurements are characterized according to the decay of the W bosons from the decay of the two top quarks as follows.

Dilepton channel. Both W bosons decay leptonically $t\bar{t} \rightarrow W^+bW^-\bar{b} \rightarrow \bar{l}\nu_l bl'\bar{\nu}_{l'}\bar{b}$, where l = electron, muon or tau lepton. The experimental signature consists of two leptons with high transverse momentum (p_T), large missing transverse energy ($\not{E}_T$) and at least two b-quark jets. The branching fraction for this decay mode is relatively small (about 10%) but this is a very clean channel with

very small background contamination from, e.g. Z + jets or WW, ZZ or WZ (diboson) production.

Lepton + jets channel. One W boson decays leptonically and other hadronically, $t\bar{t} \to W^+bW^-\bar{b} \to q\bar{q}'bl\bar{\nu}_l\bar{b} + \bar{l}\nu_l bq\bar{q}'\bar{b}$. Experimental signature for this channel is one high p_T lepton, $\not{E}_T$ and at least four jets, two of which b-quark jets. The branching fraction for this decay mode is about 44%. This is considered to be the best search channel and experiments have generally performed their most sensitive top measurements in this channel. The cross-section is relatively large for this decay mode with manageable backgrounds, mainly from W + jets and multijet production.

Hadronic channel. Both W bosons decay hadronically $t\bar{t} \to W^+bW^-\bar{b} \to q\bar{q}'bq''\bar{q}'''\bar{b}$. The experimental signature is at least six jets, two of them b-jets. Even though the branching fraction for this decay mode is about 46% this channel is very challenging because of the large background from multijet production.

Since the final states with hadronically decaying taus are experimentally much more challenging, as a result most of the channel combinations in the lepton + jets and dilepton channel include only electron and muon channels.

The measurements in single top quark production are generally limited to lepton + jets channel. The main backgrounds to EW single top quark measurements arise from $t\bar{t}$, W + jets and multijet production.

4.3. *Top quark pair production*

4.3.1. *Cross-section measurements*

The cross-section for $t\bar{t}$ production has been measured to a great precision, in different channels and at different energies, by four experiments, CDF and DØ at Tevatron and ATLAS and CMS at the LHC. So far all measurements are in good agreement with the SM predictions.

Cross-section measurements have been done in all general topologies, discussed in Subsec. 4.2 by CDF,[168–179] DØ,[180–187] ATLAS[188–193] and CMS[194–202] experiments.

CDF and DØ collaborations have performed combination of measurements within the experiments as well as with one another using a method of best linear unbiased estimate BLUE.[203,204] In these combinations, both statistical and systematic correlations among these channels are taken into account and any bias in the procedure is determined using ensembles of simulated experiments.

CDF internal combination includes two measurements in lepton + jets channel, one from the dilepton channel, and one measurement in alljets channel, using up to 4.6 fb^{-1}, 9 fb^{-1} and 2.9 fb^{-1} integrated luminosity, respectively. CDF combinations yields a total uncertainty of 0.5 pb on the combined CDF cross-section. The maximum correlation between these channels is found to be about 50%. DØ internal combination includes two measurements one from dilepton channel and the other

Table 3. Latest results for top quark pair production cross-section measurements from Tevatron and LHC experiments.

CDF, up to 8.8 fb^{-1} at 1.96 TeV (Ref. 205)	$\sigma_{t\bar{t}} = 7.63 \pm 0.31$ (stat.) ± 0.39 (syst.) pb
DØ, 5.4 fb^{-1} at 1.96 TeV (Ref. 205)	$\sigma_{t\bar{t}} = 7.56 \pm 0.20$ (stat.) ± 0.56 (syst.) pb
Tevatron, up to 8.8 fb^{-1} at 1.96 TeV (Ref. 205)	$\sigma_{t\bar{t}} = 7.60 \pm 2.0$ (stat.) ± 0.36 (syst.) pb
ATLAS, up to 1.02 fb^{-1} at 7 TeV (Ref. 206)	$\sigma_{t\bar{t}} = 177 \pm 3$ (stat.)$^{+8}_{-7}$ (syst.) ± 7 (lum.) pb
CMS, 2.3 fb^{-1} at 7 TeV (Ref. 197)	$\sigma_{t\bar{t}} = 161.9 \pm 2.5$ (stat.)$^{5.1}_{5.0}$ (syst.) ± 3.6 (lum.) pb
LHC, up to 1.1 fb^{-1} at 7 TeV (Ref. 207)	$\sigma_{t\bar{t}} = 173.3 \pm 2.3$ (stat.) ± 9.8 (syst.) pb

from lepton + jets channel, both using up to 5.4 fb^{-1} integrated luminosity. ATLAS combines its measurements in lepton + jets, dilepton and all hadronic channel.

Table 3 summarizes the internal combinations from CDF and DØ and their final Tevatron combination, the internal combination of ATLAS experiment, and the best measurement from the CMS experiment. The LHC results correspond to data collected at 7 TeV CM energy.

The contributions of different sources to systematic uncertainties for these measurements vary depending on the channel. Main uncertainties in these measurements include modeling of signal and background, luminosity and detector modeling. Here detector modeling includes uncertainties in the final state object identification efficiencies, trigger, energy and resolution, the calculation of the missing transverse momentum, trigger and in the b-jet identification, and estimated background fractions. The Tevatron combination has a relative uncertainty of 5.4% and for the LHC combination this total uncertainty is 5.8%. A summary of the most precise cross-section ($\sigma_{t\bar{t}}$) measurements performed by experiments at Tevatron, in various channels, are shown in Fig. 5. A comparison of these measurements with theory predictions is also shown. All measurements, within uncertainties, are in good agreement with one another and with SM predictions.

In addition to these benchmark measurements for the production of top quark pairs, experiments are always looking for methods to improve their acceptance or reduce uncertainties. One example is the measurement in lepton + jets channel by CDF.[170] In this analysis they reduce the large uncertainty on luminosity by measuring a ratio of $\sigma_{t\bar{t}}/\sigma_{Z/\gamma^* \to \ell\ell}$. Since Z/γ^* cross-section[30] is much more precisely known, the larger uncertainty in luminosity is replaced by a smaller uncertainty on the Z/γ^* cross-section.

4.3.2. *Measurement of branching fraction R*

Within SM the branching fraction $R = \frac{\mathrm{BR}(t \to Wb)}{\mathrm{BR}(t \to Wq)}$ $(q = d, s, b)$ is expected to be 1 and any deviations could be an indication of a fourth-generation of fermions.

The DØ and CDF experiments at Tevatron have published measurements of this ratio[208–212] and found it to be in good agreement with SM expectation with a deviation of 2.5 SD at most.[210]

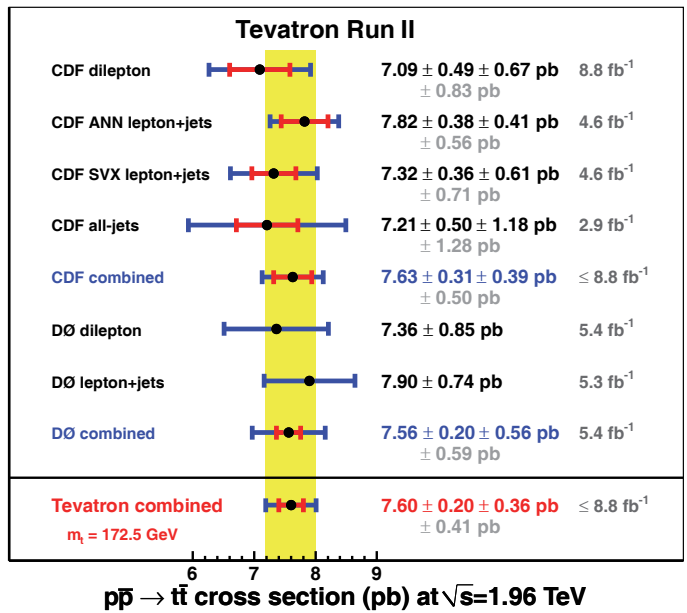

Fig. 5. Summary of the most precise cross-section ($\sigma_{t\bar{t}}$) measurements performed by CDF and DØ experiments in various channels compared with theory predictions.

4.3.3. *Additional jet activity in $t\bar{t}$ production*

Many measurements presented in this paper suffer from significant systematic uncertainties due to the modeling of additional quark and gluon radiation in $t\bar{t}$ production. Experimental data are needed to validate the MC models and reduce these uncertainties.

ATLAS performed a measurement of $t\bar{t}$ production with a veto on additional jet activity using 2 fb^{-1} of 2011 data in the dilepton channel and the results are compared to theoretical predictions from MC generators MC@NLO,[214] POWHEG,[213] ALPGEN[214] and SHERPA.[216] A reasonable, overall agreement between data and predictions is observed when the additional jets are vetoed in the rapidity interval $|y| < 2.1$. However, the agreement is not as good for some generators for jet veto in the most central or most forward bins in rapidity. For details see Ref. 217.

4.3.4. *Measurement of the fraction of gg in $t\bar{t}$ production*

A measurement of the fraction of gg fusion process (f_{gg}) in the $t\bar{t}$ production performed at CDF exploits the difference in kinematic characteristics of gg and $q\bar{q}$ contributions to distinguish the two mechanisms. Using the Feldman–Cousins prescription,[218] measured values are mapped to a range of MC-generated true fractions. For the lepton + jets channel, in a sample of 1 fb^{-1} of data CDF finds $f_{gg} < 0.33$ at a 68% CL.[219] This result is combined with another measurement[220] that relies

on the higher probability for a primary gluon, than for a quark, to radiate a low energy gluon in the production process, obtaining a value of $f_{gg} = 0.07^{+0.15}_{-0.07}$, in agreement with the SM prediction.

4.3.5. *Measurement of $t\bar{t}\gamma$ production*

The EW couplings of the top quark can be studied by investigating events where top quark pairs are produced in association with a gauge boson. CDF reported first evidence for $t\bar{t}\gamma$ production at the Tevatron[221] and the result is consistent with the SM predictions.

4.3.6. *Lorentz invariance*

Because of Earth's rotation about its axis, if Lorentz invariance is violated, with reference to Sun-centered frame in the Earth-based laboratory frame we would observe periodic oscillation in the number of $t\bar{t}$ events observed in the detector as a function of sidereal time. This violation can be quantified using the SM Extension (SME) framework,[222,223] which provides an effective field theoretical treatment for violation of Lorentz and CPT symmetry in particle interactions by introducing Lorentz-violating terms to the Lagrangian density of the SM. As yet, no constraints have yet been placed on Lorentz invariance violation in the top quark sector. Using 5.3 fb^{-1} of integrated luminosity, DØ searched for violation of Lorentz invariance by examining the $t\bar{t}$ production cross-section in lepton + jets final states.[224] Within uncertainties, these coefficients are found to be consistent with zero.

4.4. *Differential cross-sections for $t\bar{t}$ production*

Measurement of differential cross-sections $d\sigma_{t\bar{t}}/dX$, where X can be any kinematic variable of final state particles, top quark or top–antitop quark system, are an important check of SM. Any deviation in these measurements from SM predictions would be an indication of new physics (e.g. see Refs. 225 and 226). All four experiments at Tevatron and LHC measure differential cross-sections for a variety of variables including transverse momentum and $m_{t\bar{t}}$.[227–230] In most cases the differential distributions are corrected for detector and acceptance effects, in order to compare with parton level theoretical calculations.

CDF measures the differential cross-section for top quark-pair production with respect to the $t\bar{t}$ invariant mass using an integrated luminosity of 2.7 fb^{-1}.[227] DØ performs similar measurement of differential cross-section as function of top quark transverse momentum with 1.0 fb^{-1} integrated luminosity.[228]

ATLAS[229] measures differential cross-sections for top quark pair production relative to the total inclusive top quark pair production cross-section as a function of the invariant mass, the transverse momentum and the rapidity of the top quark pair system. A data sample of 2 fb^{-1} collected at 7 TeV is used for this measurement.

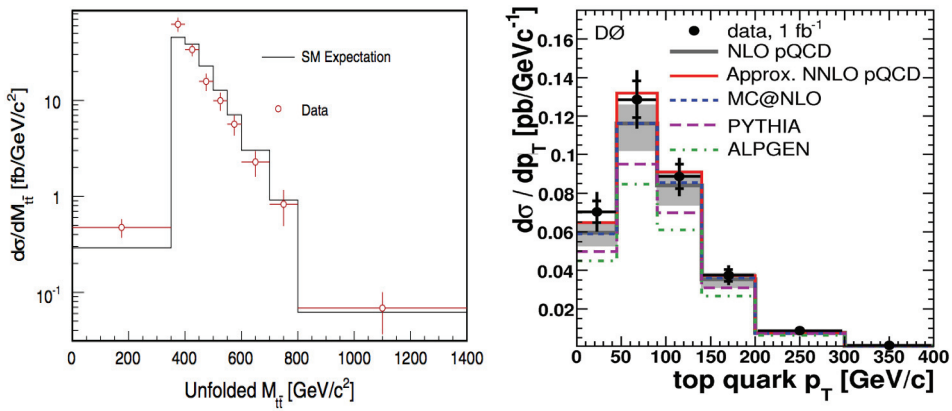

Fig. 6. Left: CDF measured mass of the $t\bar{t}$ system with 2.7 fb^{-1} of integrated luminosity. Here data are compared with the SM expectation as modeled by PYTHIA. Right: DØ inclusive $d\sigma/dp_T$ for $t\bar{t}$ production (two entries per event) in data is compared with expectations from theoretical calculations and output from several event generators.

CMS[230] also measures normalized differential top quark pair production cross-sections using data corresponding to an integrated luminosity of 5 fb^{-1} collected at 7 TeV. The $t\bar{t}$ differential cross-section is measured as a function of kinematic properties of the final-state particles, top quark and top–antitop system.

Results are shown in Figs. 6 and 7. These measurements are also compared with predictions from MC event generators and NLO perturbative QCD calculations. No significant deviations from SM predictions have been observed so far.

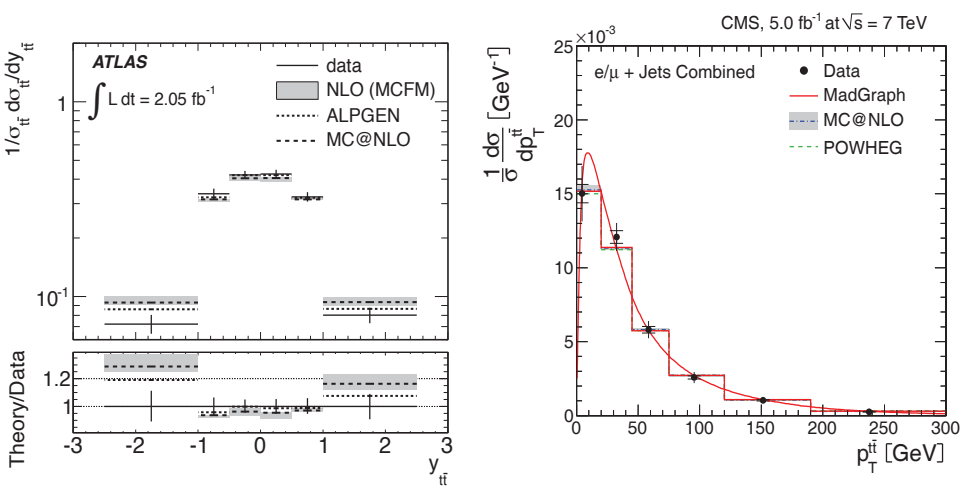

Fig. 7. Left: ATLAS relative differential cross-section versus rapidity $y_{t\bar{t}}$ compared to the NLO prediction from MCFM. Right: CMS normalized differential $t\bar{t}$ production cross-section in the lepton + jets channels as a function of the p_T^{tt}.

4.5. *Top quark mass measurements*

The top quark mass is the most precisely measured mass in the quark sector. The goal of Tevatron was to measure top mass with an uncertainty of up to 2 GeV. Today, a single analysis at Tevatron has achieved precision of 1.3 GeV and the combined measurement of top quark mass by the DØ and CDF collaboration is below 1 GeV, corresponding to 0.5% uncertainty. A number of methods have been developed over the years by all collaborations to measure top quark mass as precisely as possible.

The top quark mass is measured directly using the final state decay products, and indirectly by comparing the measured cross-section for top quark production with theoretical predictions. Both of these measurements are discussed below.

4.5.1. *Direct measurements of the top quark mass*

The top quark mass has been measured in all general topologies by CDF[176,177,231–251] and DØ[187,252–262] experiments at the Tevatron, and ATLAS[263] and CMS[264–266] experiments at the LHC.

Figure 8 shows the most recent combination of CDF and DØ top quark mass measurements.[267] This combination is an update from Ref. 268 and combines 12 statistically independent or uncorrelated measurements, including measurements from Run I done using about 100 pb^{-1} integrated luminosity collected at CM energy

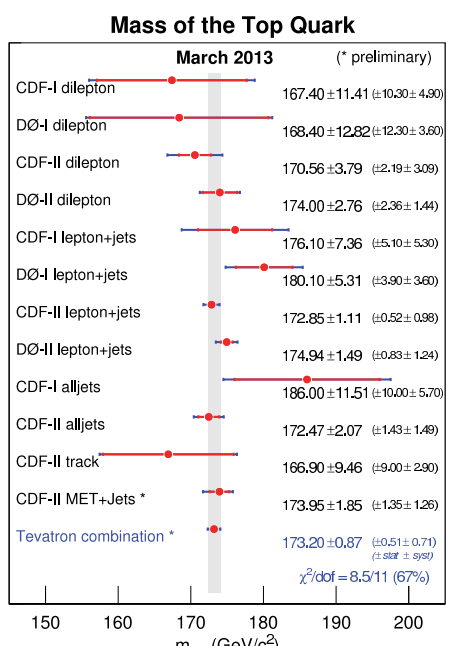

Fig. 8. Summary of measurements of m_t performed at the Tevatron.

of 1.8 TeV during period from 1992 to 1996.[233,257] The Run II measurements are done using up to 8.7 fb^{-1} integrated luminosity collected at CM energy 1.96 TeV by CDF[231,235,237,239,241,246,248,249] and up to 5.4 fb^{-1} collected by DØ[253,256,258,260] experiment.

The Run I measurements were mainly counting experiments, whereas in Run II both collaborations have used a number of different analysis techniques to increase the sensitivity. The Run I measurements all have relatively large statistical uncertainties and their systematic uncertainties are dominated by the total JES uncertainty. In Run II, both CDF and DØ take advantage of the larger $t\bar{t}$ samples available and employ new analysis techniques to reduce both of these uncertainties. In particular, jets from the W boson are used to recalibrate the JES through an *in situ* jet calibration. This calibration is possible because for true $t\bar{t}$ events, the invariant mass of the two jets from the W boson can be constrained to the world average value of M_W and the result is used to adjust the energy scale of jets. This procedure reduces the impact of the uncertainty on the absolute JES in the measurement of m_t. The Run II DØ analysis in the lepton + jets channel and the Run II CDF analyses in the lepton + jets, alljets and $\not\!\!E_T$ channels use jets from the W boson to recalibrate the JES through this *in situ* jet calibration. Run II DØ dilepton measurement uses the JES determined in the lepton + jets channel by *in situ* calibration. These analysis method also rely on the calibration of the measured m_t through MC pseudo-experiments to correct for simplifications and assumptions of each method.

Taking correlations of uncertainties into account, the resulting measured mass of the top quark at Tevatron is

$$m_t = 173.20 \pm 0.51\ (\text{stat.}) \pm 0.71\ (\text{syst.})\ \text{GeV} \quad (\text{Ref. } 267)\,,$$

corresponding to a relative precision of 0.50%.

The ATLAS experiment performs this measurement in the lepton+jets channel with 1 fb^{-1} integrated luminosity and measures top mass to be

$$m_{\text{top}} = 174.5 \pm 0.6\ (\text{stat.}) \pm 2.3\ (\text{syst.})\ \text{GeV} \quad (\text{Ref. } 263)\,.$$

And measurement by CMS using 5 fb^{-1} integrated luminosity in the same channel results in a value:

$$m_{\text{top}} = 173.5 \pm 0.4\ (\text{stat.} + \text{JES}) \pm 1.0\ (\text{syst.})\ \text{GeV} \quad (\text{Ref. } 264)\,.$$

CMS also measures top quark mass in the dilepton channel using 5 fb^{-1} integrated luminosity[265] to be

$$m_{\text{top}} = 172.5 \pm 0.4\ (\text{stat.}) \pm 1.5\ (\text{syst.})\ \text{GeV}\,.$$

CMS recently also performed a simultaneous measurement of the top quark, W boson and neutrino masses[266] using endpoints of kinematic variables. This sort of technique can be used to measure masses of new, unknown particles. By measuring mass of a known particle, this analysis provides not only a test of the method but also measures top quark mass with minimal MC input compared to more

traditional methods. When the neutrino and W boson masses are constrained to 0 and 80.4 GeV (world-average), respectively, a top quark mass value of

$$m_{\text{top}} = 173.9 \pm 0.9 \text{ (stat.)}^{+1.7}_{-2.1} \text{ (syst.) GeV}$$

is obtained.

4.5.2. *Indirect measurement of mass from the measured cross-section*

Interpretation of measured mass in terms of theoretical conventions is important when using this input in higher-order QCD calculations or in the fits of EW precision observables and the resulting indirect Higgs boson mass bounds.[22] Since the top quark mass measurement has entered into precision era, one question comes up frequently — which mass this value corresponds to? For example, is it the pole mass m_t^{pole} or the MSbar $m_t^{\overline{\text{MS}}}$ mass?

In a direct measurement of top quark mass, either kinematic quantities measured in data are compared with MC templates for different assumed values of top quark mass or the top quark mass is measured using distributions of kinematic quantities in data and the method of extraction of top mass is calibrated using MC simulation. Thus, either way, the mass is measured with respect to a quantity defined as top quark mass in the MC generator. While the MC top quark mass, m_t^{MC}, is considered to be pole mass, the MC simulations used for top quark mass at hadron colliders use LO QCD calculations and higher-order effects are simulated through parton showering at leading logarithms (LL) level, introducing an ambiguity in the definition of the pole mass of $\mathcal{O}(\Lambda_{\text{QCD}})$.[269–273] Given this ambiguity, it is hard to determine how close the measured top quark mass is to the pole mass.

The method mostly free of these ambiguities is based on extracting m_t by comparing the observed $t\bar{t}$ cross-section with theoretical predictions. Determining the mass from the cross-section is less precise than using the direct methods of measuring top quark mass, but it provides m_t in a well defined renormalization scheme.

DØ and CMS experiments have performed comparison of $t\bar{t}$ production cross-section with different higher-order perturbative QCD calculations.[185,274,275] DØ has performed extraction of m_t^{pole} and $m_t^{\overline{\text{MS}}}$ mass using 5.3 fb^{-1} integrated luminosity.[274] The direct measurement of the top quark mass are found to be consistent with measured m_t^{pole} mass within 2 SD, and different from $m_t^{\overline{\text{MS}}}$ mass by more than 2 SD. This is the first such extraction of top quark $m_t^{\overline{\text{MS}}}$ mass. This result is in accordance with theoretical arguments that m_t^{MC} should be close to the pole mass.[276]

CMS uses same method as used by the DØ experiment to measure top quark pole mass using 2.3 fb^{-1} integrated luminosity at 7 TeV. The measured value of pole mass is found to be $176.7^{+3.8}_{-3.4}$ GeV by comparing the measured cross-section for inclusive $t\bar{t}$ production to QCD calculations at NNLO + NNLL. CMS also performs the first determination at hadron collider of $\alpha_S(M_Z)$ at full NNLO QCD using m_t^{pole} to the value 173.2 ± 1.4 GeV. Figure 9 shows comparison CMS measurement

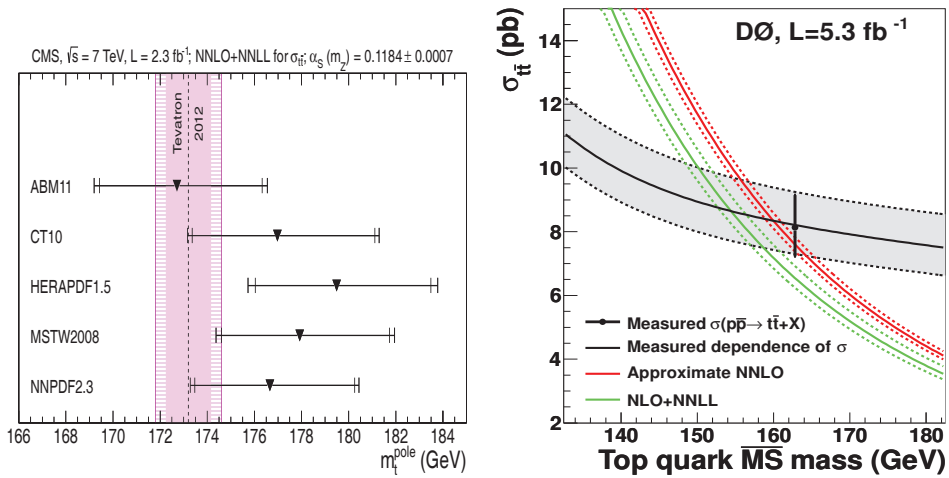

Fig. 9. Left: CMS measurement of $m_t^{\rm pole}$ from the measured $\sigma_{t\bar{t}}$ together with the prediction at NNLO+NNLL using different NNLO PDF sets. The inner error bars include the uncertainties on the measured cross-section and on the LHC beam energy as well as the PDF and scale uncertainties on the predicted cross-section. The outer error bars correspond to the uncertainty on the $\alpha_S(m_Z)$ world average. The vertical band shows the latest the direct top mass measurements. Here the inner (solid) area corresponds to the original uncertainty of the direct m_t average, while the outer (hatched) area additionally accounts for the possible difference between this mass and $m_t^{\rm pole}$.[275] Right: DØ measured $\sigma_{t\bar{t}}$ and theoretical NLO+NNLL and approximate NNLO calculations of $t\bar{t}$ cross-section as a function of $m_t^{\overline{\rm MS}}$, assuming that $m_t^{\rm MC} = m_t^{\rm pole}$.[274]

of $m_t^{\rm pole}$ from the measured $\sigma_{t\bar{t}}$ along with the prediction at NNLO + NNLL using different NNLO PDF sets (left), and DØ measured $\sigma_{t\bar{t}}$ and theoretical NLO+NNLL and approximate NNLO calculations of $t\bar{t}$ cross-section as a function of $m_t^{\overline{\rm MS}}$.

4.6. *Mass difference between top and antitop quark*

The fact that top quark decays before it can hadronize makes it the only place where the mass of a quark can be directly measured. If such a difference exists and is measured, it would be an indication of violation of the CPT symmetry. Both Tevatron and LHC experiments have measured top–antitop quark mass difference.[277–281] The most recent measurements are listed in Table 4. So far, all measurements are in good agreement with the SM expectation of no top–antitop quark mass difference.

Table 4. The top–antitop quark difference measurements from Tevatron and LHC experiments.

Exp., Lumi	$\Delta m_{\rm top} = m_t - m_{\bar{t}}$
CDF, 8.7 fb^{-1}	-1.95 ± 1.11 (stat.) ± 0.59 (syst.) (Ref. 277)
DØ, 3.6 fb^{-1}	0.8 ± 1.8 (stat.) ± 0.5 (syst.) GeV (Ref. 279)
CMS, 5 fb^{-1}	-0.44 ± 0.46 (stat.) ± 0.27 (syst.) GeV (Ref. 281)

4.7. *Charge of the top quark*

Within SM, the charge of the top quark is $+2/3e$, but this value can differ from the expectation. For example it can be $-4/3e$ in some exotic models.[282] The charge of the top quark can be inferred from charges of its decay products or in associated production of top quarks in channels which are sensitive to top quark charge.[283] Measurements at Tevatron and LHC both have excluded the presence of a top quark with exotic charge of $-4/3e$ at the 95% CL.[284–288]

4.8. *$t\bar{t}$ spin correlation*

Since the top quark decays before hadronization, the spin information is passed on to its decay products.[105] In SM top quarks are expected to be produced unpolarized at the lowest-order but in the $t\bar{t}$ pair production, the spin of two quarks is expected to be correlated. The spin information may be extracted from angular correlations between the top and antitop quark decay products, allowing tests of SM and new physics beyond SM.[134,289–305] Owing to the fact that the dominant production modes are different between Tevatron and LHC, spin correlation measurements at these colliders provide complementary information.

CDF and DØ experiments at Tevatron have measured these correlations in lepton + jets and dilepton channels with integrated luminosity of up to 5.4 fb^{-1}.[306–309] The most recent combination of DØ spin correlation measurements provides a 3.1 SD evidence for spin correlation using 5.3 fb^{-1} dataset.[307]

At the LHC, ATLAS also analyzed $t\bar{t}$ spin correlation using 2.1 fb^{-1} integrated luminosity in dilepton channel and provides a conclusive observation of spin correlation in $t\bar{t}$ events produced in pp collisions.[310] The difference in azimuthal angle between the two charged leptons in the laboratory frame is used to extract the correlation between the top and antitop quark spins. In the helicity basis the measured degree of correlation corresponds to $0.40^{+0.09}_{-0.08}$, in agreement with the NLO SM prediction. The hypothesis of zero spin correlation is excluded at 5.1 SD.

Figure 10 shows distributions in data compared with simulated $t\bar{t}$ samples with correlation as predicted by the SM and the case of no spin correlation, as predicted by the SM, for ATLAS and DØ experiments.

4.9. *Charge asymmetry in $t\bar{t}$ production*

The top quark pair production at the Tevatron $p\bar{p}$ collider proceeds mainly through $q\bar{q} \to t\bar{t}$, and at the pp LHC through $gg \to t\bar{t}$. Both of these production modes are charge conjugation symmetric at the lowest-order. However, at higher-orders this remains no longer true.[136,312–323] It turns out that processes involving initial state valence quarks exhibit a forward–backward asymmetry with respect to the incoming proton and antiproton beams. Thus, $p\bar{p}$ collisions at Tevatron provide a unique opportunity to test SM predictions as well as many new physics models that predict deviations from SM expectations.[324–336]

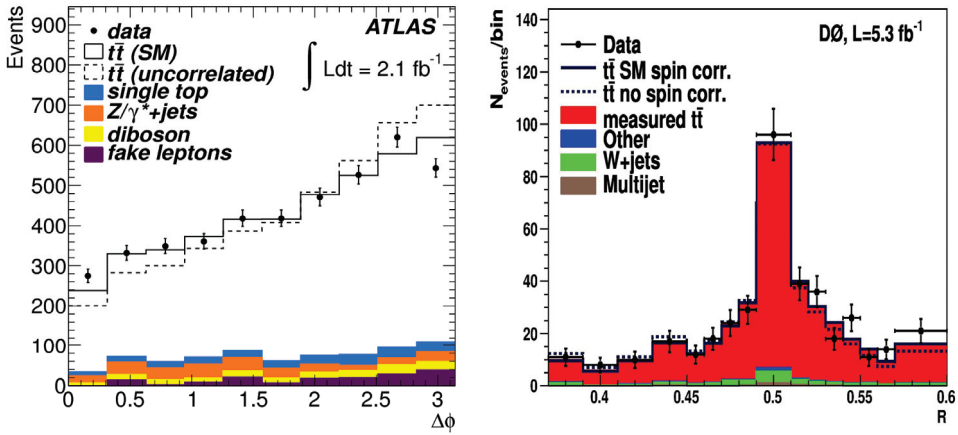

Fig. 10. Distributions in data compared with simulated $t\bar{t}$ samples with correlation as predicted by the SM and the case of no spin correlation. Left: ATLAS reconstructed charged lepton $\Delta\phi$ distribution for the dilepton channel. Right: DØ distribution of the discriminant R for lepton+jets events. The first and last bins include contributions from $R < 0.37$ and $R > 0.60$, respectively.

In case of Tevatron, the charge asymmetry is manifested as a difference in the rapidities between the top quark and antitop quark,

$$\Delta y = y_t - y_{\bar{t}}\,.$$

This difference is invariant under boosts along the beam axis. The corresponding forward–backward asymmetry in the $t\bar{t}$ rest frame is then defined as,

$$A_{\mathrm{FB}} = \frac{N_{\mathrm{F}} - N_{\mathrm{B}}}{N_{\mathrm{F}} + N_{\mathrm{B}}}\,,$$

where N_{F} is the number of "forward" events with $\Delta y > 0$ and N_{B} is the number of "backward" events with $\Delta y < 0$.

Being proton–proton collider, there is no forward–backward asymmetry at the LHC, since the initial state is symmetric. However, due to the proton density functions (PDF), the incoming quarks have on average more momentum compared with the antiquarks, which means that the charge asymmetry results in a rapidity distribution of top quarks that is slightly broader than that of top antiquarks. That is, at large rapidities, more top quarks than antiquarks are produced, while in the central region, more top antiquarks than quarks are produced. At LHC, the charge asymmetry A_C measured by the CMS Collaboration is the relative difference between events with $|\eta_t| > |\eta_{\bar{t}}|$ and $|\eta_t| < |\eta_{\bar{t}}|$, with $\eta_t(\eta_{\bar{t}})$ being the pseudorapidity of the top (anti)quark, and $\eta = \ln(\tan\theta/2)$, in the laboratory frame.

These measurements are done at the detector level where selection and reconstruction has been done. These quantities are also defined at the generator or parton level, where they are corrected for detector effects and are directly comparable to the QCD calculations.

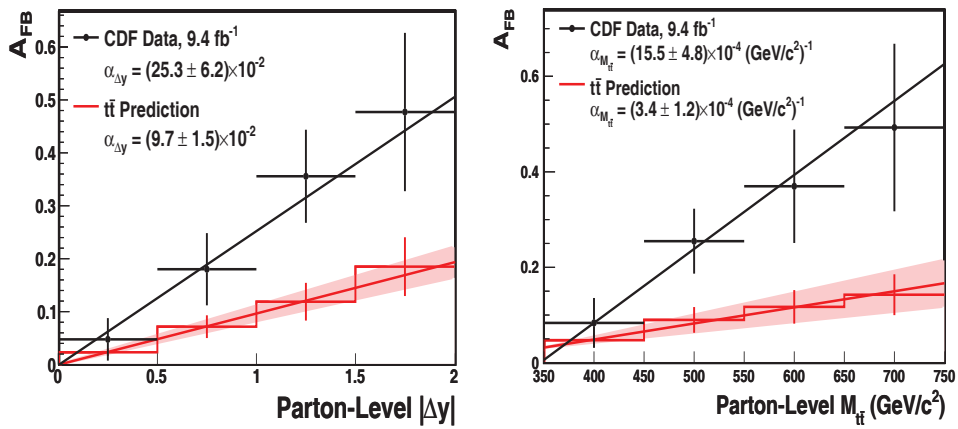

Fig. 11. CDF charge asymmetry measurements compared with theoretical predictions. Left: The parton-level forward–backward asymmetry as a function of $|\Delta y|$ with a best-fit line superimposed. Right: the parton-level forward–backward asymmetry as a function of $M_{t\bar{t}}$ with a best-fit line superimposed.

Recently, a charge asymmetry in $t\bar{t}$ events was reported by Tevatron experiments and since then Tevatron and LHC experiments have measured this property in various distributions.[337–344] DØ and CDF experiments measure forward–backward asymmetry $A_{\rm FB}$ and explore the dependence of asymmetry in terms of Δy and invariant mass of the top–antitop quark system. CDF, using an integrated luminosity of 9.4 fb^{-1}, measures the inclusive asymmetry at the parton-level to be

$$A_{\rm FB} = (16.4 \pm 4.7)\% \quad \text{(Ref. 337)}$$

which is compared to NLO prediction from POWHEG,[213] and found to be different by about 2 SD. CDF also observes a linear dependence of $A_{\rm FB}$ on the top quark pair mass $M_{t\bar{t}}$ and the rapidity difference $|\Delta y|$ at detector and parton levels. At the parton level, these dependencies exceed expected dependence by more than 2 SD. Figure 11 shows CDF parton-level forward–backward asymmetry as a function of $|\Delta y|$ and as a function of $M_{t\bar{t}}$ with a best-fit line superimposed.

DØ performs a similar analysis and finds

$$A_{\rm FB} = (19.6 \pm 6.5)\% \quad \text{(Ref. 340)}\,,$$

compared to $(5.0 \pm 0.1)\%$, predicted by MC event generator MC@NLO.[214] This value disagrees with expectations by up to 3 SD.

Instead of full reconstruction of top and antitop quark in the event, an alternative approach is to measure asymmetry based on the rapidity of the lepton in the top quark decay, which avoids the additional difficulties in accounting for migrations and reconstructing the top quark. In the most recent measurement from DØ, no excess in asymmetry compared to SM predictions was observed in the dilepton channel.[339] This measurement of leptonic asymmetry in the dilepton channel is combined with the similar measurement in the lepton + jets channel[340] The final

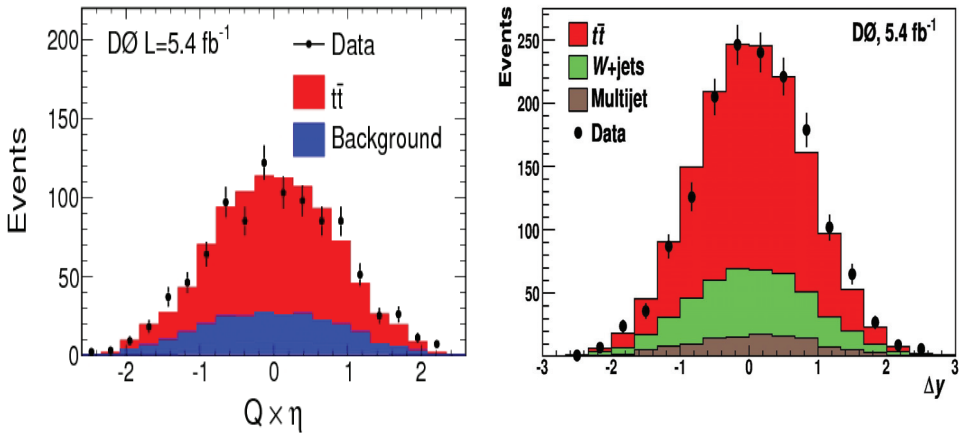

Fig. 12. DØ charge asymmetry measurements Left: Pseudorapidity × charge distribution for the charged leptons;[339] Right: The reconstructed Δy. Bin widths correspond to about half the detector resolution in Δy.[340]

asymmetry at the parton level is found to be

$$A_{\rm FB}^{l} = (11.8 \pm 3.2)\% \quad \text{(Ref. 339)}$$

which is predicted to be $A_{\rm FB}^{l} = (4.7 \pm 0.1)\%$, including higher-order QCD + EW corrections. The observed asymmetry in this case is measured to be 2.2 SD above the predicted value.

DØ does not report any statistically significant enhancement of $A_{\rm FB}$ dependence on the invariant mass of the $t\bar{t}$ system ($m_{t\bar{t}}$) or on rapidity difference $|\Delta y|$. Figure 12 shows DØ pseudorapidity × lepton charge distribution[339] and the rapidity difference Δy.[340]

ATLAS has measured charge asymmetry in single lepton + jets channel, using 1.04 fb^{-1} integrated luminosity at the CM energy 7 TeV.[342] Both $|\Delta y|$ and $m_{t\bar{t}}$ distributions are analyzed. The measured asymmetry is compatible with theoretical prediction from the MC@NLO MC generator, at parton level

$$A_C = -0.109 \pm 0.028\ (\text{stat.}) \pm 0.024\ (\text{syst.})\,,$$

compared to MC@NLO MC generator of $A_C = 0.006 \pm 0.0025$. Figure 13 shows the unfolded $\delta|y|$ distribution and unfolded asymmetries in two regions of $m_{t\bar{t}}$ compared to the prediction from MC@NLO.

CMS uses 5.0 fb^{-1} integrated luminosity collected at 7 TeV to measure charge asymmetry in single lepton+jets events in the $t\bar{t}$ sample. The inclusive measurement yields

$$A_C = 0.004 \pm 0.010\ (\text{stat.}) \pm 0.011\ (\text{syst.})\,,$$

compared to theoretical prediction (SM) $A_C = 0.0115 \pm 0.0006$.[321] CMS also measures $t\bar{t}$ charge asymmetry as a function of rapidity, transverse momentum and

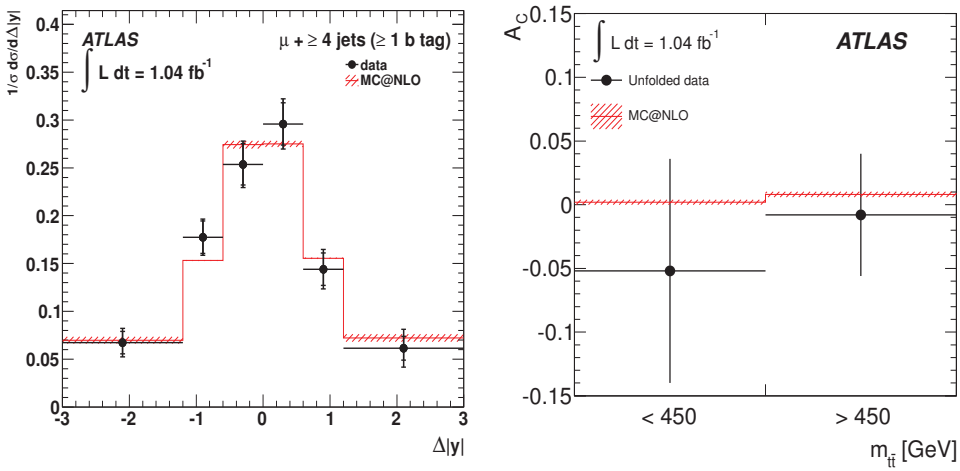

Fig. 13. ATLAS charge asymmetry measurement. Left: The unfolded $\Delta|y|$ distribution for the muon channel compared to the prediction from MC@NLO. The inner (outer) part of the error bars corresponds to the statistical (systematic) uncertainty. Right: unfolded asymmetries in two regions of $m_{t\,\bar{t}}$ compared to the prediction from MC@NLO.

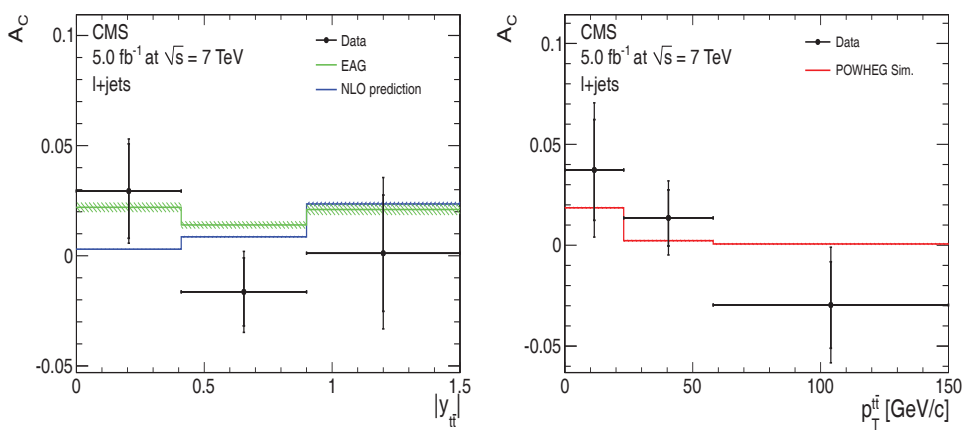

Fig. 14. Left: corrected asymmetry as a function of $|y_{t\bar{t}}|$ (right) and $p_T^{t\bar{t}}$ (left). The measured values are compared to NLO calculations.[321] and to the predictions of a model featuring an effective axial-vector coupling of the gluon (EAG).[332] The error bars on the differential asymmetry values indicate the statistical and total uncertainties, determined by adding statistical and systematic uncertainties in quadrature. The shaded areas indicate the theoretical uncertainties on the NLO calculations.

invariant mass of the $t\bar{t}$ system. Figure 14 shows corrected asymmetry as a function of $|y_{t\bar{t}}|$ and $p_T^{t\bar{t}}$ compared to NLO calculations.[321]

Within current uncertainties, the LHC data do not show any significant asymmetry and all measured values are consistent with a null asymmetry as well as with the SM predictions. Given the results and precision of measurements at LHC and Tevatron, more studies, with larger datasets are needed before any conclusion is reached.

4.10. *Width of top quark*

In the SM, decay width of the top quark, Γ_t, can be calculated given the top quark mass m_t. For $m_t = 172.5$ GeV, the top quark width is expected to be $\Gamma_t = 1.33$ GeV at NLO.[104] The value of Γ_t can be affected by the presence of new physics, but, given that the mass resolution of the reconstructed top quark at the current hadron colliders is much larger compared to Γ_t, determining this property directly is very challenging.

The CDF experiment has performed such direct searches[345,346] by comparing reconstructed top quark mass for each event with templates of different top quark widths (Γ_t). Using 4.3 fb^{-1} of integrated luminosity, CDF establishes an upper limit at 95% confidence level (CL) of $\Gamma_t < 7.6$ GeV and a two-sided 68% CL interval of 0.3 GeV $< \Gamma_t <$ 4.4 GeV for a top quark mass of 172.5 GeV.

The DØ experiment employs an indirect method[347,348] and extracts Γ_t from its partial width $\Gamma(t \to Wb)$, which is determined from the t-channel of the single top quark production cross-section. This coupled with the top quark branching fraction $B(t \to Wb)$ measured using the ratio $R = B(t \to Wb)/B(t \to Wq)$,[210] and the assumption that $\Gamma_t = \Gamma(t \to Wb)/B(t \to Wb)$, (namely that $B(t \to Wq) = 1$) and that the Wtb coupling is the same in the production and decay of the top quark, provides a measure of Γ_t. Using the above inputs from analyses using 5.4 fb^{-1} of data, DØ obtains $\Gamma_t = 2.00^{+0.47}_{-0.43}$ GeV for $m_t = 172.5$ GeV,[347] in agreement with the SM. This translates to a top quark lifetime of $\tau_t = \left(3.29^{+0.90}_{-0.63}\right) \times 10^{-25}$ s. In the same analysis, a direct limit is also obtained on the CKM matrix element $0.81 < |V_{tb}| \leq 1$ at 95% CL.

So far all measurements of top quark width are in agreement with SM expectations.

4.11. *The Wtb coupling and W polarization*

The polarization of the W bosons produced in top quark decays can be either longitudinal, left-handed or right-handed (helicity 0, helicities -1 and $+1$, respectively). In the SM, for $m_t = 172.5$ GeV, W helicity is expected to have left-handed component of $f_- = 0.303$ and a longitudinal component of $f_0 = 0.696$.[349–358] The production of right-handed W bosons is strongly suppressed.

In an effective field theory approach, the most general Wtb vertex involving terms up to dimension five can be written as[359]

$$\begin{aligned}\mathcal{L}_{Wtb} = &-\frac{g}{\sqrt{2}}\bar{b}\gamma^{\mu}\left(V_L P_L + V_R P_R\right)tW^-_{\mu} \\ &- \frac{g}{\sqrt{2}}\bar{b}\frac{i\sigma^{\mu\nu}q_{\nu}}{M_W}\left(g_L P_L + g_R P_R\right)tW^-_{\mu} + \text{h.c.}\,, \end{aligned} \tag{2}$$

where V_R, g_L and g_R are anomalous left- and right-handed couplings, and are absent in SM at tree level. The left-handed coupling $V_L = V_{tb} = 1$ within SM. In the presence of such anomalous Wtb couplings, the angular correlations of the top

quark decay products are also modified. This can, for example, change the single top quark production cross-section. Thus, measurement of helicity fractions can be used to set limits on anomalous couplings and vice versa. Direct limits on these couplings can be obtained from single top production cross-section measurements which proceeds through EW interaction and can be combined to further constrain the measurements of helicity fractions.[349,350,352,354,355]

The CDF[360–362] and DØ[363,364] experiments have measured W boson polarization in $t\bar{t}$ decays. The Tevatron combination of their individual measurements[365] is based on 2.7–5.4 fb^{-1} integrated luminosity dataset. The simultaneous determination of longitudinal (f_0) and right-handed (f_+) helicities results in

$$f_0 = 0.722 \pm 0.062\ (\text{stat.}) \pm 0.052\ (\text{syst.})\,,$$
$$f_+ = -0.033 \pm 0.034\ (\text{stat.}) \pm 0.031\ (\text{syst.})\,.$$

Assuming left-handed helicity fractions is fixed to the value expected in the SM,

$$f_0 = 0.682 \pm 0.035\ (\text{stat.}) \pm 0.046\ (\text{syst.})\,,$$
$$f_+ = -0.015 \pm 0.018\ (\text{stat.}) \pm 0.030\ (\text{syst.})\,.$$

DØ has placed limits on anomalous right-handed vector and right- and left-handed tensor couplings in single top quark production using data up to 5.4 fb^{-1}.[366–369] DØ has also performed a combination of these results from single top with W helicity fraction measurement[366] in $t\bar{t}$ decays using the general framework described in Ref. 350.

ATLAS[370] and CMS also combine their measurements[371] of the W boson polarization in top quark decays. The measurements are based on integrated luminosities of up to 2.2 fb^{-1} collected at 7 TeV and result in longitudinal (F_0) and left-handed (F_L) fractions,

$$F_0 = 0.626 \pm 0.034\ (\text{stat.}) \pm 0.048\ (\text{syst.})\,,$$
$$F_L = 0.359 \pm 0.021\ (\text{stat.}) \pm 0.028\ (\text{syst.})\,.$$

The fraction of W bosons with right-handed polarization (F_R) is calculated assuming the sum of all fractions to be unity and is found to be

$$F_R = 0.015 \pm 0.034\,.$$

Exclusion limits on anomalous Wtb couplings are derived from these results as well.

Figure 15 shows combined 2D helicity measurements of left-handed versus longitudinal helicity fractions (F_L versus F_0) for LHC and right-handed versus longitudinal helicity fractions (f_+ versus f_0) for Tevatron. Also shown are the helicity fractions predicted by NNLO QCD calculations. So far all measurements are consistent with one another as well as with SM predictions.

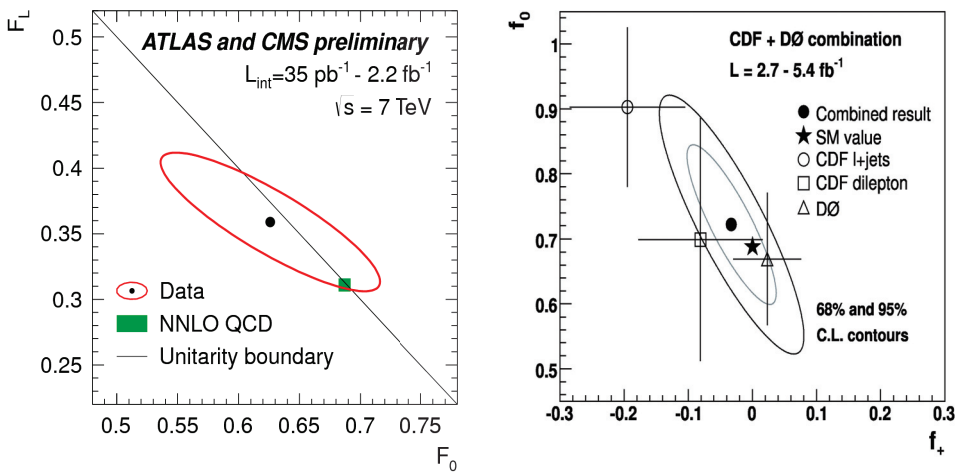

Fig. 15. Left: LHC combined values of F_L and F_0 as well as the 68% CL interval. Also shown are the helicity fractions predicted by NNLO QCD calculations. The black line indicates the boundary of the unitarity constraint that the helicity fractions sum up to unity. Right: CDF and DØ combined contours of 68% and 95% CL for the 2D helicity measurements. Error bars on the input measurements correspond to 1 SD uncertainty on f_0 and f_+.

4.12. *Study of color flow*

Color charge is a conserved quantity in QCD and two final-state particles on the same line of color flow are termed to be color-connected to each other. DØ performed the first study of color flow in terms of the color representation of the hadronically decaying W boson in $t\bar{t}$ events, using 5.3 fb^{-1} of integrated luminosity. This study is performed using a vectorial variable called "jet pull,"[372] which is based on the measurement of the pattern of jet energy distributed in the η–ϕ plane in the calorimeter, and measures the color flow between a pair of jets. This variable sensitive to the color-flow structure of the final state and is used to distinguish color-octet from color-singlet states. DØ measures the fraction of uncolored W bosons to be 0.56 ± 0.42 (stat. + syst.), in agreement with SM expectation.[373]

4.13. *Electroweak production of single top quarks*

As discussed in Subsec. 4.2, apart from top quark pair production through strong force, SM also predicts production of a single top quark through EW force. All three modes of production of single top quark are important and under constant investigation because of their complementary sensitivity to the effects of new physics in the Wtb vertex (see, e.g. Refs. 154, 374–376). Also, the cross-section is proportional to the CKM matrix element $|V_{tb}|$,[377,378] making it the only place where this matrix element can be measured directly, without any assumptions. Single top quarks are produced 100% polarized and this polarization can be observed in angular distributions of their decay products. Although the predicted cross-section for this production mode is only about half that of the top pair production, for the low jet

multiplicity final state, the background contribution from W + jets production is overwhelming. This remains true even after the identification of b-jets in the event. Given this challenging situation, use of MVA techniques has proved to be invaluable in search for single top quark production. It was largely due to the techniques used by CDF and DØ that made the initial evidence,[382,389,390] and observation[379–381] of single top production possible in 2007 and 2009, respectively.

Experiments at Tevatron and LHC have measured production cross-section for single top using different analysis techniques.[379–396] The most recent $s+t$-channel production cross-section at the Tevatron has been performed by CDF using 3.2 fb^{-1} and by DØ using 9.7 fb^{-1} integrated luminosity collected at CM energy 1.96 TeV:

$$\sigma_{p\bar{p}}(s+t) = 2.3^{+0.6}_{-0.5} \text{ pb} \quad (\text{CDF}^{379,382}),$$
$$\sigma_{p\bar{p}}(s+t) = 4.11^{+0.60}_{-0.55} \text{ pb} \quad (\text{DØ}^{383}).$$

The t-channel production of single top has the largest cross-section among the three production modes at the Tevatron as well as at the LHC and has been observed at both colliders.[385,392,394] The measured cross-section in pp and $p\bar{p}$ collisions is found to be consistent with SM predictions at CM 1.96 TeV and 7 TeV, respectively:

$$\sigma_{p\bar{p}}(t\text{-channel}) = 3.07^{+0.54}_{-0.49} \text{ (stat.} + \text{syst.) pb} \quad (\text{DØ},^{383}),$$
$$\sigma_{pp}(t\text{-channel}) = 83 \pm 4 \text{ (stat.)}^{20}_{-19} \text{ (syst.) pb} \quad (\text{ATLAS}^{392}),$$
$$\sigma_{pp}(t\text{-channel}) = 67.2 \pm 6.1 \text{ (stat.} + \text{syst.) pb} \quad (\text{CMS}^{394}).$$

The tW production mode has been observed at the LHC,[393,395] and no deviations from SM predictions have been reported:

$$\sigma_{pp}(tW) = 16.8 \pm 2.9 \text{ (stat.)} \pm 4.9 \text{ (syst.) pb} \quad (\text{ATLAS}^{393}),$$
$$\sigma_{pp}(tW) = 16^{5}_{4} \text{ (stat.} + \text{syst.) pb} \quad (\text{CMS}^{395}).$$

Recently, evidence for the most challenging mode, the s-channel production, has been reported by the DØ experiment and is found to be consistent with SM prediction within about 30% uncertainty:[383]

$$\sigma_{pp}(s\text{-channel}) = 1.10^{+0.33}_{-0.31} \text{ pb} \quad (\text{DØ}^{383}).$$

Figure 16 shows the Tevatron single top results for combined, t-channel cross-section and s-channel cross-section measurements.

All experiments also report direct measurement and lower bounds on the value of CKM matrix element $|V_{tb}|$. So far, no significant deviations from SM predictions have been observed.

5. Higgs Physics at Hadron Colliders

5.1. *Introduction*

Understanding the mechanism through which EW bosons and fermions acquire mass is at the heart of research program at hadron colliders. It is related to most

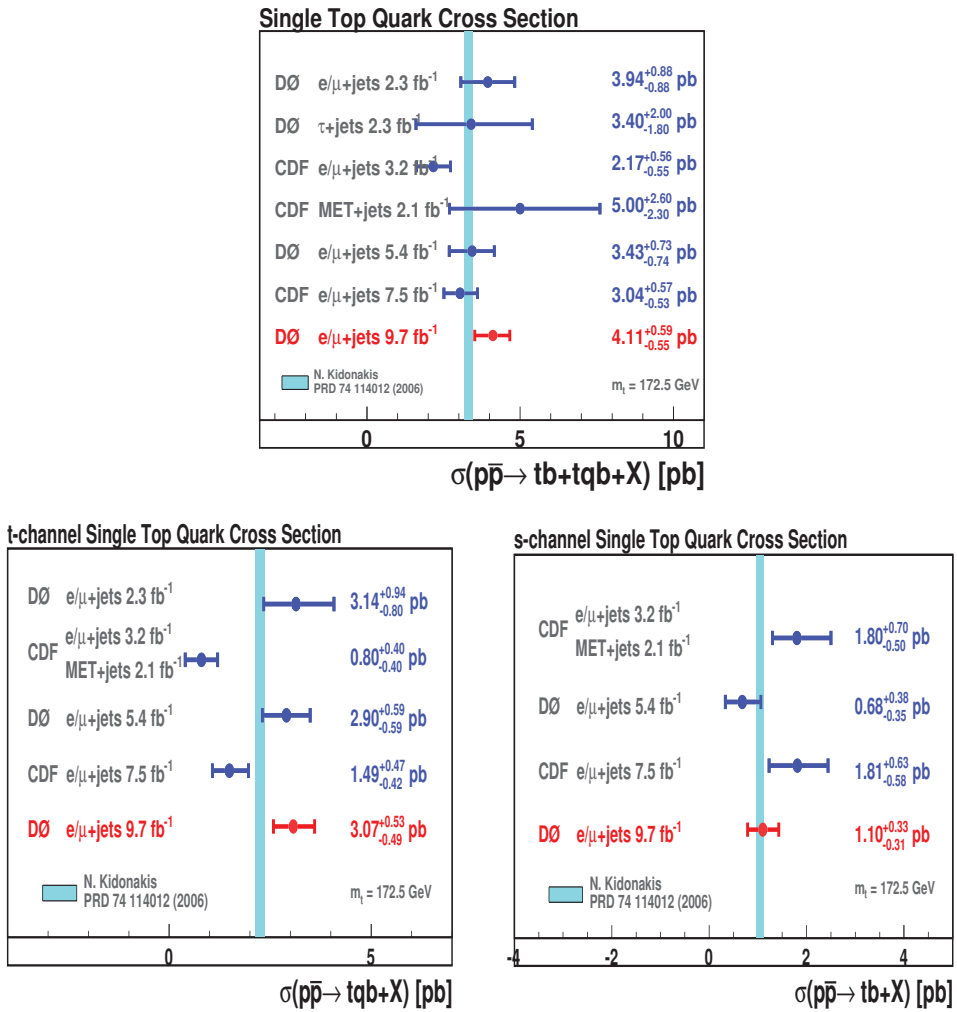

Fig. 16. Summary of single top measurements from Tevatron for combined cross-section (upper), t-channel cross-section (lower left) and s-channel cross-section (lower right) measurements.

of the major problems in particle physics today. Within SM, spontaneous breaking of EW symmetry gives mass to the W and Z bosons, imparting component of observed longitudinal polarization. In addition, fundamental fermions get their masses through Yukawa interactions with the Higgs field. In the SM, the symmetry breaking mechanism predicts the existence of a neutral scalar particle, the Higgs boson. Even though SM has been extraordinarily successful, and there are indirect indications of Higgs mechanism, for example, by the observed W/Z longitudinal polarization, the direct discovery of the Higgs boson and the EWSB mechanism is needed. This critical discovery was made in 2012, when a boson, very similar to Higgs boson predicted by SM was found. This section briefly describes the searches

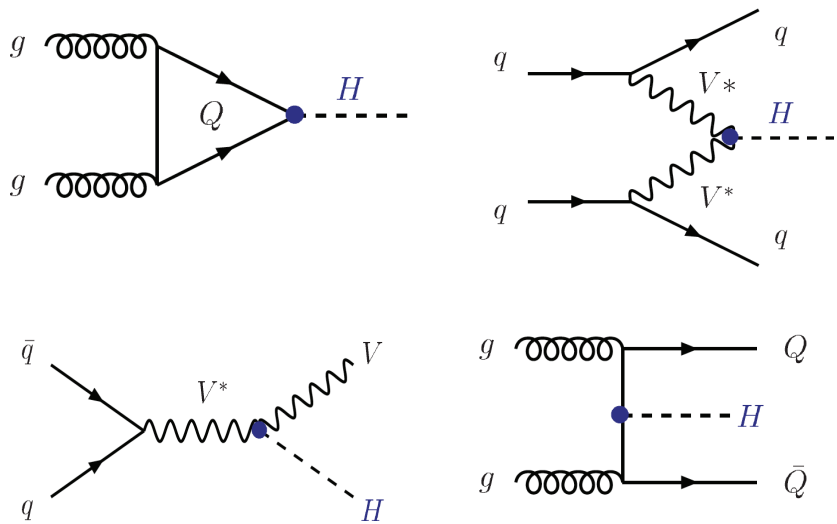

Fig. 17. Feynman diagrams for dominant Higgs boson production processes. Upper left: gluon–gluon fusion; upper right: vector boson fusion; lower left: Higgs-strahlung; lower right: Higgs boson produced in association with fermion pair.

that culminated into evidence and discovery of this particle at Tevatron and the LHC, respectively.

This section is arranged as follows. In Subsec. 5.2, Higgs boson production and decay at Tevatron and LHC is discussed. Direct and indirect constraints are discussed in Subsec. 5.3. Searches strategies at Tevatron (Subsec. 5.4) and LHC (Subsec. 5.5) are discussed next, followed by results from evidence and discovery of Higgs-like boson (Subsec. 5.6). Finally, some studies done at the Tevatron and LHC to verify the identity of this newly discovered particle are presented in Subsec. 5.7.

5.2. *Higgs boson production and decay at the hadron colliders*

The current hadron colliders have focused on the Higgs boson mass range 100 GeV $< M_H <$ 200 GeV, favored by the overall fit of the SM to precision data and the results of the direct searches. The most important Higgs production modes at the hadron colliders are gluon–gluon fusion, vector boson fusion (VBF), Higgs-strahlung, and associated production with top quark pairs. Some of the leading Higgs boson production Feynman diagrams are shown in Fig. 17. Figures 18 and 19 show the total cross-sections of the main production channels for Tevatron at $\sqrt{s} = 1.96$ TeV (Ref. 398) and for the LHC at $\sqrt{s} = 8$ TeV (Ref. 399), respectively. For the LHC at $\sqrt{s} = 7$ TeV, the Higgs production cross-section in gluon–gluon fusion process increases about 10-fold compared to Tevatron. LHC gains another 20%–30% in the Higgs boson production cross-sections for $M_H \sim$ 100–200 GeV from an increase in energy from 7 TeV to 8 TeV. The transition from 7 TeV to 14 TeV in energy increases the cross-sections by another factor of at least 3 or 4.

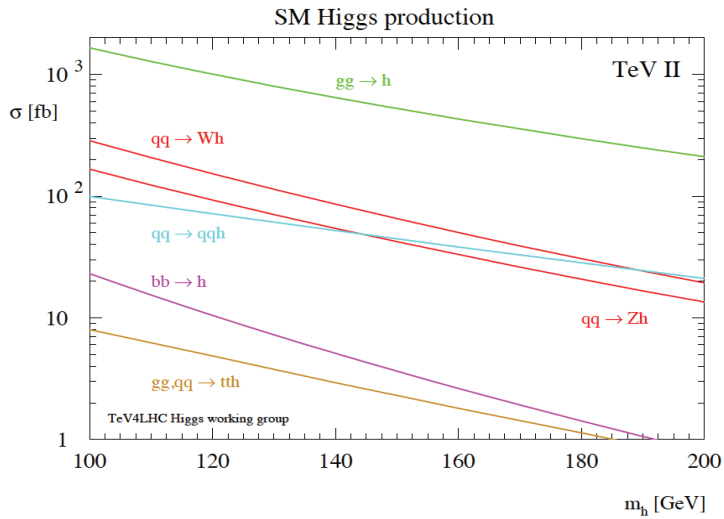

Fig. 18. Cross-sections for the various SM Higgs boson production channels at Tevatron (in fb) with a CM energy of 1.96 TeV, as predicted by the TeV4LHC Section Working Group.[398]

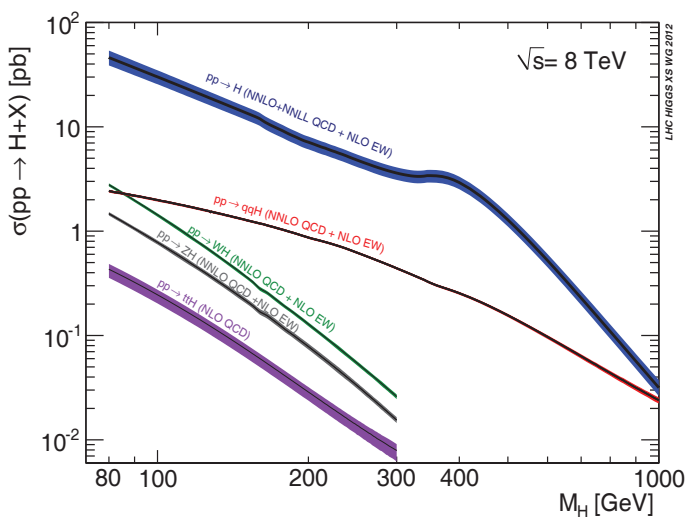

Fig. 19. Cross-sections and respective uncertainties, indicated by the band widths, for the various SM Higgs boson production channels at the LHC (in pb) with a CM energy of 8 TeV, as predicted by the LHC Higgs Cross Section Working Group.[399]

The $gg \to H$ production mode occurring through a top quark loop is the dominant production mode at hadron colliders. Cross-section for this channel is at least an order of magnitude larger than other production modes. Higgs-strahlung is one of the main search channel for Higgs bosons at Tevatron, but at the LHC this channel suffers from large background. In the case of VBF, Higgs boson is produced by

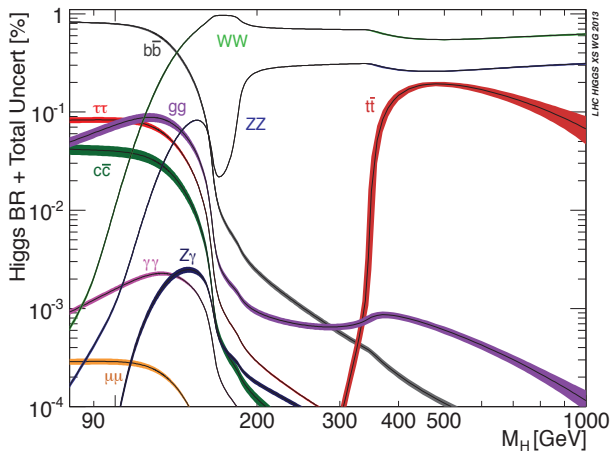

Fig. 20. The branching ratios of the SM Higgs boson as function of Higgs mass. Bands correspond to total uncertainties.[400,401]

fusion of vector bosons radiated by outgoing quarks that appear in the detector as two hard back-to-back jets, a signature that makes it easier to tag such events. Even though the cross-section from the Higgs boson production in association with $t\bar{t}$ pair is much smaller than other modes considered for the search, the motivation to study this process comes from the fact that it provides direct access to top Yukawa coupling.

Figure 20 shows branching ratios for the SM Higgs as function of Higgs mass.[400,401] The decay width of the Higgs boson extends from 10^{-4} GeV for $M_H \lesssim 10$ GeV to 10^3 GeV for $M_H \sim 1$ TeV.[399] For m_H in the low Higgs mass range 114–130 GeV, the width is below 5 MeV.[402] The dominant decay channel in the low mass range is $H \to b\bar{b}$.

Because of larger decay width, a heavy Higgs boson would show up as an extremely broad resonance, whose width becomes of the same size as its mass for $M_H \lesssim 1$ TeV.[399,400]

Theoretical calculations involving Higgs boson production and decay, and event simulation have received a big boost from the LHC (see, for example, Refs. 398–402). New powerful techniques for amplitude calculations and for the simulation of processes with complicated final states are being developed continuously.

The gluon–gluon fusion process through triangular heavy quark (dominantly top quark) loops, receives large QCD radiative corrections.[403,404] The NLO corrections in QCD have been calculated and turn out to be up to 100%. The NNLO corrections are known in the large top quark mass limit and add another 25%. Resummation of the soft-gluon contributions is known up to next-to-next-to-leading logarithm (NNLL) and add another few percentages. The EW corrections for this process are known up to two-loop level. They increase the cross-section by a factor that changes +5% for $M_H = 120$ GeV to about 2% for $M_H = 300$ GeV.[405–422]

For the VBF process, full QCD and EW calculations up to NLO and approximate NNLO QCD calculations are used to calculate the cross-section.[423–430] Cross-sections of the associated WH/ZH processes are calculated including QCD corrections up to NNLO and EW contributions up to NLO.[431–437] Finally, the cross-sections for the $t\bar{t}H$ process are calculated up to NLO QCD.[438–442]

The branching ratios of the SM Higgs boson as a function of the Higgs mass, as well as their uncertainties, are calculated using the PROPHECY4F[443,444] and HDECAY[445,446] programs. The uncertainty in the signal cross-section from the choice of PDFs is determined with the PDF4LHC prescription.[447–451]

For detailed discussion of predicted cross-sections, branching ratios and uncertainties, see Refs. 399 and 400.

5.3. *Constraints on the Higgs mass*

In SM, Higgs boson mass is a free parameter. However, there are some theoretical arguments about the low and high bounds on the Higgs mass. The upper boundary comes from the argument whether SM is viable theory up to high energies (Planck scale, $\Lambda_{\text{Planck}} = 2 \times 10^{18}$ GeV)[452,453] and lower bound comes from the need for the theory to be perturbative (i.e. calculable) up to large energies.[454–458]

Figure 21 illustrates these bounds on the SM Higgs boson mass.[459] For a Higgs boson within the mass window 130 GeV $\lesssim H \lesssim$ 170 GeV, the SM is expected to be consistent up to scales as high as the Planck scale, where effects of gravity are as large as the strong and EW interactions.

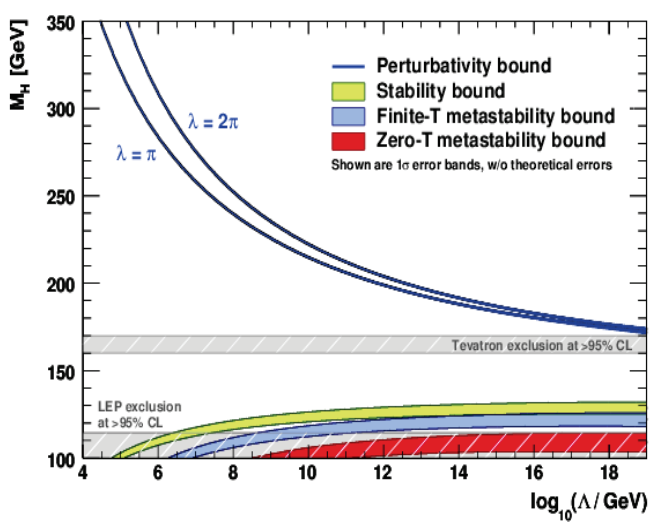

Fig. 21. Perturbativity (triviality) upper bound and vacuum-stability lower bound on M_H as function of the scale Λ at which new physics has to appear (at the latest) in order to avoid the bounds.[459] The two different versions of the perturbativity bound reflects the intrinsic uncertainty of the limit, and the bands of the (meta)stability bounds reflect parametric uncertainties.

On the experimental side, since 1980s, there have been direct and indirect experimental bounds on the Higgs mass as well. LEP1, LEP2, SLC and Tevatron have performed a large variety of high-precision measurements. These experiments provide direct and indirect constraints on the Higgs mass, along with the limits from EW precision fits to these measurements. Four experiments at LEP2 excluded the SM Higgs boson mass below 114.4 GeV with 95% CL.[460] Figure 1 shows the status of direct and indirect experimental constraints[22] as of March 2012. Here the blue band, includes both the experimental and the theoretical uncertainties. The precision EW measurements lead to $m - H = 94^{+29}_{-24}$ GeV or an upper bound of $m_H < 152$ GeV at 95% CL. Combined, LEP, Tevatron and LHC exclude most of the Higgs mass range shown in this plot, except for a small window around 130 GeV.

5.4. *Higgs boson searches at Tevatron*

At the Tevatron, searching for Higgs boson is about a decade long effort. First limits on SM Higgs boson production were placed with about 0.2 fb^{-1} data in 2003. In 2012, Tevatron announced the evidence of excess of events in Higgs boson searches.[461] Compared to the LHC, where experiments are more sensitive to $H \to \gamma\gamma/VV$, Tevatron's sensitivity primarily comes from $H \to b\bar{b}$. In this case, the fact that cross-section for Higgs boson production is much smaller than at the LHC, combined with limited jet energy resolution, has made Higgs search at the Tevatron a search for a broad excess rather than a bump hunt. This also signifies the use of MVA techniques in this search. Many of these techniques have been pioneered, refined and validated for high energy use in variety of measurements, in many different initial and final states at the Tevatron.

An overview of the production rates for most of the search channels considered at Tevatron is shown in Fig. 22. Searches in channels with leptons and missing transverse momentum prove to be more sensitive, even if the production cross-section

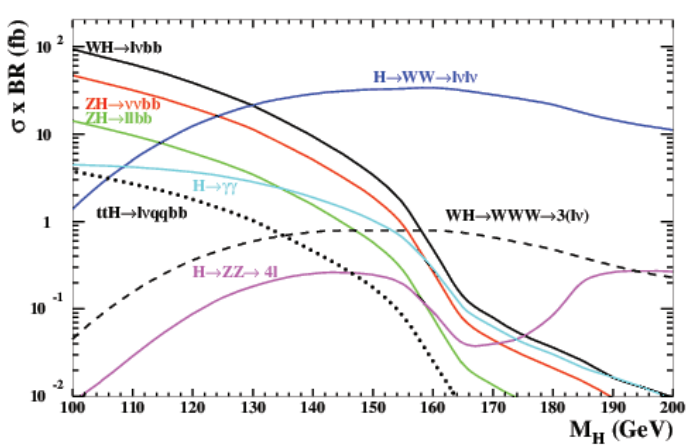

Fig. 22. Production cross-sections in the most sensitive search channels at the Tevatron.

is smaller in these channels. To increase sensitivity, both CDF and DØ experiments have put enormous effort into improving lepton reconstruction and selection efficiencies, invariant dijet mass resolution and b-jet tagging algorithms and use of MVA methods. Combining all possible channels that added even a little bit to the combined result also increased overall sensitivity. About 30 analyses have been included in the final Tevatron combination[462] for search of SM Higgs boson production in mass range 90–200 GeV. Production modes considered are gluon–gluon fusion, WH, ZH, $t\bar{t}H$ and VBF processes. The main categories that these analyses are divided into, depending on their topology, are $H \to b\bar{b}$,[463–472] $H \to W^+W^-$,[473–476] $H \to \tau^+\tau^-$,[477,478] $H \to \gamma^+\gamma^-$,[479,480] and $H \to ZZ$.[481]

The suppression of background processes, in particular from $W(Z)$+light-flavor production, depends crucially on the performance of the algorithm to identify the b-quark flavored jets from the Higgs boson decay. Significant improvements were achieved in this regard, which greatly enhanced the sensitivity. The mass of the Higgs boson candidate can be reconstructed from the invariant mass of the two jets assigned to the Higgs boson decay with a mass resolution of 10%–15%. This dijet mass is an important observable to discriminate the signal process from background processes, in particular from diboson production VZ with $Z \to b\bar{b}$. The correlations in the systematic uncertainties across channels and also across experiments were carefully taken into account in the cross-section measurement.

The combined background-subtracted dijet-mass distribution for the diboson analysis is shown in Fig. 23. Here, all channels contributing to the WZ and ZZ production modes are included. The signal and background contributions are fit to data, and the fitted background is then subtracted. Also shown is the background-subtracted distribution of the final discriminant histograms, summed for bins with

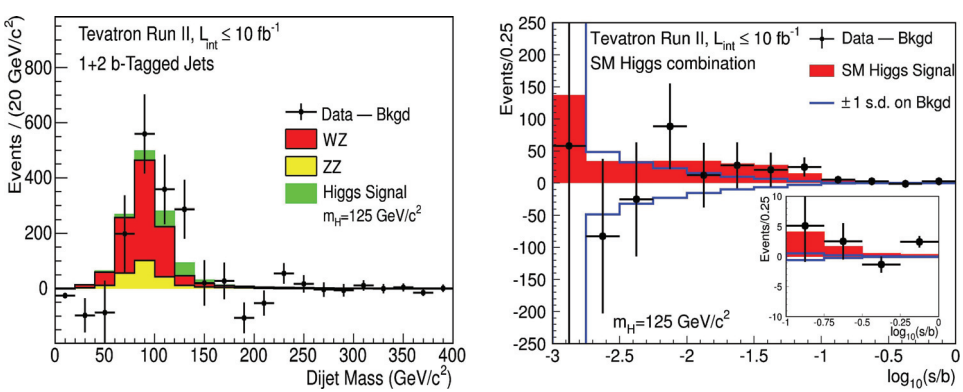

Fig. 23. Left: Background-subtracted distribution of the reconstructed dijet mass, combined Tevatron channels contributing to the WZ and ZZ analysis. Right: Background-subtracted distribution of the discriminant histograms, summed for bins with similar signal-to-background ratio (S/B) over all contributing Higgs boson search channels, for $m_H = 125$ GeV. The background is fit to the data, and the uncertainty on the background, shown with the unfilled histogram, is after the fit.[462]

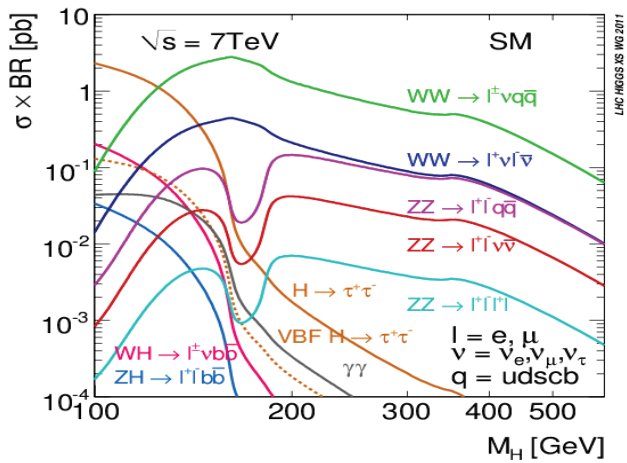

Fig. 24. Higgs boson production rates at the LHC for CM energies of 7 TeV in final states which are used to search for the Higgs boson.[399]

similar signal-to-background ratio (S/B) over all contributing Higgs boson search channels from both experiments. The background model is fit to the data, allowing the nuisance parameters to vary within their constraints. The uncertainties on the background predictions in each bin are after the fit. An excess of events in the highest S/B bins, relative to the background-only expectation is observed.

5.5. *Higgs boson searches at the LHC*

The production rates for most sensitive decay channels at the LHC are shown in Fig. 24. Here, again, the most sensitive channels for Higgs search are the ones that contain leptons, photons and large missing transverse momentum in the final decay products.

The Higgs boson search at the LHC is divided into three regions depending on the Higgs boson mass:

(1) Low-mass region, 110 GeV $\leq M_H \leq$ 150 GeV.
(2) Intermediate mass region, 150 GeV $\leq M_H \leq$ 200 GeV.
(3) High mass region, 200 GeV $\leq M_H \leq$ 600 GeV.

The channels $H \to W^+W^- \to l^+\nu l^-\bar{\nu}$ and $H \to ZZ \to l^+l^-l'^+l'^-$ contribute significantly to the overall sensitivity over the full mass range.

In the low-mass region, search is performed mostly in channels where Higgs boson decays to photons, to a pair of gauge bosons (WW, ZZ), tau leptons or bottom quarks. The decays $H \to \gamma\gamma$ and $H \to ZZ \to l^+l^-l'^+l'^-$, even though having lower rate, provide an excellent resolution for the reconstruction of the invariant mass of the decay products of the Higgs boson candidate with an accuracy of about 1%–2%. For other decays considered, either the invariant mass cannot be

reconstructed due to the presence of missing transverse momentum, or the reconstruction resolution is limited.

For the intermediate-mass range the $H \to W^+W^- \to l^+\nu l^-\bar{\nu}$ decay mode provides the most sensitivity.

In the high-mass region, in addition to the two channels discussed above, where the full mass range is covered, the channel $H \to ZZ \to l^+l^-\nu\nu$ provides the largest sensitivity and dominates the sensitivity for M_H values larger than 300 GeV. Also, for large M_H, the signal rates for $H \to ZZ \to l^+l^-l'^+l'^-$ and $H \to W^+W^- \to l^+\nu l^-\bar{\nu}$ get quite small. The sensitivity in this case is increased by including decay modes of the weak gauge bosons, which has larger branching ratios in this range. The final search channels for high mass range include $H \to W^+W^- \to l^+\nu l^-\bar{\nu}$, $H \to ZZ \to l^+l^-l'^+l'^-$, $H \to ZZ \to l^+l^-q\bar{q}$, $H \to ZZ \to l^+l^-\nu\nu$, and are analyzed by both collaborations. In addition, $H \to ZZ \to l^+l^-\tau\tau$ is analyzed only by CMS, and $H \to W^+W^- \to l\nu q\bar{q}$ only by ATLAS.

In the $H \to ZZ \to l^+l^-l'^+l'^-$ channel an excess in the invariant-mass spectrum of the four isolated leptons over a small continuum background is searched for. The main irreducible background from nonresonant ZZ production is mainly estimated from simulation. The smaller reducible backgrounds from Z+jets production, which mostly impacts the low four-lepton invariant-mass region, and top quark pair production are estimated from control regions in data, or at least the normalization is validated in dedicated control regions. The ATLAS collaboration uses the four-lepton invariant-mass spectrum as their final discriminant. The CMS collaboration uses the four-lepton invariant mass and an observable reconstructed by combined information from the five angles that describe the production and decay kinematics in the Higgs boson rest frame.[482] Figure 25 shows four-lepton invariant mass spectra for ATLAS and CMS and a clear excess can be seen at invariant mass around 125 GeV.

The $H \to \gamma\gamma$ analysis selects events with two isolated photons with large transverse momenta. The dominant reducible backgrounds are multi-jet production and single-photon production in association with jets with cross-sections several orders of magnitude larger than the signal cross-section. These backgrounds can be suppressed to a level of less than 25% due to the excellent discrimination capabilities of the LHC detectors between photon and jets. The irreducible background from diphoton production can only be discriminated from the signal process by an excellent reconstruction of the invariant mass of the diphoton system. The diphoton mass spectra after requiring two isolated photon candidates for the data from 2011 and 2012 are shown in Fig. 26. Again, a clear excess of events is observed above the continuum of background, around diphoton mass 125 GeV.

The $H \to \tau^+\tau^-$ analysis searches for a broad excess in the reconstructed ditau invariant-mass distribution. The $H \to b\bar{b}$ analysis selects events produced in association with a W or Z decaying via $Z \to l^+l^-$, $Z \to \nu\bar{\nu}$ or $W \to l\nu$.

In the combination of the different search channels the ratio of the cross-section for the different production modes and the ratio of the decay branching fraction

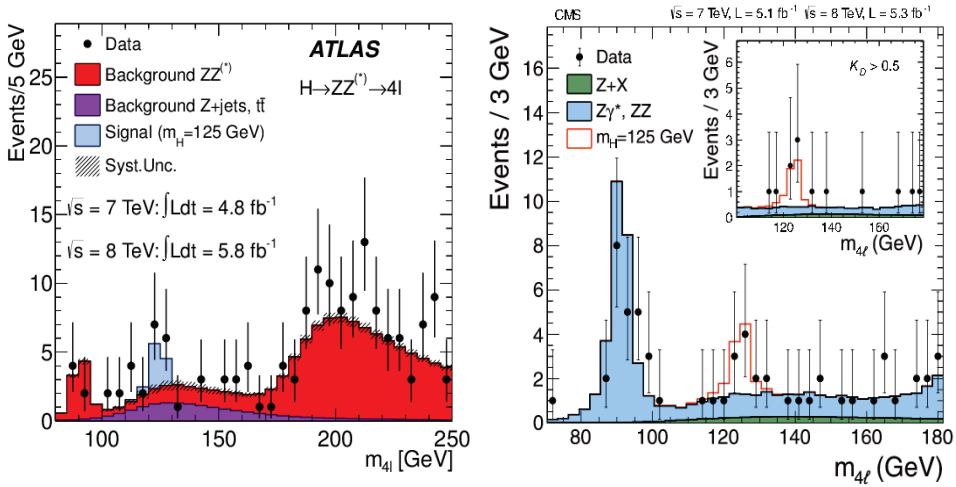

Fig. 25. Four-lepton invariant-mass spectra in ATLAS[483] (left) and CMS[484] (right) for the combined 2011 and 2012 data.

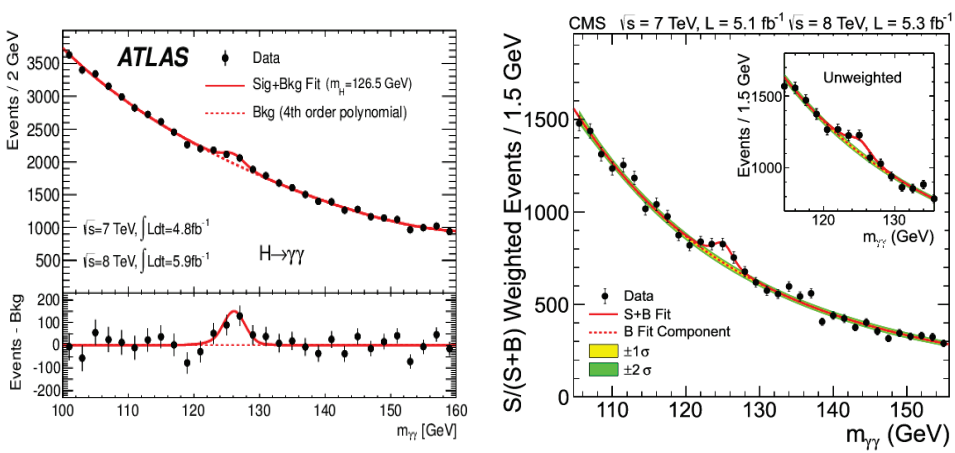

Fig. 26. Diphoton invariant-mass spectra in ATLAS[483] (left) and CMS[484] (right) for the combination of the 2011 and 2012 data.

are taken from the SM prediction.[400] Correlations in the theoretical and systematic uncertainties, which are included via nuisance parameters in the likelihood function, among the various search channels and event categories are taken into account (see Refs. 483 and 484 for details).

5.6. *Summer of 2012 — A particle is born*

In July 2012, CDF and DØ experiments at Tevatron, and ATLAS and CMS experiments at the LHC, announced evidence and discovery of a Higgs-like particle, respectively. Latest results are discussed briefly here.

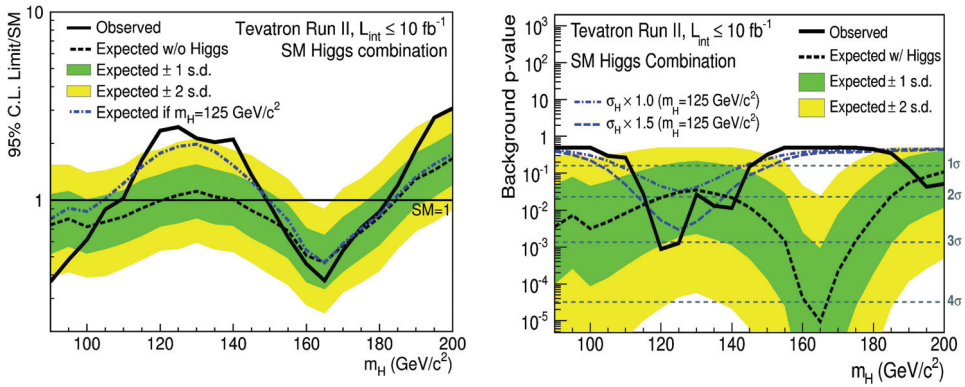

Fig. 27. (Color online) Left: Observed and median expected (for the background-only hypothesis) 95% CL Bayesian upper production limits expressed as multiples of the SM cross-section as a function of Higgs boson mass for the combined CDF and DØ searches in all decay modes. The blue short-dashed line shows median expected limits assuming the SM Higgs boson is present at $M_H = 125$ GeV. Right: The solid black line shows the background p-value as a function of M_H for CDF and DØ SM Higgs boson searches in all decay modes combined. The dotted black line shows the median expected values assuming SM signal is present, evaluated separately at each mass point. The blue lines show the median expected p-values assuming the SM Higgs boson is present with $M_H = 125$ GeV at signal strengths of 1.0 times and 1.5 times the SM prediction.[462]

5.6.1. *Evidence at the Tevatron*

Tevatron observes a broad excess in the $b\bar{b}$ final state, consistent with a wide range of SM Higgs boson-mass hypothesis.[461] Both CDF and DØ analyze up to 10 fb^{-1} integrated luminosity collected at CM $\sqrt{s} = 1.96$ TeV.[485,486] Figure 27 shows upper cross-section limit for Higgs production relative to the SM prediction. Every analysis is repeated for values of Higgs mass in 5 GeV steps. The expected sensitivity for the Tevatron combination is $1.15 \times$ SM or better for Higgs mass below 190 GeV. The Tevatron is expected to exclude for SM Higgs boson production between mass range 90–120 GeV and 140–184 GeV. An excess of events is found around 130 GeV. The local significance of this excess for Higgs mass at 125 GeV is found to be 3.0 SD with an expected local significance of 1.9 SD. This excess in events is consistent with the Higgs boson observed at the LHC. Combined cross-section measurement at Higgs mass of 125 GeV is $1.44^{+0.59}_{-0.56} \times$ SM.[462] The Tevatron experiments quote a best fit value for the signal cross-section $(\sigma_{WH} + \sigma_{ZH}) \times \mathrm{BR}(H \to b\bar{b})$ at $M_H = 125$ GeV of $0.23^{+0.09}_{-0.08}$ pb to be compared to the SM Higgs boson of 0.12 ± 0.01 pb, consistent within 1.5 SD. Based on these findings the Tevatron experiments reported evidence for the production of a new particle produced in association with weak bosons and decaying to a b-quark pair. Both experiments conclude that the excess is compatible with the production of the SM Higgs boson with a mass of 125 GeV within large uncertainties. Systematic uncertainties are evaluated for each channel including shape and normalization uncertainties, and combined by taking correlations between the channels and between CDF and DØ experiments into account. Major

systematic uncertainties arise from integrated luminosity, theoretical cross-sections used to normalize backgrounds, jet energy scale and resolution, lepton identification and b-tagging. For analyses considering $H \to b\bar{b}$ decay mode, largest source of uncertainty on the background comes from estimated rate of V + heavy-flavor production. This uncertainty is constrained using data samples before applying b-tagging requirements.

The observed signal strengths in all channels are consistent with the presence of a SM Higgs boson with a mass of 125 GeV. The best fit values for the signal strength at $M_H = 125$ GeV is $\mu\ (\sigma/\sigma_{\rm SM}) = 1.44^{+0.59}_{-0.56}$, consistent with the SM expectation of 1.

5.6.2. *Discovery at the LHC*

In July 2012, both CMS and ATLAS experiments also presented the results of their search for the SM Higgs boson using about 5 fb^{-1} integrated luminosity collected at $\sqrt{s} = 7$ TeV. A clear excess in the four-lepton invariant-mass distribution is observed in both experiments at masses of 125 GeV in ATLAS and 126 GeV in CMS. Both experiments found the presence of a Higgs-like boson with about 5 SD significance.[487]

For the latest results, both ATLAS and CMS perform this search in $H \to \gamma\gamma$,[488,489] $H \to ZZ$,[490–496] $H \to WW$,[496–499] $H \to b\bar{b}$,[500–504] and $H \to \tau\tau$ [505,506] channels for $\sqrt{s} = 7$ TeV data collected in 2011 and $\sqrt{s} = 8$ TeV integrated luminosity collected in 2012. ATLAS improved $H \to ZZ \to \ell^+\ell^-\ell^+\ell^-$ and $H \to \gamma\gamma$ searches and combined 7 TeV results obtained for 5 fb^{-1} dataset with searches in $H \to ZZ \to \ell^+\ell^-\ell^+\ell^-$, and $H \to WW \to e\nu\mu\nu$ channels carried out in 5 fb^{-1} data collected at $\sqrt{s} = 8$ TeV. The CMS experiment combines results from above five channels using up to 5.1 (5.3) fb^{-1} integrated luminosity collected at $\sqrt{s} = 7(8)$ TeV.

Figure 28 shows exclusion limits on the signal-strength parameter $\mu\ (\sigma/\sigma_{\rm SM})$ as a function of Higgs boson mass obtained from the analysis of 2011 and 2012 data by ATLAS[483] and confidence level $\rm CL_S$ for rejecting the signal+background hypothesis as a function of the Higgs boson mass by CMS.[484] Figure 29 shows corresponding local p-values as function of Higgs boson mass. The ATLAS experiment observes a significant excess of events consistent with the presence of a neutral, SM-like Higgs boson with a measured mass of 126.0 ± 0.4 (stat.) ± 0.4 (syst.) GeV, with a significance of 5.9 SD. The significance corresponds to a background fluctuation probability (p-value) of 1.7×10^{-9}. The global significance of this excess, taking into account the entire mass range 110–600 GeV, is 5.1 SD.[483] The CMS experiment observes an excess of events above the expected background, with a local significance of 5.0 SD at a mass of approximately 125 GeV, with measured mass of 125.3 ± 0.4 (stat.) ± 0.5 (syst.) GeV. The expected significance for a SM Higgs boson of that mass is 5.8 SD. CMS finds the global significance of the signal to be 4.6 (4.5) SD for the mass range 115–130 (110–145) GeV.[484]

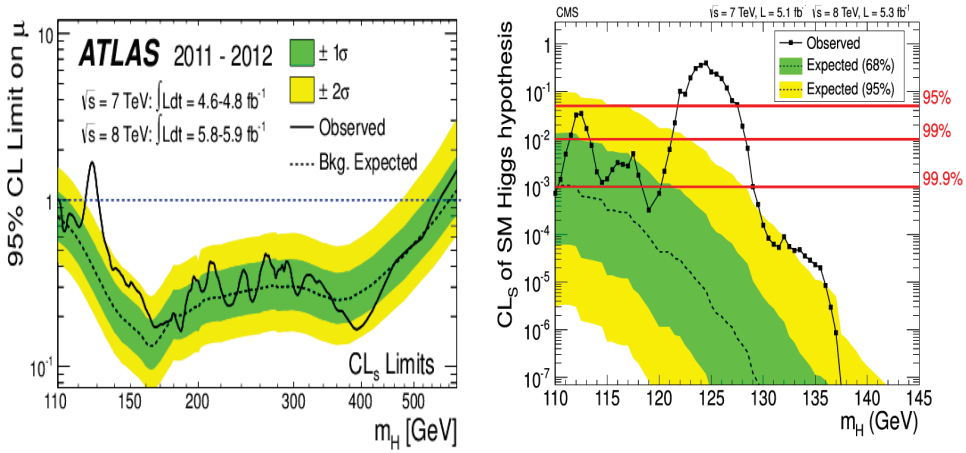

Fig. 28. Exclusion limits on the signal-strength parameter μ as a function of the hypothetical Higgs boson mass obtained from the analysis of 2011 and 2012 data by ATLAS[483] (left) and confidence level CL_S for rejecting the signal+background hypothesis as a function of the hypothetical Higgs boson mass by CMS[484] (right).

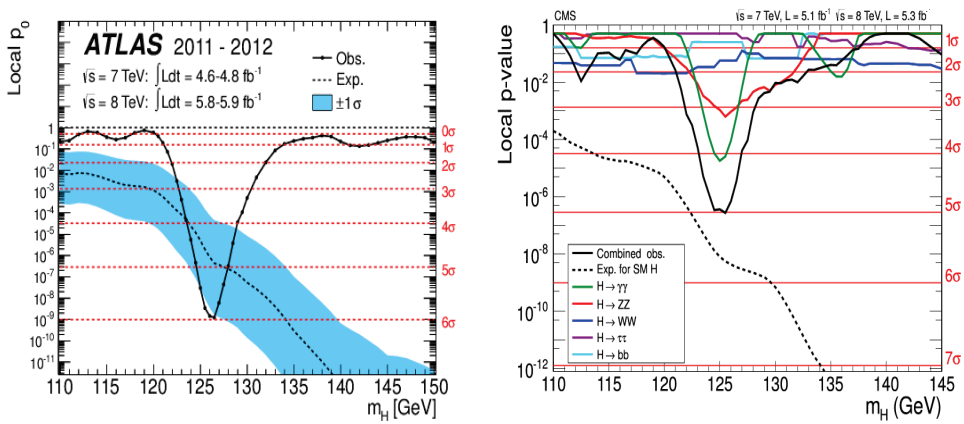

Fig. 29. Local p-values as function of the hypothetical Higgs boson mass in ATLAS[483] (left) and CMS[484] (right).

The ATLAS experiment excludes three mass regions at 99% CL, 113–114, 117–121 and 132–527 GeV, while the expected exclusion range at 99% CL is 113–532 GeV.[483] CMS excludes an SM Higgs boson at 95% CL with mass ranges 110–121.5 GeV and 128–145 GeV. In absence of a signal, CMS expects to exclude the entire mass range of 110–145 GeV at the 99.9% CL or higher.[484]

Both ATLAS and CMS have published combined results with 7 TeV and 8 TeV data.[483,484,487,507–511]

In both experiments, the systematic uncertainty is dominated by the knowledge of the absolute energy scale of photons and to a lesser extent of that of electrons.

The mass values determined in the different final states within one experiment as well as the mass values determined in the two experiments are consistent with each other. Already now the precision of the determination of the mass is better than 1%.

5.7. *Is this really the Higgs boson?*

Answer to this question requires detailed study of the discovered particle. In order to make sure that the observed particle is in fact the SM Higgs boson, one must confirm that the spin-parity is 0^+ and that the couplings are as predicted by the theory. In the SM, the properties of the Higgs boson are fully determined once its mass is known. Within SM, all cross-sections and decay fractions are predicted,[399,400] and can be measured in current data, providing test for SM predictions. The fact that both ATLAS and CMS collaborations observe significant excess of events in the $H \to \gamma\gamma$ mode, proves that the new particle is neutral and that its spin cannot be 1, and that the spin must be either 0 or 2. With large enough statistics the spin-parity can be determined from the distributions of $H \to ZZ^* \to 4\ leptons$, or $WW^* \to 4\ leptons$. Information can also be obtained from the HZ invariant mass distributions in the associated production (see, e.g. Refs. 512–516).

Since the tree level couplings of the fermions and bosons with the SM Higgs boson are in proportion to their masses, they have very special pattern. The gluon–gluon and gamma–gamma channels proceed via loops and cross-section of these channels could be different from SM expectation if non-SM particles contribute to these loops. Thus, study of Higgs boson couplings with fermions and bosons opens up another window to new physics. The coupling strengths can be determined from the measurement of the production cross-section times branching fraction in different channels. For low mass Higgs, however, the total Higgs boson width is predicted to be very small, much smaller than the experimental resolution. Therefore, either only ratios of couplings can be determined in a completely model-independent way or assumptions have to be made, e.g. the couplings to massive weak gauge bosons are not larger than predicted by the SM. Both Tevatron and LHC experiments do a model-independent analysis of Higgs couplings based on a simple rescaling of SM cross-sections, a strategy put forward by the LHC Higgs Cross Section Working Group.[400] The data is fit to corresponding coupling scale factors (κ), where $\kappa = 1$ for coupling strengths predicted by the SM.

Figure 30 shows signal strength μ for Tevatron Higgs boson measurements in several channels. Combined results for the analysis of the Higgs boson coupling to fermions and bosons from Tevatron experiments are shown as two-dimensional constraints in the fermion coupling (κ_f) either to W and Z bosons ($\kappa_{W,Z}$) or more generically to vector bosons (κ_V), as shown in Fig. 31. Within uncertainties, no deviations from SM expectation are observed. The ATLAS and CMS experiments have also performed similar measurements for coupling scale factors.

Both experiments at the LHC have measured the couplings of the new particle to vector bosons, fermions, gluons and photons. Observed event yield is compared

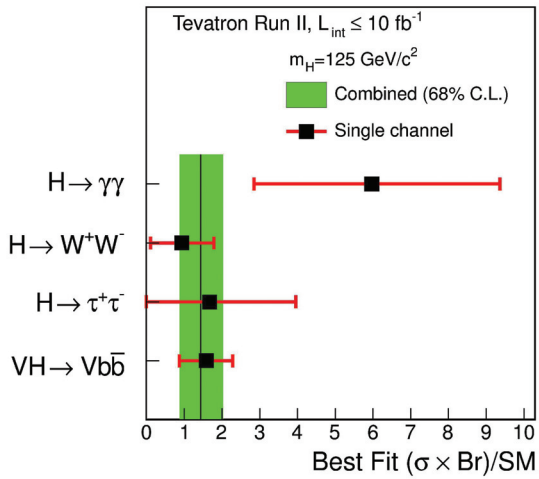

Fig. 30. Best-fit values of $\mu = (\sigma B)/\sigma_{\rm SM}$ for the combinations of CDF a DØ Higgs boson search channels for a Higgs boson mass of 125 GeV. The shaded band corresponds to the one SD uncertainty on the best-fit value of μ for all SM Higgs boson decay modes combined.[462]

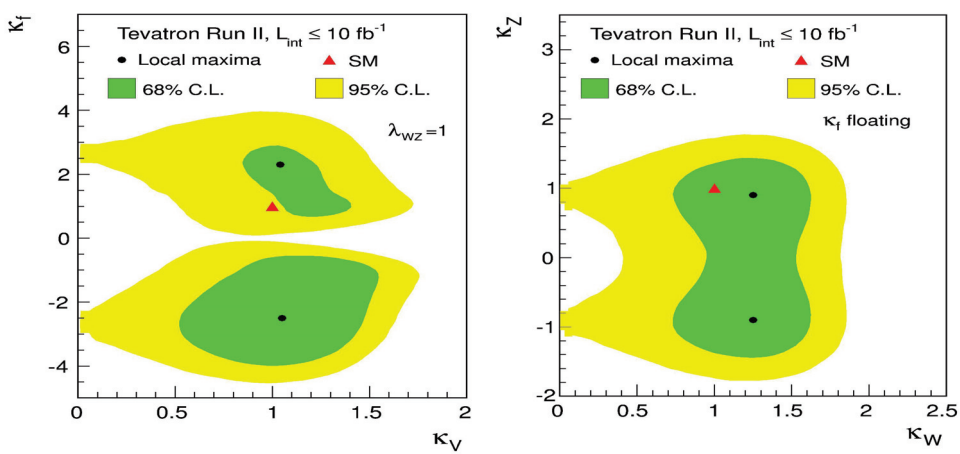

Fig. 31. Right: Two-dimensional constraints in the (κ_V, κ_f) plane, for the combined Tevatron searches for a SM-like Higgs boson with mass 125 GeV/c^2 assuming custodial symmetry ($\lambda_{WZ} = 1$). Left: Two-dimensional constraints in the (κ_W, κ_Z) plane, for the combined Tevatron searches for a SM-like Higgs boson with mass 125 GeV, allowing κ_f to float. The SM prediction for (κ_W, κ_Z) is marked with a triangle.[462]

with the prediction for the SM Higgs boson through a fit of the signal strength μ. The overall signal strength relative to the SM prediction, assuming the ratio of production cross-sections and ratio of branching ratios as predicted by the SM, is shown in Fig. 32 as function of the hypothetical Higgs boson mass. The compatibility of a simultaneous determination of the best signal strength μ and the best mass value m_H in several final states is demonstrated in Fig. 33. The largest

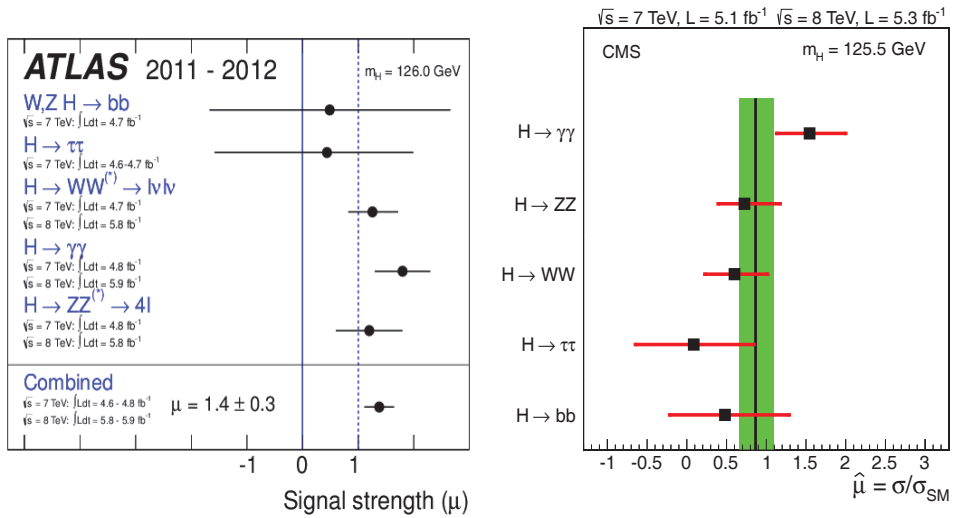

Fig. 32. Best fit values for the signal strength μ in ATLAS[483] (left) and CMS[484] (right).

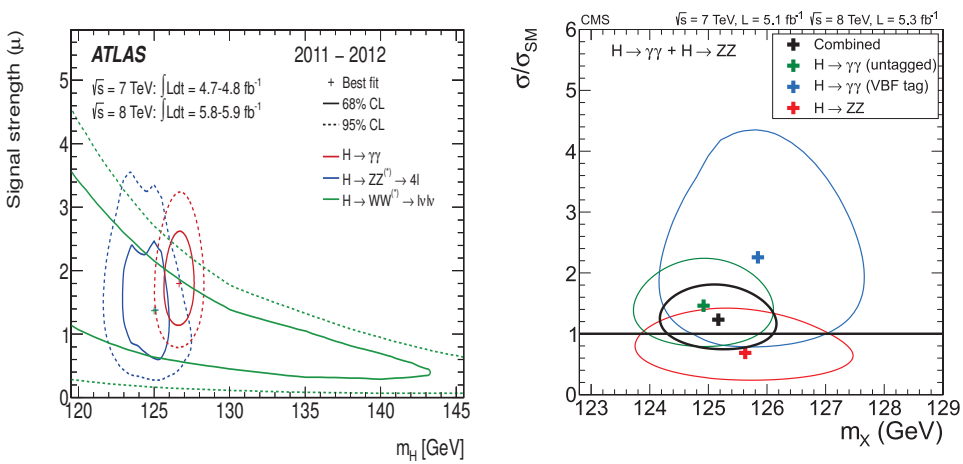

Fig. 33. Best fit values for the signal strength μ versus hypothetical Higgs boson mass M_H in ATLAS[483] (left) and CMS[484] (right).

signal strengths of 1.4 ± 0.3, observed at a mass of 126.0 GeV (ATLAS) and of 0.87 ± 0.23 observed at a mass of 125.5 GeV (CMS), are compatible with unity. The four main Higgs boson production mechanisms at LHC can be associated with either top quark couplings (gluon–gluon fusion and $t\bar{t}H$) or vector–boson couplings (VBF and VH). Therefore, combinations of channels corresponding to these productions modes can be used to test the relative strengths of the couplings of the new state to the vector bosons and top quark and shown in Fig. 34. So far, all results are consistent, within uncertainties, with expectations for a SM Higgs boson.

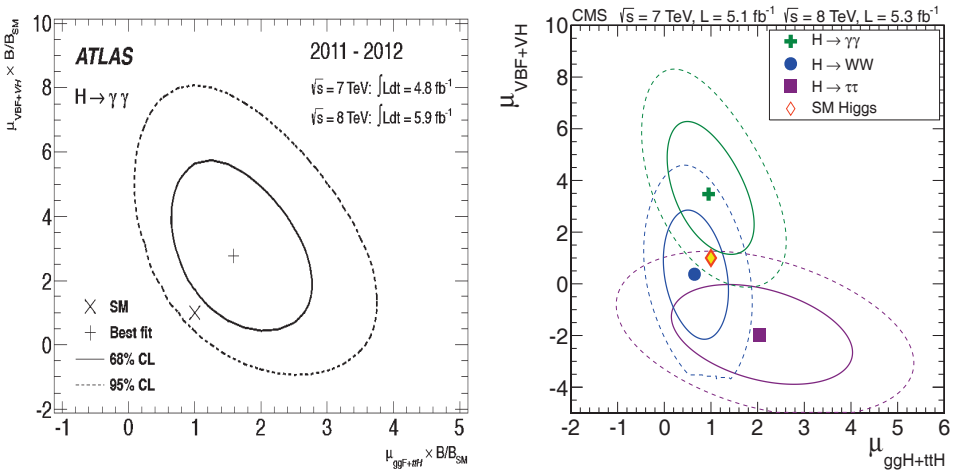

Fig. 34. The 68% (solid lines) and 95% (dashed lines) CL contours for the signal strength in $(\mu_{ggF+t\bar{t}H}, \mu_{VBF+VH})$ plane. Left: ATLAS likelihood contours including the branching ratio factor B/BSM. The best fit to the data (SM expectation) $+(x)$ and 68% (full) and 95% (dashed) CL contours are shown as well.[483] Right: CMS likelihood contours for decay modes gg, WW and tt. The markers indicate the best-fit values for each mode. The diamond at $(1, 1)$ indicates the expected values for the SM Higgs boson.[484]

6. Conclusions

These are very exciting and historic times. More than 40 years ago, Higgs mechanism was proposed to describe the spontaneous breaking of the EW symmetry. This mechanism is accompanied by a neutral scalar known as the Higgs boson. Experimental proof of Higgs, both the mechanism and the particle, would be a great breakthrough and a step further towards deeper understanding of nature. In July 2012, a new neutral boson with a mass of 126 GeV was discovered. This is the first evidence of a fundamental, scalar particle, related to a field with nonzero vacuum expectation value.

So far no significant hints of physics beyond SM have been seen either at Tevatron or the LHC. Couplings of the newly discovered boson with fermions and bosons have been studied and, so far, all measured properties are consistent with the expectations for the SM Higgs boson within current, rather large, uncertainties. Most measurements in the top quark sector are in accordance with the SM expectations and the deviations seen so far are not significant enough.

The measured mass of newly discovered boson is compatible with the m_H in the range preferred by the EW precision measurements. Figure 35 shows the stability domains as functions of the top quark mass, m_t and the Higgs boson mass, m_H. The observed value of m_H corresponds to a metastable value with a lifetime longer than the age of the universe, so the SM could be a viable theory up to the Planck mass.[517]

Regardless of its exceptional success, SM is not complete and some new physics has to exist beyond SM. It would be very disappointing if all the properties of the

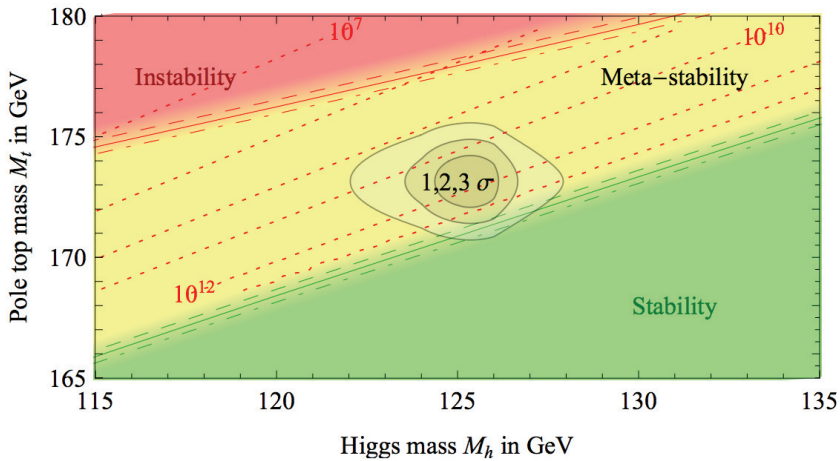

Fig. 35. Vacuum stability domains in the SM for the observed values of m_t and m_H.[517] The dotted contour-lines show the scale Λ in GeV where the instability sets in, for $\alpha_s(m_Z) = 0.1184$.

newly discovered boson match exactly the SM predictions. Therefore, precision measurements of its properties are critical. Precise measurement of Higgs boson self-coupling is especially needed, in order to determine the Higgs potential. Similarly, a nonvanishing value for λ provides a test of spontaneous symmetry breaking. An increase of the integrated luminosity to 3000 fb^{-1} reduces the experimental uncertainties in the signal strength ($\sigma/\sigma_{\rm SM}$) by roughly a factor of 2,[518] so that the uncertainties of the Higgs boson couplings should be reduced by a factor of about 1.5. The precise value of λ and hence, the exact method of spontaneous symmetry breaking, will perhaps have to wait for future experiments. Studies show that at the LHC design luminosity, for Higgs boson with mass between 150 GeV and 200 GeV, nonzero self-coupling and a range of 0–3.8$\lambda/\lambda_{\rm SM}$ at 95% CL can be established.[519]

Because of its special nature, the top quark plays very central role in many new physics models as well. Exact nature of the Higgs boson will not be completely clear until crucial information from study of its couplings with the top quark is provided. Given, EW symmetry breaking does employ Higgs mechanism, any extension of SM would include Higgs-like bosons. Many SM extensions in the Higgs sector include Dark Matter candidates, providing another reason to study the new particle with as much precision as possible. Finally, Higgs fields could in fact play a key role in the inflationary phase of the cosmological expansion that is driven by Dark Energy.

Thus, precise measurements of Higgs boson and top quark properties, understanding of Higgs potential, the search for additional Higgs bosons and other new particles and corresponding processes, will be of utmost priority not only at the current LHC experiments but in future upgrades and in planning of new machines.

Acknowledgments

The author is thankful to colleagues working at DØ, CDF, CMS and ATLAS experiments, for their hard work that went into the beautiful measurements presented in this paper. Many thanks to Tevatron and LHC accelerator division, without whom these measurements would not have been possible. Finally, the author is especially grateful to colleagues Anwar Bhatti, Robert Craig Group, Andreas Jung, Nikolaos Kidonakis and Lidija Zivkovic, for their useful feedback on the contents of this review.

References

1. S. L. Glashow, *Nucl. Phys.* **22**, 579 (1961).
2. S. Weinberg, *Phys. Rev. Lett.* **19**, 1264 (1967).
3. A. Salam, *Proc. 8th Nobel Symposium*, Lerum, Sweden, 19–25 May 1968, p. 367.
4. S. L. Glashow, J. Iliopoulos and L. Maiani, *Phys. Rev. D* **2**, 1285 (1970).
5. S. L. Glashow, *Nucl. Phys.* **22**, 579 (1961).
6. S. Weinberg, *Phys. Rev. Lett.* **19**, 1264 (1967).
7. A. Salam, *Elementary Particle Theory*, ed. N. Svartholm (Almquist and Wiksells, Stockholm, 1969), p. 367.
8. M. Gell-Mann, *Acta Phys. Austriaca Suppl.* **IX**, 733 (1972).
9. H. Fritzsch and M. Gell-Mann, *Proc. XVI Int. Conf. on High Energy Physics*, Chicago–Batavia, 1972.
10. H. Fritzsch, M. Gell-Mann and H. Leutwyler, *Phys. Lett. B* **47**, 365 (1973).
11. D. Gross and F. Wilczek, *Phys. Rev. Lett.* **30**, 1343 (1973).
12. S. Weinberg, *Phys. Rev. Lett.* **31**, 494 (1973).
13. M. Veltman, *Nucl. Phys. B* **21**, 288 (1970).
14. G. 't Hooft, *Nucl. Phys. B* **33**, 173 (1971).
15. B. W. Lee and J. Zinn-Justin, *Phys. Rev. D* **5**, 3121 (1972).
16. F. Englert and R. Brout, *Phys. Rev. Lett.* **13**, 321 (1964).
17. P. W. Higgs, *Phys. Lett.* **12**, 132 (1964).
18. G. S. Guralnik, C. R. Hagen and T. W. B. Kibble, *Phys. Rev. Lett.* **13**, 585 (1964).
19. P. W. Higgs, *Phys. Rev.* **145**, 1156 (1966).
20. T. W. B. Kibble, *Phys. Rev.* **155**, 1554 (1967).
21. The LEP Electroweak Working Group, http://lepewwg.web.cern.ch/LEPEWWG/.
22. The ALEPH, CDF, DØ, DELPHI, L3, OPAL and SLD Collabs., The LEP Electroweak Working Group, the Tevatron Electroweak Working Group, and the SLD Electroweak and Heavy Flavour Working Groups, arXiv:1012.2367 [hep-ex].
23. Gfitter Group (M. Baak *et al.*), *Eur. Phys. J. C* **72**, 2205 (2012), arXiv:1209.2716 [hep-ph].
24. P. Gambino, *Int. J. Mod. Phys. A* **19**, 808 (2004), arXiv:hep-ph/0311257.
25. CDF Public Results, http://www-cdf.fnal.gov/physics/physics.html.
26. DØ Public Results, http://www-d0.fnal.gov/Run2Physics/WWW/results.htm.
27. ATLAS Public Results, https://twiki.cern.ch/twiki/bin/view/AtlasPublic.
28. CMS Public Results, https://twiki.cern.ch/twiki/bin/view/CMSPublic/PhysicsResults.
29. CDF Collab. (D. Acosta *et al.*), *Phys. Rev. D* **71**, 032001 (2005).
30. CDF Collab. (A. Abulencia *et al.*), *J. Phys. G*: *Nucl. Part. Phys.* **34**, 2457 (2007).
31. DØ Collab. (S. Abachi *et al.*), *Nucl. Instrum. Methods Res. A* **338**, 185 (1994).

32. DØ Collab. (V. M. Abazov *et al.*), *Nucl. Instrum. Methods Phys. Res. A* **565**, 463 (2006).
33. ATLAS Collab. (G. Aad *et al.*), CERN-OPEN-2008-020, arXiv:0901.0512 [hep-ex].
34. ATLAS Collab. (G. Aad *et al.*), *J. High Energy Phys.* **1009**, 056 (2010), arXiv:1005.5254 [hep-ex].
35. CMS Collab. (G. Bayatian *et al.*), CERN-LHCC-2006-001 (2006).
36. CMS Collab. (G. Bayatian *et al.*), *J. Phys. G* **34**, 995 (2007).
37. CDF Collab. (F. Abe *et al.*), *Phys. Rev. D* **45**, 1448 (1992).
38. A. Bhatti *et al.*, *Nucl. Instrum. Methods A* **566**, 375 (2006).
39. G. Blazey *et al.*, *Proc. Run II QCD and Weak Boson Physics Workshop* (2000), arXiv:hep-ex/0005012.
40. DØ Collab. (B. Abbott *et al.*), *Nucl. Instrum. Methods Phys. Res. A* **424**, 352 (1999), arXiv:hep-ex/9805009.
41. DØ Collab. (V. M. Abazov *et al.*), *Phys. Rev. D* **85**, 052006 (2012), arXiv:1110.3771 [hep-ex].
42. CDF Collab. (T. Affolder *et al.*), *Phys. Rev. D* **64**, 032002 (2001).
43. J. Freeman, W. Ketchum, J. D. Lewis, S. Poprocki, A. Pronko, V. Rusu and P. Wittich, *Nucl. Instrum. Methods A* **663**, 37 (2011), arXiv:1108.4738 [hep-ex].
44. J. Freeman *et al.*, *Nucl. Instrum. Methods A* **697**, 64 (2012).
45. DØ Collab. (V. M. Abazov *et al.*), *Nucl. Instrum. Methods Phys. Res. A* **620**, 490 (2010), arXiv:1002.4224 [hep-ex].
46. D. Acosta *et al.*, *Nucl. Instrum. Methods A* **494**, 57 (2002).
47. ATLAS Collab. (G. Aad *et al.*), *J. Instrum.* **3**, S08003 (2008).
48. CMS Collab. (R. Adolphi *et al.*), *J. Instrum.* **3**, S08004 (2008).
49. CMS Collab., CMS physics analysis summary, CMS-PAS-PFT-10-002 (2011).
50. CMS Collab., CMS physics analysis summary, CMS-PAS-EGM-10-004 (2010).
51. CMS Collab. (S. Chatrchyan *et al.*), *J. High Energy Phys.* **1110**, 132 (2011), arXiv:1107.4789 [hep-ex].
52. ATLAS Collab. (G. Aad *et al.*), *Phys. Rev. D* **85**, 072004 (2012), arXiv:1109.5141 [hep-ex].
53. CMS Collab., CMS physics analysis summary, CMS-PAS-MUO-10-002 (2010).
54. M. Cacciari, G. P. Salam and G. Soyez, *J. High Energy Phys.* **0804**, 063 (2008), arXiv:0802.1189 [hep-ph].
55. M. Cacciari and G. P. Salam, *Phys. Lett. B* **641**, 57 (2006), arXiv:hep-ph/0512210.
56. M. Cacciari, G. P. Salam and G. Soyez, *Eur. Phys. J. C* **72**, 1896 (2012), arXiv:1111.6097 [hep-ph].
57. CMS Collab. (S. Chatrchyan *et al.*), *J. Instrum.* **6**, P11002 (2011), arXiv:1107.4277 [physics.ins-det].
58. ATLAS Collab., ATLAS Note, ATLAS-CONF-2010-054 (2010).
59. ATLAS Collab. (G. Aad *et al.*), *Eur. Phys. J. C* **73**, 2304 (2013), arXiv:1112.6426 [hep-ex].
60. CMS Collab., CMS physics analysis summary, CMS-PAS-BTV-09-001 (2009).
61. ATLAS Collab., ATLAS Note ATLAS-CONF-2010-091 (2010).
62. CMS Collab., CMS-PAS-BTV-11-002 (2011).
63. ATLAS Collab., CMS physics analysis summary, ATLAS-CONF-2010-042 (2010).
64. CMS Collab., CMS physics analysis summary, CMS-PAS-BTV-07-003 (2009).
65. ATLAS Collab., ATLAS Note ATLAS-CONF-2011-102 (2011).
66. CMS Collab., CMS physics analysis summary, CMS-PAS-BTV-11-004 (2012).
67. ATLAS Collab., ATLAS Note, ATLAS-CONF-2011-089 (2011).
68. ATLAS Collab., ATLAS Note, ATLAS-CONF-2011-143 (2011).

69. ATLAS Collab., ATLAS Note, ATLAS-CONF-2012-043 (2012).
70. CMS Collab., CMS physics analysis summary, CMS-PAS-BTV-11-003 (2012).
71. CMS Collab., CMS physics analysis summary, CMS-PAS-BTV-11-001 (2011).
72. ATLAS Collab. (G. Aad *et al.*), *Eur. Phys. J. C* **72**, 1844 (2012), arXiv:1108.5602 [hep-ex].
73. CMS Collab. (S. Chatrchyan *et al.*), *J. Instrum.* **6**, P09001 (2011), arXiv:1106.5048 [physics.ins-det].
74. ATLAS Collab. (G. Aad *et al.*), *Eur. Phys. J. C* **71**, 1630 (2011), arXiv:1101.2185 [hep-ex].
75. ATLAS Collab., ATLAS Note, ATLAS-CONF-2011-011 (2011).
76. ATLAS Collab., ATLAS Note, ATLAS-CONF-2011-116 (2011).
77. CMS Collab., CMS physics analysis summary, CMS-PAS-SMP-12-008 (2012).
78. CMS Collab., Detector performance summary, CMS-DP-2011-002 (2011).
79. CMS Collab., CMS physics analysis summary, CMS-PAS-EWK-11-001 (2011).
80. CMS Collab., CMS physics analysis summary, CMS-PAS-EWK-10-004 (2010).
81. ATLAS Collab., accepted for publication in *Eur. Phys. J. C.*, arXiv:1302.4393 [hep-ex].
82. D. W. Ruck, S. K. Rogers, M. Kabrinsky, M. E. Oxley and B. W. Suter, *IEEE Trans. Neural Networks* **1**, 296 (1990).
83. E. A. Wan, *IEEE Trans. Neural Networks* **1**, 303 (1990).
84. C. M. Bishop, *Neural Networks for Pattern Recognition* (Clarendon Press, Oxford, 1998).
85. E. K. Blum and L. K. Li, *Neural Networks* **4**, 511 (1991).
86. R. M. Neal, *Bayesian Learning of Neural Networks* (Springer-Verlag, New York, 1996).
87. L. Breiman, J. Friedman, C. J. Stone and R. A. Olshen, *Classification and Regression Trees* (Wadsworth, Stanford, 1984).
88. D. Bowser-Chao and D. L. Dzialo, *Phys. Rev. D* **47**, 1900 (1993).
89. Y. Freund and R. E. Schapire, in *Proc. 13th International Conference on Machine Learning*, ed. L. Saitta (Morgan Kaufmann, San Francisco, 1996).
90. B. P. Roe, H.-J. Yang, J. Zhu, Y. Liu, I. Stancu and G. McGregor, *Nucl. Instrum. Methods Phys. Res. A* **543**, 577 (2005).
91. H.-J. Yang, B. P. Roe and J. Zhu, *Nucl. Instrum. Methods Phys. Res. A* **555**, 370 (2005).
92. T. Sjostrand, S. Mrenna and P. Z. Skands, *J. High Energy Phys.* **05**, 026 (2006).
93. S. Gieseke *et al.*, arXiv:hep-ph/0609306.
94. GEANT4 Collab. (S. Agostinelli *et al.*), *Nucl. Instrum. Methods A* **506**, 250 (2003).
95. T. Junk, *Nucl. Instrum. Methods A* **434**, 435 (1999).
96. I. Bertram *et al.*, FERMILAB-TM-2104 (2000).
97. A. L. Read, *J. Phys. G* **28**, 2693 (2002).
98. E. Gross and O. Vitells, *Eur. Phys. J. C* **70**, 525 (2010), arXiv:1005.1891 [physics.data-an].
99. L. Moneta *et al.*, in *Proc. 13th Int. Workshop on Advanced Computing and Analysis Techniques in Physics Research* (*ACAT2010*) *SISSA* (2010), arXiv:1009.1003 [physics.data-an].
100. ATLAS and CMS Collab., Technical Report ATL-PHYS-PUB 2011-11, CMS NOTE 2011/005 (2011).
101. G. Cowan *et al.*, *Phys. J. C* **71**, 1554 (2011), arXiv:1007.1727 [physics.data-an].
102. CDF Collab. (F. Abe *et al.*), *Phys. Rev. Lett.* **74**, 2626 (1995).
103. DØ Collab. (S. Abachi *et al.*), *Phys. Rev. Lett.* **74**, 2632 (1995).

104. M. Jezabek and J. H. Kuhn, *Nucl. Phys. B* **314**, 1 (1989).
105. I. Bigi, Y. Dokshitzer, V. Khoze, J. Kühn and P. Zerwas, *Phys. Lett. B* **181**, 157 (1986).
106. F. Deliot, Y. Peters and V. Sorin, *Int. J. Mod. Phys. A* **28**, 08 (2013), arXiv:1302.3628 [hep-ex].
107. F.-P. Schilling, *Int. J. Mod. Phys. A* **27**, 1230016 (2012), arXiv:1206.4484v2 [hep-ex].
108. A. Heinson, *Mod. Phys. Lett. A* **25**, 309 (2010), arXiv:1002.4167 [hep-ex].
109. P. Nason, S. Dawson and R. K. Ellis, *Nucl. Phys. B* **303**, 607 (1988).
110. P. Nason, S. Dawson and R. K. Ellis, *Nucl. Phys. B* **327**, 49 (1989) [Erratum: *ibid.* **335**, 260 (1990)].
111. W. Beenakker, H. Kuijf, W. L. van Neerven and J. Smith, *Phys. Rev. D* **40**, 54 (1989).
112. W. Beenakker, W. L. van Neerven, R. Meng, G. A. Schuler and J. Smith, *Nucl. Phys. B* **351**, 507 (1991).
113. G. Bevilacqua, M. Czakon, A. van Hameren, C. G. Papadopoulos and M. Worek, *J. High Energy Phys.* **1102**, 083 (2011), arXiv:1012.4230 [hep-ph].
114. J. A. Maestre *et al.*, arXiv:1203.6803 [hep-ph].
115. S. Dittmaier, P. Uwer and S. Weinzierl, *Phys. Rev. Lett.* **98**, 262002 (2007), arXiv:hep-ph/0703120.
116. W. Beenakker *et al.*, *Nucl. Phys. B* **411**, 343 (1994).
117. W. Bernreuther, M. Fuecker and Z. Si, *Phys. Lett. B* **633**, 54 (2006), arXiv:hep-ph/0508091.
118. W. Bernreuther, M. Fuecker and Z. Si, *Phys. Rev. D* **74**, 113005 (2006), arXiv:hep-ph/0610334.
119. W. Bernreuther, M. Fucker and Z. Si, *Phys. Rev. D* **78**, 017503 (2008), arXiv:0804.1237 [hep-ph].
120. J. H. Kuhn, A. Scharf and P. Uwer, *Eur. Phys. J. C* **45**, 139 (2006), arXiv:hep-ph/0508092.
121. J. H. Kuhn, A. Scharf and P. Uwer, *Eur. Phys. J. C* **51**, 37 (2007), arXiv:hep-ph/0610335.
122. W. Hollik and M. Kollar, *Phys. Rev. D* **77**, 014008 (2008), arXiv:0708.1697 [hep-ph].
123. N. Kidonakis, *Phys. Rev. D* **82**, 114030 (2010), arXiv:1009.4935 [hep-ph].
124. M. Aliev, H. Lacker, U. Langenfeld, S. Moch, P. Uwer and M. Wiedemann, *Comput. Phys. Commun.* **182**, 1034 (2011), arXiv:1007.1327 [hep-ph].
125. V. Ahrens, A. Ferroglia, M. Neubert, B. D. Pecjak and L. L. Yang, *Phys. Lett. B* **703**, 135 (2011), arXiv:1105.5824 [hep-ph].
126. M. Beneke, P. Falgari, S. Klein and C. Schwinn, *Nucl. Phys. B* **855**, 695 (2012), arXiv:1109.1536 [hep-ph].
127. M. Cacciari, M. Czakon, M. Mangano, A. Mitov and P. Nason, *Phys. Lett. B* **710**, 612 (2012), arXiv:1111.5869 [hep-ph].
128. U. Langenfeld, S. Moch and P. Uwer, *Phys. Rev. D* **80**, 054009 (2009), arXiv:0906.5273 [hep-ph].
129. M. Beneke, P. Falgari and C. Schwinn, *Nucl. Phys. B* **828**, 69 (2010), arXiv:0907.1443 [hep-ph].
130. V. Ahrens, A. Ferroglia, M. Neubert, B. D. Pecjak and L. L. Yang, *J. High Energy Phys.* **1009**, 097 (2010), arXiv:1003.5827 [hep-ph].
131. M. Czakon, A. Mitov and G. F. Sterman, *Phys. Rev. D* **80**, 074017 (2009), arXiv:0907.1790 [hep-ph].
132. N. Kidonakis, arXiv:1304.7775 [hep-ph].

133. W. Bernreuther, A. Brandenburg, Z. Si and P. Uwer, *Phys. Rev. Lett.* **87**, 242002 (2001), arXiv:hep-ph/0107086.
134. W. Bernreuther, A. Brandenburg, Z. Si and P. Uwer, *Nucl. Phys. B* **690**, 81 (2004), arXiv:hep-ph/0403035.
135. K. Melnikov and M. Schulze, *J. High Energy Phys.* **908**, 049 (2009), arXiv:0907.3090 [hep-ph].
136. W. Bernreuther and Z. Si, *Nucl. Phys. B* **837**, 90 (2010), arXiv:1003.3926 [hep-ph].
137. J. M. Campbell and R. K. Ellis, arXiv:1204.1513 [hep-ph].
138. M. Czakon, P. Fiedler and A. Mitov, *Phys. Rev. Lett.* **110**, 252004 (2013), arXiv:1303.6254 [hep-ph].
139. S. Dittmaier, P. Uwer and S. Weinzierl, *Eur. Phys. J. C* **59**, 625 (2009), arXiv:0810.0452 [hep-ph].
140. K. Melnikov and M. Schulze, *Nucl. Phys. B* **840**, 129 (2010), arXiv:1004.3284 [hep-ph].
141. K. Melnikov, A. Scharf and M. Schulze, *Phys. Rev. D* **85**, 054002 (2012), arXiv:1111.4991 [hep-ph].
142. G. Bevilacqua, M. Czakon, C. Papadopoulos and M. Worek, *Phys. Rev. Lett.* **104**, 162002 (2010), arXiv:1002.4009 [hep-ph].
143. G. Bevilacqua, M. Czakon, C. Papadopoulos and M. Worek, *Phys. Rev. D* **84**, 114017 (2011), arXiv:1108.2851 [hep-ph].
144. W. Bernreuther, *J. Phys. G* **35**, 083001 (2008), arXiv:0805.1333 [hep-ph].
145. S. Moch and P. Uwer, *Phys. Rev. D* **78**, 034003 (2008), arXiv:0804.1476 [hep-ph].
146. S. Weinzierl, in *Proc. of HCP2011*, Paris, France, 2011, arXiv:1201.4025 [hep-ph].
147. N. Kidonakis and B. D. Pecjak, *Eur. Phys. J. C* **72**, 2084 (2012), arXiv:1108.6063 [hep-ph].
148. S. S. Willenbrock and D. A. Dicus, *Phys. Rev. D* **34**, 155 (1986).
149. C. P. Yuan, *Phys. Rev. D* **41**, 42 (1990).
150. S. Cortese and R. Petronzio, *Phys. Lett. B* **253**, 494 (1991).
151. R. K. Ellis and S. Parke, *Phys. Rev. D* **46**, 3785 (1992).
152. D. O. Carlson and C. P. Yuan, *Phys. Lett. B* **306**, 386 (1993).
153. T. Stelzer and S. Willenbrock, *Phys. Lett. B* **357**, 125 (1995).
154. A. P. Heinson, A. S. Belyaev and E. E. Boos, *Phys. Rev. D* **56**, 3114 (1997).
155. T. Stelzer, Z. Sullivan and S. Willenbrock, *Phys. Rev. D* **56**, 5919 (1997), arXiv:hep-ph/9705398.
156. T. Stelzer, Z. Sullivan and S. Willenbrock, *Phys. Rev. D* **58**, 094021 (1998), arXiv:hep-ph/9807340.
157. Z. Sullivan, *Phys. Rev. D* **70**, 114012 (2004), arXiv:hep-ph/0408049.
158. J. M. Campbell, R. K. Ellis and F. Tramontano, *Phys. Rev. D* **70**, 094012 (2004), arXiv:hep-ph/0408158.
159. Q.-H. Cao, R. Schwienhorst and C. P. Yuan, *Phys. Rev. D* **71**, 054023 (2005), arXiv:hep-ph/0409040.
160. Q.-H. Cao, R. Schwienhorst, J. A. Benitez, R. Brock and C. P. Yuan, *Phys. Rev. D* **72**, 094027 (2005), arXiv:hep-ph/0504230.
161. N. Kidonakis, *Phys. Rev. D* **74**, 114012 (2006).
162. B. Harris, E. Laenen, L. Phaf, Z. Sullivan and S. Weinzierl, *Phys. Rev. D* **66**, 054024 (2002), arXiv:hep-ph/0207055.
163. S. Zhu, *Phys. Lett. B* **524**, 283 (2002).
164. N. Kidonakis, *Phys. Rev. D* **83**, 091503 (2011), arXiv:1103.2792 [hep-ph].
165. N. Kidonakis, *Phys. Rev. D* **81**, 054028 (2010), arXiv:1001.5034 [hep-ph].

166. H. X. Zhu, C. S. Li, J. Wang and J. J. Zhang, *J. High Energy Phys.* **1102**, 099 (2011), arXiv:1006.0681 [hep-ph].
167. N. Kidonakis, *Phys. Rev. D* **82**, 054018 (2010), arXiv:1005.4451 [hep-ph].
168. CDF Collab. (T. Aaltonen *et al.*), *Phys. Rev. D* **84**, 031101(R) (2011), arXiv:1103.4821 [hep-ex].
169. CDF Collab. (T. Aaltonen *et al.*), *Phys. Rev. D* **83**, 071102 (2011), arXiv:1007.4423 [hep-ex].
170. CDF Collab. (T. Aaltonen *et al.*), *Phys. Rev. Lett.* **105**, 012001 (2010), arXiv:1004.3224 [hep-ex].
171. CDF Collab. (T. Aaltonen *et al.*), *Phys. Rev. D* **79**, 052007 (2009), arXiv:0901.4142 [hep-ex].
172. CDF Collab. (A. Abulencia *et al.*), *Phys. Rev. D* **74**, 072006 (2006), arXiv:hep-ex/0607035.
173. CDF Collab. (T. Aaltonen *et al.*), submitted to *Phys. Rev. D*, arXiv:1304.7961 [hep-ex].
174. CDF Collab. (T. Aaltonen *et al.*), *Phys. Rev. D* **82**, 052002 (2010), arXiv:1002.2919 [hep-ex].
175. CDF Collab. (T. Aaltonen *et al.*), *Phys. Rev. Lett.* **100**, 062005 (2008), arXiv:0710.4037 [hep-ex].
176. CDF Collab. (T. Aaltonen *et al.*), *Phys. Rev. Lett.* **109**, 192001 (2012), arXiv:1208.5720 [hep-ex].
177. CDF Collab. (T. Aaltonen *et al.*), *Phys. Rev. D* **81**, 052001 (2010), arXiv:1002.0365 [hep-ex].
178. CDF Collab. (T. Aaltonen *et al.*), *Phys. Rev. D* **76**, 072009 (2007), arXiv:0706.3790 [hep-ex].
179. CDF Collab. (A. Abulencia *et al.*), *Phys. Rev. D* **74**, 072005 (2006), arXiv:hep-ex/0607095 [hep-ex].
180. DØ Collab. (V. M. Abazov *et al.*), *Phys. Rev. D* **84**, 012008 (2011), arXiv:1101.0124 [hep-ex].
181. DØ Collab. (V. M. Abazov *et al.*), *Phys. Rev. Lett.* **100**, 192004 (2008), arXiv:0803.2779 [hep-ex].
182. DØ Collab. (V. M. Abazov *et al.*), *Phys. Rev. D* **76**, 092007 (2007), arXiv:0705.2788 [hep-ex].
183. DØ Collab. (V. M. Abazov *et al.*), *Phys. Lett. B* **704**, 403 (2011), arXiv:1105.5384 [hep-ex].
184. DØ Collab. (V. M. Abazov *et al.*), *Phys. Rev. D* **80**, 071102 (2009), arXiv:0903.5525 [hep-ex].
185. DØ Collab. (V. M. Abazov *et al.*), *Phys. Lett. B* **679**, 177 (2009), arXiv:0901.2137 [hep-ex].
186. DØ Collab. (V. M. Abazov *et al.*), *Phys. Rev. D* **82**, 071102 (2010), arXiv:1008.4284 [hep-ex].
187. DØ Collab. (V. M. Abazov *et al.*), *Phys. Rev. D* **82**, 032002 (2010), arXiv:0911.4286 [hep-ex].
188. ATLAS Collab. (G. Aad *et al.*), *Phys. Lett. B* **711**, 244 (2012), arXiv:1201.1889 [hep-ex].
189. ATLAS Collab. (G. Aad *et al.*), *J. High Energy Phys.* **05**, 059 (2012), arXiv:1202.4892 [hep-ex].
190. ATLAS Collab. (G. Aad *et al.*), *Phys. Lett. B* **707**, 459 (2012), arXiv:1108.3699 [hep-ex].

191. ATLAS Collab. (G. Aad *et al.*), *Eur. Phys. J. C* **71**, 1577 (2011), arXiv:1012.1792 [hep-ex].
192. ATLAS Collab. (G. Aad *et al.*), *Eur. Phys. J. C* **73**, 2328 (2013), arXiv:1211.7205 [hep-ex].
193. ATLAS Collab. (G. Aad *et al.*), *Phys. Lett. B* **717**, 89 (2012), arXiv:1205.2067 [hep-ex].
194. CMS Collab. (S. Chatrchyan *et al.*), *Phys. Lett. B* **720**, 83 (2013), arXiv:1212.6682 [hep-ex].
195. CMS Collab. (S. Chatrchyan *et al.*), *Phys. Rev. D* **84**, 092004 (2011), arXiv:1108.3773 [hep-ex].
196. CMS Collab. (S. Chatrchyan *et al.*), *Eur. Phys. J. C* **71**, 1721 (2011), arXiv:1106.0902 [hep-ex].
197. CMS Collab. (S. Chatrchyan *et al.*), *J. High Energy Phys.* **11**, 067 (2012), arXiv:1208.2671 [hep-ex].
198. CMS Collab. (S. Chatrchyan *et al.*), *J. High Energy Phys.* **07**, 049 (2011), arXiv:1105.5661 [hep-ex].
199. CMS Collab. (S. Chatrchyan *et al.*), *Phys. Lett. B* **695**, 424 (2011), arXiv:1010.5994 [hep-ex].
200. CMS Collab. (S. Chatrchyan *et al.*), *Eur. Phys. J. C.* **73**, 2386 (2013), arXiv:1301.5755 [hep-ex].
201. CMS Collab. (S. Chatrchyan *et al.*), *Phys. Rev. D* **85**, 112007 (2012), arXiv:1203.6810 [hep-ex].
202. CMS Collab. (S. Chatrchyan *et al.*), *J. High Energy Phys.* **1305**, 065 (2013), arXiv:1302.0508 [hep-ex].
203. L. Lyons, D. Gibaut and P. Clifford, *Nucl. Instrum. Methods A* **270**, 110 (1988).
204. L. Lyons, A. Martin and D. Saxon, *Phys. Rev. D* **41**, 3 (1990).
205. CDF and DØ Collab. (T. Aaltonen *et al.*), DØ Note 6363.
206. ATLAS Collab. (G. Aad *et al.*), ATLAS NOTE, ATLAS-CONF-2012-024 (2012).
207. ATLAS and CMS Collabs., ATLAS-CONF-2012-134.
208. CDF Collab. (T. Aaltonen *et al.*), submitted to *Phys. Rev. Lett.* (2013).
209. CDF Collab. (D. Acosta *et al.*), *Phys. Rev. Lett.* **95**, 102002 (2005), arXiv:hep-ex/0505091 [hep-ex].
210. DØ Collab. (V. M. Abazov *et al.*), *Phys. Rev. Lett.* **107**, 121802 (2011), arXiv:1106.5436 [hep-ex].
211. DØ Collab. (V. M. Abazov *et al.*), *Phys. Rev. D* **80**, 071102(R) (2009).
212. DØ Collab. (V. M. Abazov *et al.*), *Phys. Rev. Lett.* **100**, 192003 (2008).
213. S. Frixione, P. Nason and G. Ridolfi, *J. High Energy Phys.* **09**, 126 (2007), arXiv:0707.3088 [hep-ph].
214. S. Frixione and B. R. Webber, *J. High Energy Phys.* **06**, 029 (2002).
215. M. L. Mangano, M. Moretti, F. Piccinini, R. Pittau and A. D. Polosa, *J. High Energy Phys.* **07**, 001 (2003).
216. T. Gleisberg *et al.*, *J. High Energy Phys.* **0902**, 007 (2009), arXiv:0811.4622 [hep-ph].
217. ATLAS Collab. (G. Aad *et al.*), *Eur. Phys. J. C* **72**, 2043 (2012), arXiv:1203.5015 [hep-ex].
218. G. J. Feldman and R. D. Cousins, *Phys. Rev. D* **57**, 3873 (1998).
219. CDF Collab. (T. Aaltonen *et al.*), *Phys. Rev. D* **78**, 111101 (2008).
220. CDF Collab. (T. Aaltonen *et al.*), *Phys. Rev. D* **79**, 031101 (2009), arXiv:0807.4262 [hep-ex].

221. CDF Collab. (T. Aaltonen *et al.*), *Phys. Rev. D* **84**, 031104 (2011), arXiv:1106.3970 [hep-ex].
222. D. Colladay and V. A. Kostelecký, *Phys. Rev. D* **58**, 116002 (1998).
223. V. A. Kostelecký, *Phys. Rev. D* **69**, 105009 (2004).
224. DØ Collab. (V. M. Abazov *et al.*), *Phys. Rev. Lett.* **108**, 261603 (2012), arXiv:1203.6106 [hep-ex].
225. C. T. Hill and S. J. Parke, *Phys. Rev. D* **49**, 4454 (1994).
226. D. Atwood *et al.*, *Phys. Rev. D* **52**, 6264 (1995).
227. CDF Collab. (T. Aaltonen *et al.*), *Phys. Rev. Lett.* **102**, 222003 (2009), arXiv:0903.2850 [hep-ex].
228. DØ Collab. (V. M. Abazov *et al.*), *Phys. Lett. B* **693**, 515 (2010), arXiv:1001.1900 [hep-ex].
229. ATLAS Collab. (G. Aad *et al.*), *Eur. Phys. J. C* **73**, 2261 (2013), arXiv:1207.5644v2 [hep-ex].
230. CMS Collab. (S. Chatrchyan *et al.*), *Eur. Phys. J. C* **73**, 2339 (2013), arXiv:1211.2220 [hep-ex].
231. CDF Collab. (F. Abe *et al.*), *Phys. Rev. Lett.* **79**, 1992 (1997).
232. CDF Collab. (F. Abe *et al.*), *Phys. Rev. Lett.* **80**, 2767 (1998).
233. CDF Collab. (F. Abe *et al.*), *Phys. Rev. Lett.* **80**, 2779 (1998).
234. CDF Collab. (F. Abe *et al.*), *Phys. Rev. Lett.* **82**, 271 (1999).
235. CDF Collab. (T. Affolder *et al.*), *Phys. Rev. D* **63**, 032003 (2001).
236. CDF Collab. (F. Abe *et al.*), *Phys. Rev. Lett.* **82**, 2808 (1999) [Erratum].
237. CDF Collab. (T. Aaltonen *et al.*), *Phys. Rev. Lett.* **109**, 152003 (2012), arXiv:1207.6758 [hep-ex].
238. CDF Collab. (T. Aaltonen *et al.*), *Phys. Rev. D* **84**, 071105 (2011), arXiv:1108.1601 [hep-ex]
239. CDF Collab. (T. Aaltonen *et al.*), *Phys. Rev. D* **83**, 111101 (2011), arXiv:1105.0192 [hep-ex].
240. CDF Collab. (T. Aaltonen *et al.*), *Phys. Lett. B* **698**, 371 (2011), arXiv:1101.4926 [hep-ex].
241. CDF Collab. (T. Aaltonen *et al.*), *Phys. Rev. Lett.* **105**, 252001 (2010), arXiv:1010.4582 [hep-ex].
242. CDF Collab. (T. Aaltonen *et al.*), *Phys. Rev. D* **79**, 072005 (2009), arXiv:0901.3773 [hep-ex].
243. CDF Collab. (T. Aaltonen *et al.*), *Phys. Rev. D* **79**, 072001 (2009), arXiv:0812.4469 [hep-ex].
244. CDF Collab. (T. Aaltonen *et al.*), *Phys. Rev. D* **81**, 031102 (2010), arXiv:0911.2956 [hep-ex].
245. CDF Collab. (T. Aaltonen *et al.*), *Phys. Rev. Lett.* **102**, 152001 (2009), arXiv:0807.4652 [hep-ex].
246. CDF Collab. (T. Aaltonen *et al.*), *Phys. Lett. B* **714**, 24 (2012), arXiv:1112.4891 [hep-ex].
247. CDF Collab. (T. Aaltonen *et al.*), *Phys. Rev. D* **79**, 072010 (2009), arXiv:0811.1062 [hep-ex].
248. CDF Collab. (T. Aaltonen *et al.*), *Phys. Rev. Lett.* **107**, 232002 (2011), arXiv:1109.1490 [hep-ex].
249. CDF Collab. (T. Aaltonen *et al.*), *Phys. Rev. D* **81**, 032002 (2010), arXiv:0910.0969 [hep-ex].
250. CDF Collab. (T. Aaltonen *et al.*), *Phys. Rev. D* **80**, 051104 (2009), arXiv:0906.5371 [hep-ex].

251. CDF Collab. (T. Aaltonen *et al.*), *Phys. Rev. D* **79**, 092005 (2009), arXiv:0809.4808 [hep-ex].
252. DØ Collab. (S. Abachi *et al.*), *Phys. Rev. Lett.* **79**, 1197 (1997).
253. DØ Collab. (B. Abbott *et al.*), *Phys. Rev. D* **58**, 052001 (1998).
254. DØ Collab. (B. Abbott *et al.*), *Phys. Rev. Lett.* **80**, 2063 (1998).
255. DØ Collab. (B. Abbott *et al.*), *Phys. Rev. D* **60**, 052001 (1999).
256. DØ Collab. (V. M. Abazov *et al.*), *Nature* **429**, 638 (2004).
257. DØ Collab. (V. M. Abazov *et al.*), *Phys. Lett. B* **606**, 25 (2005).
258. DØ Collab. (V. M. Abazov *et al.*), *Phys. Rev. D* **84**, 032004 (2011), arXiv:1105.6287 [hep-ex].
259. DØ Collab. (V. M. Abazov *et al.*), *Phys. Rev. Lett.* **101**, 182001 (2008), arXiv:0807.2141 [hep-ex].
260. DØ Collab. (V. M. Abazov *et al.*), *Phys. Rev. D* **86**, 051103(R) (2012), arXiv:1201.5172 [hep-ex].
261. DØ Collab. (V. M. Abazov *et al.*), *Phys. Rev. Lett.* **107**, 082004 (2011), arXiv:1105.0320 [hep-ex].
262. DØ Collab. (V. M. Abazov *et al.*), *Phys. Rev. D* **80**, 092006 (2009), arXiv:0904.3195 [hep-ex].
263. ATLAS Collab. (G. Aad *et al.*), *Eur. Phys. J. C* **72**, 2046 (2012), arXiv:1203.5755 [hep-ex].
264. CMS Collab. (S. Chatrchyan *et al.*), *J. High Energy Phys.* **12**, 105 (2012), arXiv:1209.2319 [hep-ex].
265. CMS Collab. (S. Chatrchyan *et al.*), *Eur. Phys. J. C* **72**, 2202 (2012), arXiv:1209.2393 [hep-ex].
266. CMS Collab. (S. Chatrchyan *et al.*), *Eur. Phys. J. C* **73**, 2494 (2013), arXiv:1304.5783 [hep-ex].
267. CDF and DØ Collabs. (T. Aaltonen *et al.*), arXiv:1305.3929v1 [hep-ex].
268. CDF and DØ Collabs. (T. Aaltonen *et al.*), *Phys. Rev. D* **86**, 092003 (2012), arXiv:1207.1069 [hep-ex].
269. M. Beneke and V. M. Braun, *Nucl. Phys. B* **426**, 301 (1994).
270. I. I. Y. Bigi, M. A. Shifman, N. G. Uraltsev and A. I. Vainshtein, *Phys. Rev. D* **50**, 2234 (1994).
271. M. C. Smith and S. S. Willenbrock, *Phys. Rev. Lett.* **79**, 3825 (1997).
272. P. Z. Skands and D. Wicke, *Eur. Phys. J. C* **52**, 133 (2007), arXiv:hep-ph/0703081 [hep-ph].
273. A. Buckley *et al.*, *Phys. Rep.* **504**, 145 (2011).
274. DØ Collab. (V. M. Abazov *et al.*), *Phys. Lett. B* **703**, 422 (2011), arXiv:1104.2887 [hep-ex].
275. CMS Collab. (S. Chatrchyan *et al.*), submitted to *Phys. Lett. B* arXiv:1307.1907 [hep-ex].
276. S. Fleming, A. H. Hoang, S. Mantry and I. W. Stewart, *Phys. Rev. D* **77**, 074010 (2008), arXiv:hep-ph/0703207.
277. CDF Collab. (T. Aaltonen *et al.*), *Phys. Rev. D* **87**, 052013 (2013), arXiv:1210.6131 [hep-ex].
278. CDF Collab. (T. Aaltonen *et al.*), *Phys. Rev. Lett.* **106**, 152001 (2011), arXiv:1103.2782 [hep-ex].
279. DØ Collab. (V. M. Abazov *et al.*), *Phys. Rev. D* **84**, 052005 (2011), arXiv:1106.2063 [hep-ex].
280. DØ Collab. (V. M. Abazov *et al.*), *Phys. Rev. Lett.* **103**, 132001 (2009), arXiv:0906.1172 [hep-ex].

281. DØ Collab. (V. M. Abazov *et al.*), *J. High Energy Phys.* **06**, 109 (2012), arXiv:1204.2807 [hep-ex].
282. D. Chang, W.-F. Chang and E. Ma, *Phys. Rev. D* **59**, 091503 (1999).
283. U. Baur, M. Buice and L. H. Orr, *Phys. Rev. D* **64**, 094019 (2001), arXiv:hep-ph/0106341 [hep-ph].
284. DØ Collab. (V. M. Abazov *et al.*), *Phys. Rev. Lett.* **98**, 041801 (2007), arXiv:hep-ex/0608044.
285. CDF Collab. (T. Aaltonen *et al.*), *Phys. Rev. Lett.* **105**, 101801 (2010), arXiv:1006.4597 [hep-ex].
286. CDF Collab. (T. Aaltonen *et al.*), *Phys. Rev. Lett.* **105**, 101801 (2010).
287. ATLAS Collab., ATLAS NOTE, ATLAS-CONF-2011-141 (2011).
288. CMS Collab., CMS physics analysis summary, CMS-PAS-TOP-11-031 (2012).
289. V. Barger, J. Ohnemus and R. Phillips, *Int. J. Mod. Phys. A* **4**, 617 (1989).
290. T. Arens and L. M. Sehgal, *Phys. Lett. B* **302**, 501 (1993).
291. G. Mahlon and S. Parke, *Phys. Rev. D* **53**, 4886 (1996), arXiv:hep-ph/9512264.
292. T. Stelzer and S. Willenbrock, *Phys. Lett. B* **374**, 169 (1996), arXiv:hep-ph/9512292.
293. A. Brandenburg, *Phys. Lett. B* **388**, 626 (1996), arXiv:hep-ph/9603333.
294. D. Chang, S. C. Lee and A. Soumarokov, *Phys. Rev. Lett.* **77**, 1218 (1996), arXiv:hep-ph/9512417.
295. G. Mahlon and S. Parke, *Phys. Lett. B* **411**, 173 (1997), arXiv:hep-ph/9706304.
296. G. L. Kane, G. Ladinsky and C. Yuan, *Phys. Rev. D* **45**, 124 (1992).
297. K. Cheung, *Phys. Rev. D* **55**, 4430 (1997), arXiv:hep-ph/9610368.
298. W. Bernreuther, M. Flesch and P. Haberl, *Phys. Rev. D* **58**, 114031 (1998), arXiv:hep-ph/9709284.
299. B. Holdom and T. Torma, *Phys. Rev. D* **60**, 114010 (1999), arXiv:hep-ph/9906208.
300. M. Arai, N. Okada, K. Smolek and V. Simak, *Phys. Rev. D* **70**, 115015 (2004), arXiv:hep-ph/0409273.
301. P. Uwer, *Phys. Lett. B* **609**, 271 (2005), arXiv:hep-ph/0412097.
302. M. Arai, N. Okada, K. Smolek and V. Simak, *Phys. Rev. D* **75**, 095008 (2007), arXiv:hep-ph/0701155.
303. M. Arai, N. Okada and K. Smolek, *Phys. Rev. D* **79**, 074019 (2009), arXiv:0902.0418 [hep-ph].
304. G. Mahlon and S. Parke, *Phys. Rev. D* **81**, 074024 (2010), arXiv:1001.3422 [hep-ph].
305. S. Fajfer, J. F. Kamenik and B. Melic, *J. High Energy Phys.* **1208**, 114 (2012), arXiv:1205.0264 [hep-ph].
306. CDF Collab. (T. Aaltonen *et al.*), *Phys. Rev. D* **83**, 031104 (2011), arXiv:1012.3093 [hep-ex].
307. DØ Collab. (V. M. Abazov *et al.*), *Phys. Rev. Lett.* **108**, 032004 (2012), arXiv:1110.4194 [hep-ex].
308. DØ Collab. (V. M. Abazov *et al.*), *Phys. Rev. Lett.* **107**, 032001 (2011), arXiv:1104.5194 [hep-ex].
309. DØ Collab. (V. M. Abazov *et al.*), *Phys. Lett. B* **702**, 16 (2011), arXiv:1103.1871 [hep-ex].
310. ATLAS Collab. (G. Aad *et al.*), *Phys. Rev. Lett.* **108**, 212001 (2012), arXiv:1203.4081 [hep-ex].
311. F. Halzen, P. Hoyer and C. S. Kim, *Phys. Lett. B* **195**, 74 (1987).
312. J. H. Kuhn and G. Rodrigo, *Phys. Rev. Lett.* **81**, 49 (1998), arXiv:hep-ph/9802268.
313. J. H. Kuhn and G. Rodrigo, *Phys. Rev. D* **59**, 054017 (1999), arXiv:hep-ph/9807420.
314. O. Antunano, J. H. Kuhn and G. Rodrigo, *Phys. Rev. D* **77**, 014003 (2008), arXiv:0709.1652.

315. M. T. Bowen, S. D. Ellis and D. Rainwater, *Phys. Rev. D* **73**, 014008 (2006), arXiv:hep-ph/0509267.
316. L. G. Almeida, G. F. Sterman and W. Vogelsang, *Phys. Rev. D* **78**, 014008 (2008), arXiv:0805.1885 [hep-ph].
317. O. Antunano, J. H. Kuhn and G. V. Rodrigo, *Phys. Rev. D* **77**, 014003 (2008), arXiv:0709.1652 [hep-ph].
318. W. Hollik and D. Pagani, *Phys. Rev. D* **84**, 093003 (2011), arXiv:1107.2606 [hep-ph].
319. V. Ahrens, A. Ferroglia, M. Neubert, B. D. Pecjak and L. L. Yang, *Phys. Rev. D* **84**, 074004 (2011), arXiv:1106.6051 [hep-ph].
320. N. Kidonakis, *Phys. Rev. D* **84**, 011504 (2011), arXiv:1105.5167 [hep-ph].
321. J. H. Kuhn and G. Rodrigo, *J. High Energy Phys.* **1201**, 063 (2012), arXiv:1109.6830 [hep-ph].
322. A. V. Manohar and M. Trott, *Phys. Lett. B* **711**, 313 (2012), arXiv:1201.3926 [hep-ph].
323. W. Bernreuther and Z.-G. Si, *Phys. Rev. D* **86**, 034026 (2012), arXiv:1205.6580 [hep-ph].
324. J. L. Rosner, *Phys. Lett. B* **387**, 113 (1996), arXiv:hep-ph/9607207.
325. P. Ferrario and G. Rodrigo, *Phys. Rev. D* **78**, 094018 (2008), arXiv:0809.3354 [hep-ph].
326. R. Diener, S. Godfrey and T. A. Martin, *Phys. Rev. D* **80**, 075014 (2009), arXiv:0909.2022 [hep-ph].
327. P. H. Frampton, J. Shu and K. Wang, *Phys. Lett. B* **683**, 294 (2010), arXiv:0911.2955 [hep-ph].
328. J. Aguilar-Saavedra and M. Perez-Victoria, *Phys. Rev. D* **84**, 115013 (2011), arXiv:1105.4606 [hep-ph].
329. J. Aguilar-Saavedra and M. Perez-Victoria, *J. High Energy Phys.* **1109**, 097 (2011), arXiv:1107.0841 [hep-ph].
330. J. A. Aguilar-Saavedra and M. Perez-Victoria, *Phys. Rev. D* **84**, 115013 (2011), arXiv:1105.4606 [hep-ph].
331. S. Jung, A. Pierce and J. D. Wells, *Phys. Rev. D* **83**, 114039 (2011), arXiv:1103.4835 [hep-ph].
332. G. Brooijmans *et al.* (eds.), Les Houches 2011: Physics at TeV Colliders New Physics Working Group Report, arXiv:1203.1488 [hep-ph].
333. J. A. Aguilar-Saavedra, in *Proc. of TOP2011, 4th Int. Workshop on Top Quark Physics*, Sant Feliu de Guixols, Spain, 25–30th September 2011, arXiv:1202.2382 [hep-ph].
334. P. Z. Skands, B. R. Webber and J. Winter, *J. High Energy Phys.* **1207**, 151 (2012), arXiv:1205.1466 [hep-ph].
335. E. Gabrielli, M. Raidal and A. Racioppi, *Phys. Rev. D* **85**, 074021 (2012), arXiv:1112.5885 [hep-ph].
336. J. F. Kamenik, J. Shu and J. Zupan, *Eur. Phys. J. C* **72**, 2102 (2012), arXiv:1107.5257 [hep-ph].
337. CDF Collab. (T. Aaltonen *et al.*), *Phys. Rev. D* **87**, 092002 (2013), arXiv:1211.1003 [hep-ex].
338. CDF Collab. (T. Aaltonen *et al.*), *Phys. Rev. D* **83**, 112003 (2011), arXiv:1101.0034 [hep-ex].
339. DØ Collab. (V. M. Abazov *et al.*), *Phys. Rev. D* **87**, 011103(R) (2013), arXiv:1207.0364 [hep-ex].

340. DØ Collab. (V. M. Abazov *et al.*), *Phys. Rev. D* **84**, 112005 (2011), arXiv:1107.4995 [hep-ex].
341. DØ Collab. (V. M. Abazov *et al.*), *Phys. Rev. Lett.* **100**, 142002 (2008), arXiv:0712.0851 [hep-ex].
342. ATLAS Collab. (G. Aad *et al.*), *Eur. Phys. J. C* **72**, 2039 (2012), arXiv:1203.4211 [hep-ex].
343. CMS Collab. (S. Chatrchyan *et al.*), *Phys. Lett. B* **717**, 129 (2012), arXiv:1207.0065 [hep-ex].
344. CMS Collab. (S. Chatrchyan *et al.*), *Phys. Lett. B* **709**, 28 (2012), arXiv:1112.5100 [hep-ex].
345. CDF Collab. (T. Aaltonen *et al.*), *Phys. Rev. Lett.* **105**, 232003 (2010), arXiv:1008.3891 [hep-ex].
346. CDF Collab. (T. Aaltonen *et al.*), *Phys. Rev. Lett.* **102**, 042001 (2009), arXiv:0808.2167 [hep-ex].
347. DØ Collab. (V. M. Abazov *et al.*), *Phys. Rev. D* **85**, 091104 (2012), arXiv:1201.4156 [hep-ex].
348. DØ Collab. (V. M. Abazov *et al.*), *Phys. Rev. Lett.* **106**, 022001 (2011), arXiv:1009.5686 [hep-ex].
349. G. Kane, G. Ladinsky and C.-P. Yuan, *Phys. Rev. D* **45**, 124 (1992).
350. C. R. Chen, F. Larios and C.-P. Yuan, *Phys. Lett. B* **631**, 126 (2005).
351. M. Fischer, S. Groote, J. G. Korner and M. C. Mauser, *Phys. Rev. D* **63**, 031501(R) (2001).
352. H. S. Do, S. Groote, J. G. Korner and M. C. Mauser, *Phys. Rev. D* **67**, 091501(R) (2003).
353. J. Aguilar-Saavedra, J. Carvalho, N. F. Castro, F. Veloso and A. Onofre, *Eur. Phys. J. C* **50**, 519 (2007).
354. C. Zhang, N. Greiner and S. Willenbrock, arXiv:1201.6670 [hep-ph].
355. C. Zhang and S. Willenbrock, *Phys. Rev. D* **83**, 034006 (2011).
356. J. A. Aguilar-Saavedra, *Nucl. Phys. B* **804**, 160 (2008), arXiv:0803.3810 [hep-ph].
357. J. A. Aguilar-Saavedra, *Nucl. Phys. B* **812**, 181 (2009).
358. J. Aguilar-Saavedra, N. Castro and A. Onofre, *Phys. Rev. D* **83**, 117301 (2011), arXiv:1105.0117 [hep-ph].
359. J. A. Aguilar-Saavedra, J. Carvalho, N. Castro, A. Onofre and F. Veloso, *Eur. Phys. J. C* **50**, 519 (2007), arXiv:hep-ph/0605190.
360. CDF Collab. (T. Aaltonen *et al.*), *Phys. Rev. D* **87**, 031104(R) (2013), arXiv:1211.4523 [hep-ex].
361. CDF Collab. (T. Aaltonen *et al.*), *Phys. Rev. Lett.* **105**, 042002 (2010), arXiv:1003.0224 [hep-ex].
362. CDF Collab. (T. Aaltonen *et al.*), *Phys. Lett. B* **479**, 160 (2009), arXiv:0811.0344 [hep-ex].
363. DØ Collab. (V. M. Abazov *et al.*), *Phys. Rev. D* **83**, 032009 (2011), arXiv:1011.6549 [hep-ex].
364. DØ Collab. (V. M. Abazov *et al.*), *Phys. Rev. Lett.* **100**, 062004 (2008), arXiv:0711.0032 [hep-ex].
365. CDF and DØ Collabs. (T. Aaltonen *et al.*), *Phys. Rev. D* **85**, 071106 (2012), arXiv:1202.5272 [hep-ex].
366. DØ Collab. (V. M. Abazov *et al.*), *Phys. Lett. B* **713**, 165 (2012), arXiv:1204.2332 [hep-ex].
367. DØ Collab. (V. M. Abazov *et al.*), *Phys. Lett. B* **708**, 21 (2012), arXiv:1110.4592 [hep-ex].

368. DØ Collab. (V. M. Abazov *et al.*), *Phys. Rev. Lett.* **102**, 092002 (2009), arXiv:0901.0151 [hep-ex].
369. DØ Collab. (V. M. Abazov *et al.*), *Phys. Rev. Lett.* **101**, 221801 (2008), arXiv:0807.1692 [hep-ex].
370. ATLAS Collab. (G. Aad *et al.*), *J. High Energy Phys.* **06**, 088 (2012), arXiv:1205.2484 [hep-ex].
371. ATLAS and CMS Collabs. (G. Aad *et al.*), ATLAS-CONF-2013-033, CMS PAS TOP-12-025.
372. J. Gallicchio and M. D. Schwartz, *Phys. Rev. Lett.* **105**, 022001 (2010).
373. DØ Collab. (V. M. Abazov *et al.*), *Phys. Rev. D* **83**, 092002 (2011), arXiv:1101.0648 [hep-ex].
374. J. Alwall *et al.*, *Eur. Phys. J. C* **49**, 791 (2007).
375. Q.-H. Cao, J. Wudka and C.-P. Yuan, *Phys. Lett. B* **658**, 50 (2007), arXiv:0704.2809 [hep-ph].
376. T. Tait and C.-P. Yuan, *Phys. Rev. D* **63**, 014018 (2001), arXiv:hep-ph/0007298.
377. N. Cabibbo, *Phys. Rev. Lett.* **10**, 531 (1963).
378. M. Kobayashi and T. Maskawa, *Prog. Theor. Phys.* **49**, 652 (1973).
379. CDF Collab. (T. Aaltonen *et al.*), *Phys. Rev. D* **82**, 112005 (2010), arXiv:1004.1181 [hep-ex].
380. CDF Collab. (T. Aaltonen *et al.*), *Phys. Rev. D* **81**, 072003 (2010), arXiv:1001.4577 [hep-ex].
381. CDF Collab. (T. Aaltonen *et al.*), *Phys. Rev. Lett.* **103**, 092002 (2009), arXiv:0903.0885 [hep-ex].
382. CDF Collab. (T. Aaltonen *et al.*), *Phys. Rev. Lett.* **101**, 252001 (2008), arXiv:0809.2581 [hep-ex].
383. DØ Collab. (V. M. Abazov *et al.*), submitted to *Phys. Lett. B*, arXiv:1307.0731 [hep-ex].
384. DØ Collab. (V. M. Abazov *et al.*), *Phys. Rev. D* **84**, 112001 (2011), arXiv:1108.3091 [hep-ex].
385. DØ Collab. (V. M. Abazov *et al.*), *Phys. Lett. B* **705**, 313 (2011), arXiv:1105.2788 [hep-ex].
386. DØ Collab. (V. M. Abazov *et al.*), *Phys. Lett. B* **690**, 5 (2010), arXiv:0912.1066 [hep-ex].
387. DØ Collab. (V. M. Abazov *et al.*), *Phys. Lett. B* **682**, 363 (2010), arXiv:0907.4259 [hep-ex].
388. DØ Collab. (V. M. Abazov *et al.*), *Phys. Rev. Lett.* **103**, 092001 (2009), arXiv:0903.0850 [hep-ex].
389. DØ Collab. (V. M. Abazov *et al.*), *Phys. Rev. D* **78**, 012005 (2008), arXiv:0803.0739 [hep-ex].
390. DØ Collab. (V. M. Abazov *et al.*), *Phys. Rev. Lett.* **98**, 181802 (2007), arXiv:hep-ex/0612052.
391. DØ Collab. (V. M. Abazov *et al.*), *Phys. Lett. B* **690**, 5 (2010).
392. ATLAS Collab. (G. Aad *et al.*), *Phys. Lett. B* **717**, 330 (2012), arXiv:1205.3130 [hep-ex].
393. ATLAS Collab. (G. Aad *et al.*), *Phys. Lett. B* **716**, 142 (2012), arXiv:1205.5764 [hep-ex].
394. CMS Collab. (S. Chatrchyan *et al.*), *J. High Energy Phys.* **12**, 035 (2012), arXiv:1209.4533 [hep-ex].
395. CMS Collab. (S. Chatrchyan *et al.*), to be published in *Phys. Rev. Lett.*, arXiv:1209.3489 [hep-ex].

396. CMS Collab. (S. Chatrchyan *et al.*), *Phys. Rev. Lett.* **107**, 091802 (2011), arXiv:1106.3052 [hep-ex].
397. CDF and DØ Collabs. (T. Aaltonen *et al.*), arXiv:0908.2171 [hep-ex].
398. U. Aglietti *et al.*, arXiv:hep-ph/0612172.
399. LHC Higgs Cross Section Working Group, arXiv:1101.0593 [hep-ph].
400. LHC Higgs Cross Section Working Group, arXiv:1201.3084 [hep-ph].
401. LHC Higgs Cross Section Working Group, https://twiki.cern.ch/twiki/bin/view/LHCPhysics/CrossSections.
402. A. Djouadi, arXiv:1203.4199 [hep-ph].
403. J. Ellis, M. K. Gaillard and D. V. Nanopoulos, *Nucl. Phys. B* **106**, 292 (1976).
404. H. M. Georgi, S. L. Glashow, M. E. Machacek and D. V. Nanopoulos, *Phys. Rev. Lett.* **40**, 692 (1978).
405. A. Djouadi, M. Spira and P. M. Zerwas, *Phys. Lett. B* **264**, 440 (1991).
406. S. Dawson, *Nucl. Phys. B* **359**, 283 (1991).
407. M. Spira, A. Djouadi, D. Graudenz and P. M. Zerwas, *Nucl. Phys. B* **453**, 17 (1995).
408. R. V. Harlander and W. B. Kilgore, *Phys. Rev. Lett.* **88**, 201801 (2002).
409. C. Anastasiou and K. Melnikov, *Nucl. Phys. B* **646**, 220 (2002).
410. R. V. Harlander and W. B. Kilgore, *Phys. Rev. Lett.* **88**, 201801 (2002), arXiv:hep-ph/0201206.
411. C. Anastasiou and K. Melnikov, *Nucl. Phys. B* **646**, 220 (2002), arXiv:hep-ph/0207004.
412. V. Ravindran, J. Smith and W. L. van Neerven, *Nucl. Phys. B* **665**, 325 (2003).
413. U. Aglietti, R. Bonciani, G. Degrassi and A. Vicini, *Phys. Lett. B* **595**, 432 (2004), arXiv:hep-ph/0404071.
414. G. Degrassi and F. Maltoni, *Phys. Lett. B* **600**, 255 (2004), arXiv:hep-ph/0407249.
415. S. Actis, G. Passarino, C. Sturm and S. Uccirati, *Phys. Lett. B* **670**, 12 (2008), arXiv:0809.1301 [hep-ph].
416. S. Catani, D. de Florian, M. Grazzini and P. Nason, *J. High Energy Phys.* **0307**, 028 (2003).
417. V. Ravindran, J. Smith and W. L. van Neerven, *Nucl. Phys. B* **665**, 325 (2003), arXiv:hep-ph/0302135.
418. D. de Florian and M. Grazzini, *Phys. Lett. B* **674**, 291 (2009), arXiv:0901.2427 [hep-ph].
419. C. Anastasiou, R. Boughezal and F. Petriello, *J. High Energy Phys.* **0904**, 003 (2009), arXiv:0811.3458 [hep-ph].
420. D. de Florian and M. Grazzini, *Phys. Lett. B* **718**, 117 (2012), arXiv:1206.4133 [hep-ph].
421. C. Anastasiou, S. Buehler, F. Herzog and A. Lazopoulos, *J. High Energy Phys.* **1204**, 004 (2012), arXiv:1202.3638 [hep-ph].
422. J. Baglio and A. Djouadi, *J. High Energy Phys.* **1103**, 055 (2011).
423. R. N. Cahn and S. Dawson, *Phys. Lett. B* **136**, 196 (1984) [Erratum: *ibid.* **138**, 464 (1984)].
424. T. Figy, C. Oleari and D. Zeppenfeld, *Phys. Rev. D* **68**, 073005 (2003), arXiv:hep-ph/0306109.
425. M. Ciccolini, A. Denner and S. Dittmaier, *Phys. Rev. Lett.* **99**, 161803 (2007), arXiv:0707.0381 [hep-ph].
426. M. Ciccolini, A. Denner and S. Dittmaier, *Phys. Rev. D* **77**, 013002 (2008), arXiv:0710.4749 [hep-ph].

427. K. Arnold *et al.*, *Comput. Phys. Commun.* **180**, 1661 (2009), arXiv:0811.4559 [hep-ph].
428. J. Baglio and A. Djouadi, *J. High Energy Phys.* **10**, 064 (2010).
429. O. Brein, R. V. Harlander, M. Weisemann and T. Zirke, *Eur. Phys. J. C* **72**, 1868 (2012).
430. P. Bolzoni, F. Maltoni, S.-O. Moch and M. Zaro, *Phys. Rev. Lett.* **105**, 011801 (2010), arXiv:1003.4451 [hep-ph].
431. S. L. Glashow, D. V. Nanopoulos and A. Yildiz, *Phys. Rev. D* **18**, 1724 (1978).
432. T. Han and S. Willenbrock, *Phys. Lett. B* **273**, 167 (1991).
433. O. Brein, A. Djouadi and R. Harlander, *Phys. Lett. B* **579**, 149 (2004), arXiv:hep-ph/0307206.
434. M. L. Ciccolini, S. Dittmaier and M. Krämer, *Phys. Rev. D* **68**, 073003 (2003), arXiv:hep-ph/0306234.
435. R. Hamberg, W. L. van Neerven and T. Matsuura, *Nucl. Phys. B* **359**, 343 (1991).
436. A. Denner *et al.*, *J. High Energy Phys.* **1203**, 075 (2012), arXiv:1112.5142 [hep-ph].
437. G. Ferrera, M. Grazzini and F. Tramontano, *Phys. Rev. Lett.* **107**, 152003 (2011), arXiv:1107.1164 [hep-ph].
438. Z. Kunszt, *Nucl. Phys. B* **247**, 339 (1984), arXiv:hep-ph/0107081.
439. W. Beenakker *et al.*, *Phys. Rev. Lett.* **87**, 201805 (2001).
440. W. Beenakker *et al.*, *Nucl. Phys. B* **653**, 151 (2003), arXiv:hep-ph/0211352.
441. S. Dawson, L. H. Orr, L. Reina and D. Wackeroth, *Phys. Rev. D* **67**, 071503 (2003), arXiv:hep-ph/0211438.
442. S. Dawson, C. Jackson, L. H. Orr, L. Reina and D. Wackeroth, *Phys. Rev. D* **68**, 034022 (2003), arXiv:hep-ph/0305087.
443. A. Bredenstein, A. Denner, S. Dittmaier and M. M. Weber, *Phys. Rev. D* **74**, 013004 (2006), arXiv:hep-ph/0604011.
444. A. Bredenstein, A. Denner, S. Dittmaier and M. M. Weber, *J. High Energy Phys.* **0702**, 080 (2007), arXiv:hep-ph/0604011.
445. A. Djouadi, J. Kalinowski and M. Spira, *Comput. Phys. Commun.* **108**, 56 (1998), arXiv:hep-ph/9704448.
446. A. Djouadi *et al.*, arXiv:1003.1643 [hep-ph].
447. S. Alekhin *et al.*, arXiv:1101.0536 [hep-ph].
448. M. Botje *et al.*, arXiv:1101.0538 [hep-ph].
449. H.-L. Lai *et al.*, *Phys. Rev. D* **82**, 074024 (2010), arXiv:1007.2241 [hep-ph].
450. A. D. Martin *et al.*, *Eur. Phys. J. C* **63**, 189 (2009), arXiv:0901.0002 [hep-ph].
451. NNPDF Collab., *Nucl. Phys. B* **849**, 296 (2011), arXiv:1101.1300 [hep-ph].
452. L. Maiani, G. Parisi and R. Petronzio, *Nucl. Phys. B* **136**, 115 (1978).
453. M. Lindner, *Z. Phys. C* **31**, 295 (1986).
454. M. Lindner, M. Sher and H. W. Zaglauer, *Phys. Lett. B* **228**, 139 (1989).
455. M. Sher, *Phys. Rep.* **179**, 273 (1989).
456. G. Altarelli and G. Isidori, *Phys. Lett. B* **337**, 141 (1994).
457. J. A. Casas, J. R. Espinosa and M. Quiros, *Phys. Lett. B* **342**, 171 (1995), arXiv:hep-ph/9409458.
458. J. A. Casas, J. R. Espinosa and M. Quiros, *Phys. Lett. B* **382**, 374 (1996), arXiv:hep-ph/9603227.
459. J. Ellis *et al.*, *Phys. Lett. B* **679**, 369 (2009), arXiv:0906.0954 [hep-ph].
460. R. Barate *et al.*, *Phys. Lett. B* **565**, 61 (2003), arXiv:hep-ex/0306033.
461. CDF and DØ Collabs. (T. Aaltonen *et al.*), *Phys. Rev. Lett.* **109**, 071804 (2012), arXiv:1207.6436 [hep-ex].

462. CDF and DØ Collabs. (T. Aaltonen *et al.*), submitted to *Phys. Rev. D*, arXiv:1303.6346 [hep-ex].
463. CDF Collab. (T. Aaltonen *et al.*), *Phys. Rev. Lett.* **109**, 111804 (2012).
464. CDF Collab. (T. Aaltonen *et al.*), *Phys. Rev. D* **87**, 052008 (2013), arXiv:1301.4440 [hep-ex].
465. CDF Collab. (T. Aaltonen *et al.*), *Phys. Rev. Lett.* **109**, 111803 (2012).
466. CDF Collab. (T. Aaltonen *et al.*), *J. High Energy Phys.* **02**, 004 (2013).
467. CDF Collab. (T. Aaltonen *et al.*), *Phys. Rev. Lett.* **109**, 181802 (2012).
468. DØ Collab. (V. M. Abazov *et al.*), *Phys. Rev. Lett.* **109**, 121804 (2012).
469. DØ Collab. (V. M. Abazov *et al.*), accepted by *Phys. Rev. D*, arXiv:1301.6122 [hep-ex].
470. DØ Collab. (V. M. Abazov *et al.*), *Phys. Rev. Lett.* **109**, 121803 (2012).
471. DØ Collab. (V. M. Abazov *et al.*), accepted by *Phys. Rev. D*, arXiv:1303.3276 [hep-ex].
472. DØ Collab. (V. M. Abazov *et al.*), *Phys. Lett. B* **716**, 285 (2012).
473. CDF Collab. (T. Aaltonen *et al.*), submitted to *Phys. Rev. D*, arXiv:1306.0023 [hep-ex].
474. DØ Collab. (V. M. Abazov *et al.*), accepted by *Phys. Rev. D*, arXiv:1301.1243 [hep-ex].
475. DØ Collab. (V. M. Abazov *et al.*), *Phys. Lett. B* **714**, 237 (2012).
476. DØ Collab. (V. M. Abazov *et al.*), accepted by *Phys. Rev. D*, arXiv:1302.5723 [hep-ex].
477. CDF Collab. (T. Aaltonen *et al.*), *Phys. Rev. Lett.* **108**, 181804 (2012).
478. DØ Collab. (V. M. Abazov *et al.*), accepted by *Phys. Rev. D*, arXiv:1211.6993 [hep-ex].
479. CDF Collab. (T. Aaltonen *et al.*), *Phys. Lett. B* **717**, 173 (2012).
480. DØ Collab. (V. M. Abazov *et al.*), accepted by *Phys. Rev. D*, arXiv:1301.5358 [hep-ex].
481. CDF Collab. (T. Aaltonen *et al.*), *Phys. Rev. D* **86**, 072012 (2012).
482. Y. Gao *et al.*, *Phys. Rev. D* **81**, 075022 (2010), arXiv:1001.3396 [hep-ph].
483. ATLAS Collab. (G. Aad *et al.*), *Phys. Lett. B* **716**, 1 (2012), arXiv:1207.7214 [hep-ex].
484. CMS Collab. (S. Chatrchyan *et al.*), submitted to *J. High Energy Phys.*, arXiv:1303.4571 [hep-ex].
485. CDF Collab. (T. Aaltonen *et al.*), accepted for publication by *Phys. Rev. D*, arXiv:1301.6668 [hep-ex].
486. DØ Collab. (V. M. Abazov *et al.*), submitted to *Phys. Rev. D*, arXiv:1303.0823 [hep-ex].
487. CMS Collab. (S. Chatrchyan *et al.*), *Phys. Lett. B* **716**, 30 (2012), arXiv:1207.7235 [hep-ex].
488. ATLAS Collab. (G. Aad *et al.*), *Phys. Rev. Lett.* **108**, 111803 (2012), arXiv:1202.1414 [hep-ex].
489. CMS Collab. (S. Chatrchyan *et al.*), *Phys. Lett. B* **710**, 403 (2012), arXiv:1202.1487 [hep-ex].
490. ATLAS Collab. (G. Aad *et al.*), *Phys. Lett. B* **710**, 383 (2012), arXiv:1202.1415 [hep-ex].
491. ATLAS Collab. (G. Aad *et al.*), *Phys. Lett. B* **717**, 29 (2012), arXiv:1205.6744 [hep-ex].
492. ATLAS Collab. (G. Aad *et al.*), *Phys. Lett. B* **717**, 70 (2012), arXiv:1206.2443 [hep-ex].

493. CMS Collab. (S. Chatrchyan *et al.*), *J. High Energy Phys.* **03**, 040 (2012), arXiv:1202.3478 [hep-ex].
494. CMS Collab. (S. Chatrchyan *et al.*), *J. High Energy Phys.* **03**, 081 (2012), arXiv:1202.3617 [hep-ex].
495. CMS Collab. (S. Chatrchyan *et al.*), *J. High Energy Phys.* **04**, 036 (2012), arXiv:1202.1416 [hep-ex].
496. CMS Collab. (S. Chatrchyan *et al.*), *Eur. Phys. J. C* **73**, 2469 (2013), arXiv:1304.0213 [hep-ex].
497. ATLAS Collab. (G. Aad *et al.*), *Phys. Lett. B* **716**, 62 (2012), arXiv:1206.0756 [hep-ex].
498. ATLAS Collab. (G. Aad *et al.*), *Phys. Lett. B* **718**, 391 (2012), arXiv:1206.6074 [hep-ex].
499. CMS Collab. (S. Chatrchyan *et al.*), *Phys. Lett. B* **699**, 25 (2011), arXiv:1102.5429 [hep-ex].
500. ATLAS Collab. (G. Aad *et al.*), *Phys. Lett. B* **718**, 369 (2012), arXiv:1207.0210 [hep-ex].
501. CMS Collab. (S. Chatrchyan *et al.*), *J. High Energy Phys.* **11**, 088 (2012), arXiv:1209.3937 [hep-ex].
502. CMS Collab. (S. Chatrchyan *et al.*), *Phys. Lett. B* **722**, 207 (2013), arXiv:1302.2892 [hep-ex].
503. CMS Collab. (S. Chatrchyan *et al.*), *Phys. Lett. B* **710**, 284 (2012), arXiv:1202.4195 [hep-ex].
504. CMS Collab. (S. Chatrchyan *et al.*), *J. High Energy Phys.* **05**, 145 (2013), arXiv:1303.0763 [hep-ex].
505. ATLAS Collab. (G. Aad *et al.*), *J. High Energy Phys.* **09**, 070 (2012), arXiv:1206.5971 [hep-ex].
506. CMS Collab. (S. Chatrchyan *et al.*), *Phys. Lett. B* **713**, 68 (2012), arXiv:1202.4083 [hep-ex].
507. ATLAS Collab. (G. Aad *et al.*), *Science* **338**, 1576 (2012).
508. ATLAS Collab. (G. Aad *et al.*), *Phys. Rev. D* **86**, 032003 (2012), arXiv:1207.0319 [hep-ex].
509. ATLAS Collab. (G. Aad *et al.*), *Phys. Lett. B* **710**, 49 (2012), arXiv:1202.1408 [hep-ex].
510. CMS Collab. (S. Chatrchyan *et al.*), *Science* **338**, 1569 (2012).
511. CMS Collab. (S. Chatrchyan *et al.*), *Phys. Lett. B* **710**, 26 (2012), arXiv:1202.1488 [hep-ex].
512. J. Ellis and D. S. Hwang, *J. High Energy Phys.* **1209**, 071 (2012), arXiv:1202.6660 [hep-ph].
513. J. Ellis, D. S. Hwang, V. Sanz and T. You, arXiv:1208.6002 [hep-ph].
514. J. Ellis, R. Fok, D. S. Hwang, V. Sanz and T. You, arXiv:1210.5229 [hep-ph].
515. L. D. Landau, *Dokl. Akad. Nauk SSSR* **60**, 207 (1948).
516. C. N. Yang, *Phys. Rev.* **77**, 242 (1950).
517. G. Degrassi *et al.*, *J. High Energy Phys.* **1208**, 098 (2012), arXiv:1205.6497 [hep-ph].
518. ATLAS Collab., ATL-PHYS-PUB-2012-004 (2012).
519. U. Baur, T. Plehn and D. L. Rainwater, *Phys. Rev. D* **67**, 033003 (2003), arXiv:hep-ph/0211224.